I 5.008

Cursusprogramma

SIMONA

Programmbeschreibung

Teil 2

SIMULATION WATER QUALITY

HISWA

HINDCAST

OF

SHALLOW WATER WAVES

Resumé windgolven-theorie

- Lineaire golftheorie

  $x(t) = A \cos(\omega t + \phi)$

- Random phase model

  $x(t) = \Sigma A_i \cos(\omega_i t + \phi_i)$

  A_i, ω_i deterministisch
  ϕ_i stochastisch, uniform verdeeld in $(-\pi , \pi)$

- Statistische beschrijving

  Fourier transformatie
  - amplitudespectrum: $A = A(\omega,\theta)$
  - energiedichtheidspectrum: $E = E(\omega,\theta) \sim A^2$

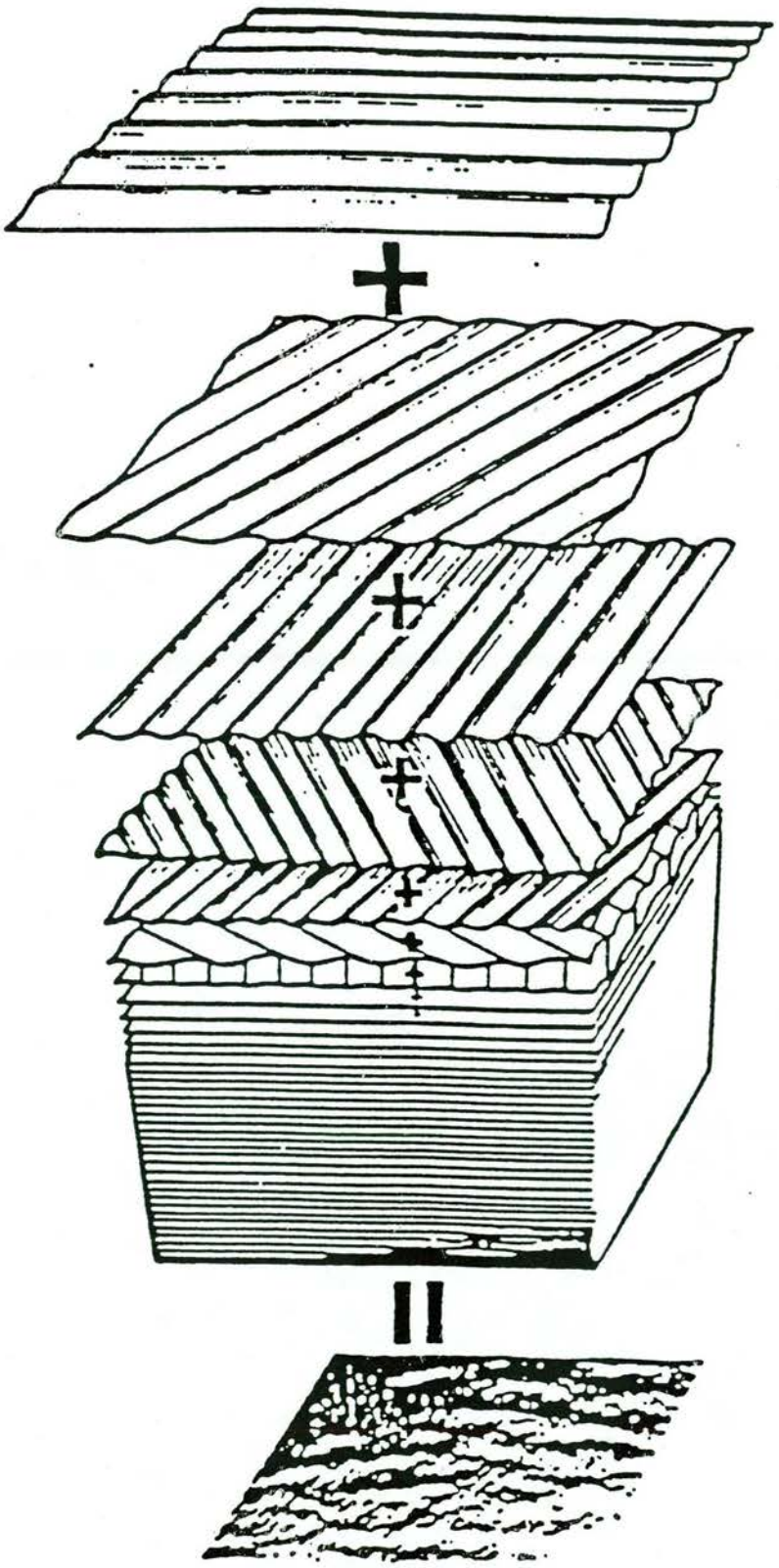

Energiedichtheidsspectrum

- 1-dimensionaal (voor 1 richting)

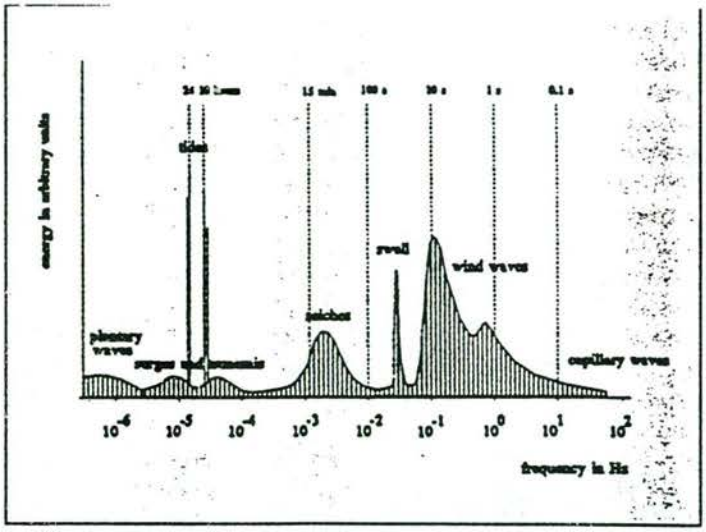

- 2-dimensionaal (voor alle richtingen)

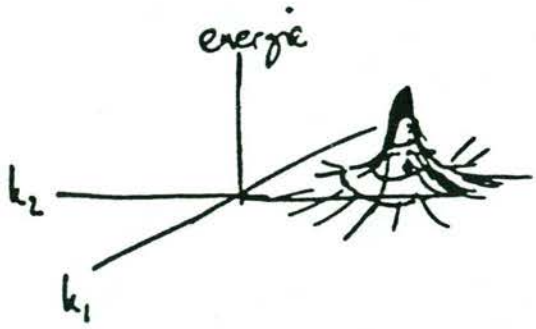

Energiebalans-vergelijking

$$dE(\omega,\theta;\underline{\mathbf{x}},t)/dt = S(\omega,\theta;\underline{\mathbf{x}},t)$$

$$S = S_{in} + S_{ds} + S_{nl}$$

S_{in} - bronterm voor input
S_{ds} - bronterm voor dissipatie
S_{nl} - bronterm voor niet-lineaire wisselwerking

Golfactie

$A(\omega,\theta;\underline{\mathbf{x}},t) = E(\omega,\theta;\underline{\mathbf{x}},t)/\sigma$

$\sigma = \omega - \underline{\mathbf{k}}.\underline{\mathbf{V}}$ relatieve frequentie
$\underline{\mathbf{V}}$ - stroomsnelheidsvector

Actiebalans-vergelijking

$$dA(\omega,\theta;\underline{\mathbf{x}},t)/dt = T(\omega,\theta;\underline{\mathbf{x}},t)$$

$$T = T_{in} + T_{ds} + T_{nl}$$

T_{in} - bronterm voor input
T_{ds} - bronterm voor dissipatie
T_{nl} - bronterm voor niet-lineaire wisselwerking

Basisvergelijkingen van HISWA

- Actiebalans-vergelijking
- Stationaire benadering (verblijftijd van golven in het model klein tov tijdschaal van wind, getij enz.)
- Parametrisatie van de actiebalans-vergelijking
- Aanname van standaard vorm van het frequentie-spectrum
- Spectrum in de (x,y)-ruimte wordt beschreven d.m.v.:
  - gemiddelde periode
  - gemiddelde frequentie

- Evolutievergelijkingen

  - an evolution equation for the zero-order moment of the action density spectrum for each spectral direction,

$$\frac{\partial}{\partial x}(c_x^* A_0) + \frac{\partial}{\partial y}(c_y^* A_0) + \frac{\partial}{\partial \theta}(c_\theta^* A_0) = T_0$$

  - an evolution equation for the first-order moment of the action density spectrum for each spectral direction,

$$\frac{\partial}{\partial x}(c_x^{**} A_1) + \frac{\partial}{\partial y}(c_y^{**} A_1) + \frac{\partial}{\partial \theta}(c_\theta^{**} A_1) = T_1$$

The physical phenomena which are accounted for in these equations are:

a) refractive propagation
b) wind growth
c) bottom dissipation
d) surf dissipation
e) current dissipation

- Brontermen

$$S(\theta) = S(\theta)_{wind} + S(\theta)_{bottom} + S(\theta)_{breaking} + S(\theta)_{blocking}$$

Beperkingen van HISWA

- Geen diffractie
- Geen spectra met meerdere pieken
- Teruglopende / gereflecteerde golven worden niet meegenomen in de berekening)

Numerieke implementatie

- Numeriek schema

  - (expliciet) leap-frog in de (x,y)-ruimte

  - (impliciet) Euler in de θ-ruimte

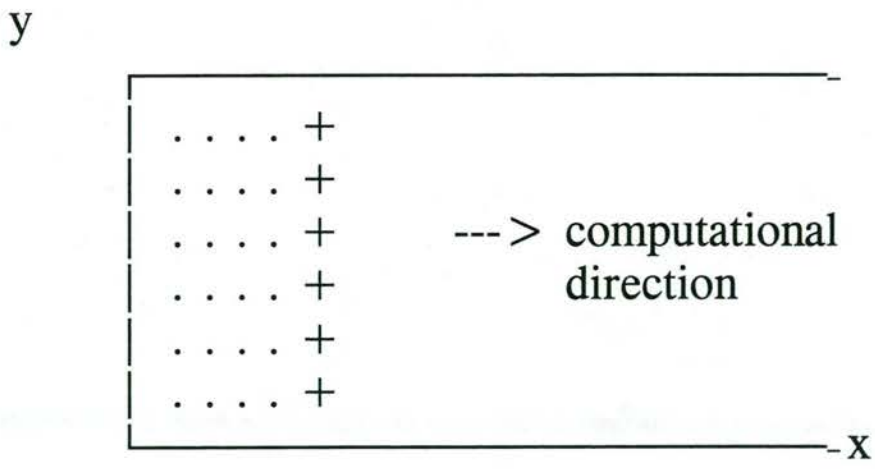

Figure 1: The computational grid
. points determined previously
\+ points being computed

- Rekensector Hoogst 180° (Daarom geen terug-lopende golven)

- Rekenrichting
- Groei van fouten

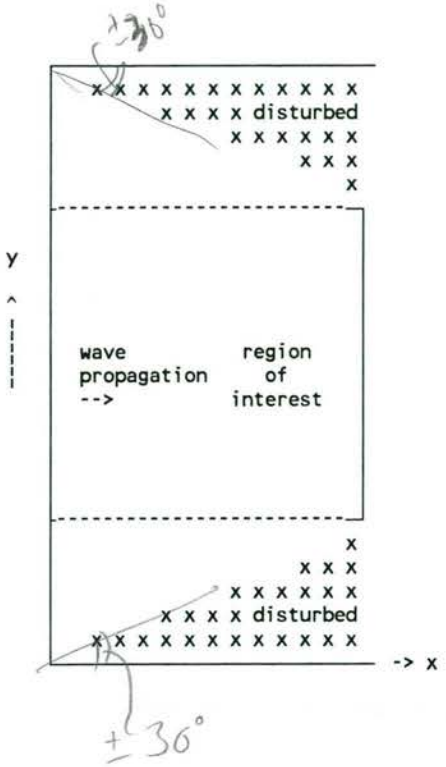

- Stabiliteitscriterium

$$\frac{|c_y \Delta x|}{|c_x \Delta y|} \leq 1$$

bij de afwezigheid van stroming:

$$\frac{\Delta x}{\Delta y} \leq cotg(\theta)$$

(bij sector = 120^0: $\Delta x \leq \frac{1}{2}\Delta y$)

- Keuze stapgrootte

  - Δy ~ stapgrootte bodemrooster
  - Δx volgt uit het stabiliteitscriterium
  - $\Delta\theta$ 10^0 , bij smalle spectrum (deining) 5^0

- Ruimtelijke interpolaties

tussen drie programma delen HISWA
- preparatie
- rekenen
- uitvoer

Input-, Reken- en Outputgrids

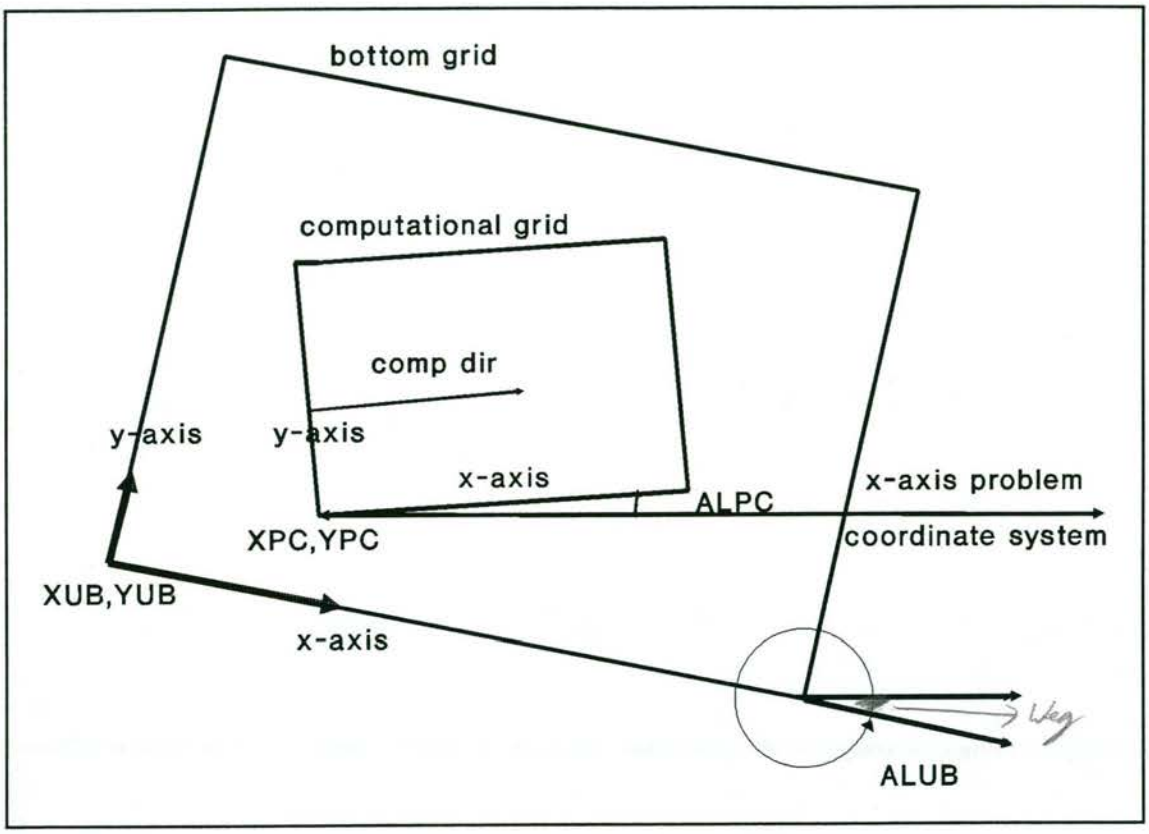

Input / Output

- Input-grootheden
  - model-geometrie
  - dieptes, stroomsnelheden
  - wind, bodemwrijving
  - randvoorwaarden: Hs, T, breedte richtingspectrum

- Output-grootheden
  - Hs
  - gemiddelde golfperiode
  - gemiddelde richting
  - golfkrachten
  - energietransport
  - energiedissipatie
  - orbitale snelheid bij de bodem
  - fractie brekende golven
  - richtingsspreiding
  - golflengte
  - golfsteilheid

Simulatie Modellen Natte Waterstaat

SIMONA

- Doelstellingen

  - koppelen van modellen
  - uniformering van programmatuur
  - hergebruik van programmatuur

- Praktische realisatie

  - software toolbox
  - WAQUA
  - HISWA

- Plannen voor de toekomst

  - koppeling HISWA-WAQUA
  - morfologie (koppeling morfologisch model-WAQUA) ISM. WL
  - ecologie
  - post-processing

Opzet SIMONA pre-processing

- batch-georiënteerd → Niet interactief
- tweetrapse verwerking → Eerst invoercontrole. Dan pas naar HISWA
- ASCII invoerfile
- blokgewijze opbouw vd invoer
- keywords en data
- default-waarden
- eenvoudig uit te breiden structuur

Opbouw SIMONA invoer file

- keywords (bijv. MESH)
- numerieke data

  - integer (bijv. 10)
  - real (bijv. 1.0 of 1.3e-10)

- character strings (bijv. 'TEXEL')
- scheidingstekens (/ , ; = : \ )
- commentaar (bijv. #dit is comment.)
- invoerlijn: max. 80 posities lang
- invoerblok (keywords en data)

User's Guide HISWA

Gebruikte conventies

For the input definition the following conventions are used:

[val]	:	real value
[tval]	:	time specification in the form: *day hours:minutes* (e.g. 2 21:15). Times are given relative to midnight of a reference date, starting at 0 0:00.
[ival]	:	integer value
[iseq]	:	sequence number to indicate a point, curve, etc.
[text]	:	string (enclosed between quotes)
< ... >	:	repetition group
| A		
<	:	choice between A and B (A and B are
| B		mutually exclusive)
&	:	continuation mark

In this document a part of the keywords is underlined (e,g, PRIN-TOUTPUT). Only the underlined characters are significant. So the user must type at least PRINT in his input, but PRINTOUT is excepted as well.

The 'Explanation' part of the description of the various sections, subsections is divided in three columns:

KEYWORD **X** Explanation
X can be O, M, D, S, R.

- **O** means keyword is optional.
- **M** means keyword is mandatory.
- **D** means keyword has a default value. When this keyword is omitted, the pre-processor will use the default value for the variable specified by means of this keyword.
- **R** means keyword can be used repeatedly.
- **S** means this keyword is a sequential keyword: a keyword followed by an integer (e.g. P4). A sequential keyword can be used repeatedly.

Speciale invoerstructuren
Datavelden

```
FIELDDATA
   GLOBAL
   LOCAL


GLOBAL
   LAYOUT = [ival]
   |     CONST_VALUES = [val]
<
   |     VARIABLE_VALUES = < [val] >


LOCAL
<    BOX:    MNMN = ( [ival], [ival] ) ( [ival], [ival] )
               | CONST_VALUES = [val]
           <
               | CORNER_VALUES = [val], [val], [val], [val]
           <
               | VARIABLE_VALUES = < [val] >
>
```

VOORBEELD:

```
GLOBAL
   CONST_VALUES = 0,  LAYOUT = 3
LOCAL
BOX:    MNMN = (10, 5), (11, 7)
        VARIABLE_VALUES =  2.0   2.3     2.4
                           1.9   2.0     3.2
```

Speciale keywords

- SET

  - echo (default)
  - noecho
  - maxerror = <waarde> (def. 10)
  - maxwarn = <waarde> (def. 50)
  - nowritesds
  - writesds (default)

- INCLUDE (lees invoer uit een andere invoer file)

- INSERT (lees gegevens van een datafile volgens opgegeven formaat)

Belangrijkste commando's

PARAMETERS (User's Guide blz. 42)
  gravity, rho, cfae

MESH (blz. 43)
  INPUTGRIDS
  COMPGRID
  RESGRID

FORCINGS (blz. 47)
  DEPTHS
  CURRENT
  FRICTION
  WIND
  INCOMING_WAVES
  BOUNDARY

BREAKING (blz. 55)

BLOCKING (blz. 56) — Wordt niet aanbevolen om aan te passen, tenzij heel bewust.

OUTPUT_LOCATIONS (blz. 59)
  FRAMES_DEFINITION
  CURVES_DEFINITION
  POINTS_DEFINITION

PRINTOUTPUT (blz. 64)
  BLOCKOUTPUT
  TABLEOUTPUT

PLOTOUTPUT (blz. 70)
  SHOWOUTPUT
  PLOTRESULTS

Het HISWA-systeem

- Rekenprogramma HISWA
- Grafisch post-processing programma HPLOT
- Conversieprocedure voor oude HISWA invoerfiles → HISCON

UNIX runprocedures

hiswa.run -runid <runid> -input <input>

hplot <plotfile> <plotdev>

hiscon <oldfile> <newfile>

Standaard HISWA-testbank

- Testverslag DGW
- Invoerfiles:

  /usr/local/simona/examples/hiswa

Wind en golven

Golven op zee nemen veel gedaanten aan, variërend van een lieflijke deining bij een tropisch strand tot verwoestende brekers in een storm. Deze golven zijn opgewekt door de wind en worden door de meeste mensen ervaren als 'de' golven op zee. Strikt genomen horen echter ook andere verschijnselen tot de golven op zee (dat wil zeggen min of meer periodieke oppervlakte-uitwijkingen). Men denke daarbij aan getijden, stormvloeden, tsunamis en seiches. In dit artikel zal de aandacht vooral gericht worden op de opwekking, voortplanting en dissipatie van windgolven.

Het lijkt voor de hand te liggen golven te definiëren als de op-en-neergaande beweging van het zee-oppervlak. Deze definitie omvat zowel de golven die door de wind opgewekt worden en die gewoonlijk zeegolven genoemd worden, als andere golven zoals getijden. Getijden zijn niet zo eenvoudig waar te nemen als golven waarvan de ene golftop volgt op de andere. In plaats daarvan zien we een langzaam rijzen en dalen van de waterlijn op het strand of in een haven. Een kort overzicht van golven, geordend naar hun periode of frequentie is weergegeven in afbeelding 1 en in de navolgende tekst.

Dr.ir. L. H. Holthuijsen

De auteur is verbonden aan de Vakgroep Waterbouwkunde van de Faculteit der Civiele Techniek van de Technische Universiteit Delft.

Dit artikel is de weergave van de voordracht die de auteur op 18 november 1992 hield tijdens het symposium 'Windtechnologie buitengaats', georganiseerd door de Stuurgroep Windtechnologie (werkzaam onder auspiciën van de Afdeling Bouw- en Waterbouwkunde van het KIvI).
Het symposiumboek met alle teksten van de lezingen is te bestellen door overmaking van *f* 60,- op gironummer 34 46 04, t.n.v. KIvI/Stuurgroep Windtechnologie, Apeldoorn.

Typen golven

Uit afbeelding 1 is af te lezen dat er verschillende typen golven bestaan. Te onderscheiden zijn:

- *capillaire golven*: dit zijn zeer kleine golven die door de wind opgewekt worden. Ze zijn slechts een paar centimeter lang en een of twee millimeter hoog. Ze zijn goed te zien op rustig water waar ze de glinstering van de zon op het water veroorzaken. Zelfs een lichte bries op een vijver of een meer veroorzaakt deze golven. De dynamica van deze golven wordt gedomineerd door de oppervlaktespanning. Hun gedrag kan daarom benvloed worden door de oppervlaktespanning van het water te veranderen, bijvoorbeeld door zeep of olie op het water te brengen;
- *windgolven*: deze golven worden eveneens door de wind opgewekt, in een wat later stadium dan de capillaire golven. Dit zijn de golven die van belang zijn voor schepen, offshoreconstructies en havens. Hun golflengte varieert van een paar centimeter tot enige honderden meters met golfhoogten tot 30 m. Deze golven worden gewoonlijk als *'zeegolven'* aangeduid. De dynamica

wordt, evenals die van de navolgende categorieën golven, gedomineerd door de zwaartekracht;

- *deining*: dit is het restant van windgolven, opgewekt in een storm op enige afstand van de waarnemer. De periode varieert van ongeveer 10 s tot 30 s;
- *seiches*: deze golven behoren noch tot windgolven, noch tot getijden. De tijdschaal varieert van een paar minuten tot een half uur. De opwekking van deze golven is nog steeds een mysterie (zij worden wellicht veroorzaakt door groepen windgolven of wellicht door atmosferische storingen zoals buien of andere verschijnselen). Ze kunnen schepen in problemen brengen, die rustig in een haven liggen omdat zij door resonantie het water in havenbekkens in slingering kunnen brengen;
- *tsunamis*: deze golven worden ook wel 'tidal waves' genoemd (dit is in zoverre een misleidend naam, om dat ze niets met getijden te maken hebben). Het zijn vrij lange golven met een tijdschaal van enige uren, ontstaan door aardbevingen of (onderzeese) aardverschuivingen;
- *stormvloeden*: deze golven worden opgewekt door meteorologische systemen (druk- en windvariaties voornamelijk in lage-drukgebieden). De tijdschaal varieert van één tot enkele dagen. Naast de zwaartekracht speelt ook de Coriolis-(schijn)kracht een rol;
- *getijden*: dit zijn de zeer lange golven (honderden tot duizenden kilometers lang) opgewekt door de onderlinge krachten en bewegingen van Aarde, Zon en Maan. Naast de zwaartekracht speelt ook de Coriolis-(schijn)kracht een rol;
- *planetary golven*: ook dit zijn zeer lange golven maar, anders dan getijden, zijn ze opgewekt door grootschalige variaties in het aardse atmosferische systeem en door interacties met de oceaanbodem en getijden.

Windgolven

Windgolven maken meestal een chaotische indruk en lijken iedere poging tot een ordelijke beschrijving te weerstaan. Toch blijkt deze chaos goed te beschrijven door deze te splitsen in een aspect van perfecte chaos en een aspect van perfecte ordening. Het chaotische aspect is voor de meeste doeleinden eenvoudig van aard en goed bekend. Een goede benadering van het zee-oppervlak binnen een klein gebied (om de gedachten te bepalen: 100 km x 100 km op de oceaan of 10 km x 10 km in een randzee) is te verkrijgen door het opgebouwd te denken uit een groot aantal individuele golfcomponenten die elk, behalve door een frequentie, gekenmerkt zijn door een amplitude, fase en richting.

Van deze parameters blijkt de fase een stochastische grootheid te zijn (dat wil zeggen niet voorspelbaar). Dit model staat daarom bekend als het 'random phase'-model van zeegolven. In feite is dit random karakter van de fase de oorzaak van het onvoorspelbare, chaotische karakter van zeegolven. De fase blijkt echter elegant stochastisch te zijn: de kansdichtheidsverdeling is uniform tussen $-\pi$ en $+\pi$.

De andere parameters (amplitude, frequentie en richting) zijn deterministisch. Het is gebruikelijk de golfcomponenten te ordenen naar hun frequentie en richting, waarbij de amplitude dan een functie wordt van frequentie en richting. Deze tweedimensionale functie wordt het *amplitudespectrum* genoemd. Deze combinatie van een stochastische (fase) en een deterministische parameter (amplitude als functie van frequentie en richting) kan gebruikt worden om alle statistische eigenschappen van de golven te bepalen (binnen de beperking dat de golven niet te steil mogen zijn). Strikt genomen moet het spectrum gegeneraliseerd worden om een oneindig aantal frequenties en richtingen te bevatten. Als dat gebeurt, dan blijkt dat het principieel beter is om het kwadraat van de amplitude te beschouwen. Dat is niet alleen uit stochastisch oogpunt beter (de variantie van het chaotische zee-oppervlak is evenredig met dit kwadraat), het geeft ook direct het verband met de fysica weer, omdat de golfenergie rechtevenredig is met dit kwadraat). Dit gegeneraliseerde amplitude(kwadraat)spectrum wordt daarom wel het *energiespectrum* van de golven genoemd.

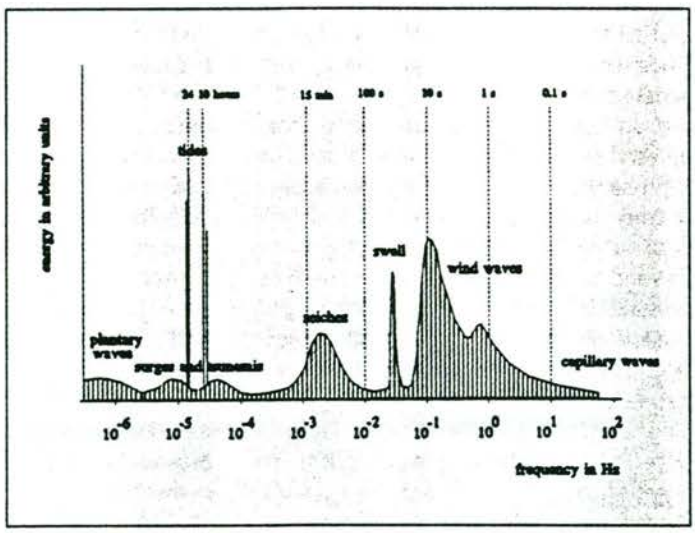

Afb. 1 Het energiespectrum van de golven in de oceaan (vrijelijk weergegeven).

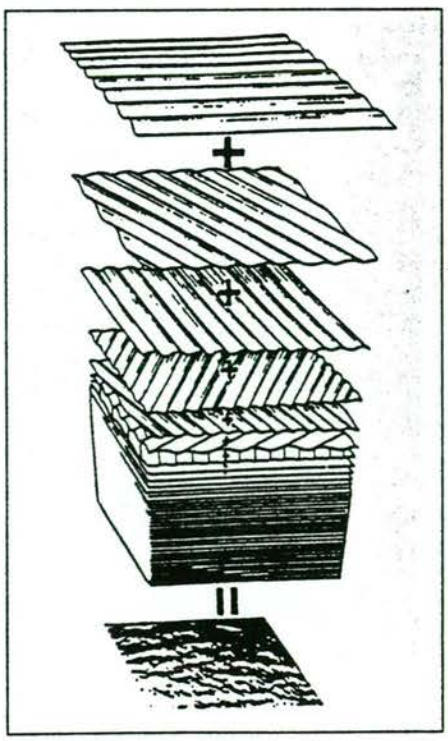

Afb. 2 Het zee-oppervlak voorgesteld als de som van een groot aantal harmonische golfcomponenten.

De fysica van windgolven

De fysica van windgolven kan globaal onderverdeeld worden in de voortplanting van de golven enerzijds en de opwekking en dissipatie van de golven anderzijds. Daarbij kan met veel nut gebruik gemaakt worden van de voorgaande beschrijving in termen van het energiespectrum van de golven.

De voortplanting van een individuele golfcomponent is goed bekend. In diep water loopt een golfcomponent (of beter: zijn golfenergie) met een bekende snelheid langs rechte lijnen loodrecht op zijn golfkam. Als men golfvoortplanting op grote (oceanische) schaal bekijkt, blijken de rechte lijnen vervangen te moeten worden door groot cirkels. De lage frequenties blijken zich sneller voort te planten dan de hoge frequenties (omgekeerd evenredig met de frequentie).

Als de golven in ondiep water komen (ondieper dan ongeveer de halve golflengte), wordt de snelheid ook afhankelijk van de waterdiepte (lagere snelheid naarmate het water ondieper wordt). Dit heeft onder andere tot gevolg dat de golfcomponent van

richting verandert (altijd naar het ondiepere water toe; refractie) en dat de golfenergie zich enigszins 'opstapelt' (de golfhoogte neemt toe; shoaling).
Bij de kust kunnen zich in het golfveld obstakels bevinden. Een deel van de golven zal dissiperen en wellicht gedeeltelijk op een dergelijk obstakel reflecteren, maar een ander deel van het golfveld verspreidt zich achter het obstakel (diffractie). Deze diffractie wordt veroorzaakt door grote verschillen in golfhoogte over korte afstanden. De golven draaien hierdoor naar de gebieden met lage golfhoogte. In de aanwezigheid van stroming is de situatie enigszins anders maar overigens goed bekend.

De opwekking van golven is in redelijke mate bekend, in ieder geval voldoende om met succes numerieke modellen toe te passen. Aanvankelijk wekt de wind golven op door het drukpatroon dat ontstaat als een turbulente wind het wateroppervlak raakt. Dit drukpatroon verplaatst zich met de gemiddelde windsnelheid over het water en verandert daarbij maar langzaam. Dit 'bevroren' en lopende drukpatroon veroorzaakt de eerste golven (schuifspanning door de wind aan het wateroppervlak speelt geen noemenswaardige rol). Zodra echter golven door dit mechanisme ontstaan zijn, gaan zij de wind zelf beïnvloeden. Aan de loefzijde ontstaat door de aanwezigheid van de golf een licht overdruk en aan de lijzijde een lichte onderdruk. Dat betekent dat daar waar het wateroppervlak een neerwaartse beweging heeft (aan de lijzijde), de wind een druk uitoefent. Dit impliceert een overdracht van energie (kracht en weg in dezelfde richting). Hetzelfde gebeurt aan de loefzijde: het wateroppervlak heeft een opwaartse beweging en er heerst een lichte onderdruk waardoor er ook energie van wind naar golven overgedragen wordt.
De mate van overdruk en onderdruk wordt onder andere bepaald door de amplitude van de golf. Maar die neemt toe door de drukverschillen, waardoor de drukverschillen zelf weer toenemen. Het is dus een niet-stabiel terugkoppelingsmechanisme dat resulteert in een exponentiële groei van de golfenergie van de beschouwde golfcomponent.
Opgemerkt moet worden dat de hoge frequenties op deze manier veel sneller groeien dan de lage frequenties. Zodra de golven door het opnemen van energie uit de atmosfeer enige steilheid opgebouwd hebben, gaan niet-lineaire effecten een rol spelen. Al vrij snel zal een golfcomponent energie ontvangen danwel afstaan aan andere golfcomponenten. Het blijkt namelijk dat door resonantie drie golfcomponenten energie uitwisselen met een vierde (quadruplet interactie; op diep water). Deze niet-lineaire

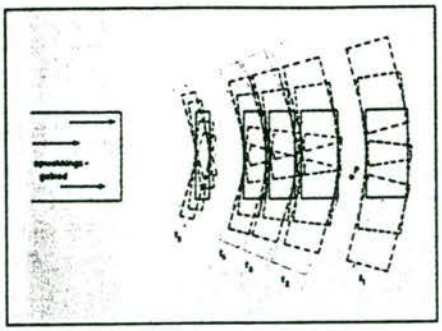

Afb. 3 De voortplanting van golven uit een stormgebied (frequentie en richtingdispersie).

golf-golf interacties blijken van groot belang te zijn voor de ontwikkeling van een golfveld zolang de golven een redelijke steilheid hebben (golfhoogte/golflengteverhouding). Uiteindelijk blijkt de steilheid van de golven zò groot te kunnen worden dat de golven gaan breken ('whitecapping').
In ondiep water geldt dat twee componenten een interactie aangaan met een derde (triad interactie; in ondiep water). Hier is overigens nog weinig onderzoek naar gedaan. Een tweede effect in ondiep water is het opwekken van turbulentie bij de bodem door waterbeweging ten gevolge van de golven. Dit veroorzaakt energieverlies voor de golven. Uiteindelijk wordt de waterdiepte zo gering dat de golven breken op zandbanken, riffen, het strand of op de rotsen.

Kort samengevat is de geschiedenis van een golfcomponent dus als volgt. Hij ontstaat ergens op zee (meestal benedenwinds van een kust) door een wind-geïnduceerde drukfluctuatie. Door zijn aanwezigheid aan het wateroppervlak verstoort hij het windveld enigszins, waardoor er een licht druk-

Afb. 4 Het richting- en frequentiefilter van stormgolven dat deining verklaart.

verschil over de golfkam ontstaat. Dat levert energie op voor de golfcomponent. Daarnaast ontvangt hij door resonantie energie van andere golfcomponenten. Als hij na enige groei een bepaalde steilheid bereikt, staat hij weer energie af aan andere componenten (door resonantie), maar niet voldoende om breken te voorkomen. Dat laatste kan midden op zee gebeuren, maar ook pas in de brandingszone op een strand. Voor hij echter een strand (of in het algemeen: een kust) bereikt, wordt de golfcomponent gedwongen om (a) zijn snelheid te minderen en (b) zijn richting naar het ondiepe water toe te draaien, meestal onder verlies van energie door bodemwrijving. Soms, bijvoorbeeld bij een golfbreker of een rotspartij, wordt de golf ook gedwongen van richting te veranderen naar gebieden met een lagere golfhoogte.

Golfmodellen

Op grond van de voorgaande beschrijvingstechniek en fysica van zeegolven is een groot aantal golfmodellen ontwikkeld om golven te kunnen berekenen voor een gegeven windveld. Afhankelijk van het feit of het een voorspeld windveld is of een gereconstrueerd (historisch) windveld, spreekt met van een 'forecast' of een 'hindcast'. Een forecast is natuurlijk van operationele waarde bij uitvoering van werk op zee, zoals het installeren van een grote offshoreconstructie. De hindcasts zijn om verschillende redenen van belang. De belangrijkste zijn wellicht het schatten van een golfklimaat aan de hand van een groot aantal historische weerkaarten en het reconstrueren van belangrijke incidenten op zee waar geen betrouwbare golfwaarnemingen zijn. Die golfmodellen zijn er in allerlei uitvoeringen, variërend van zeer eenvoudig uitvoerbaar op een zakrekenmachine (maar zeer onbe-

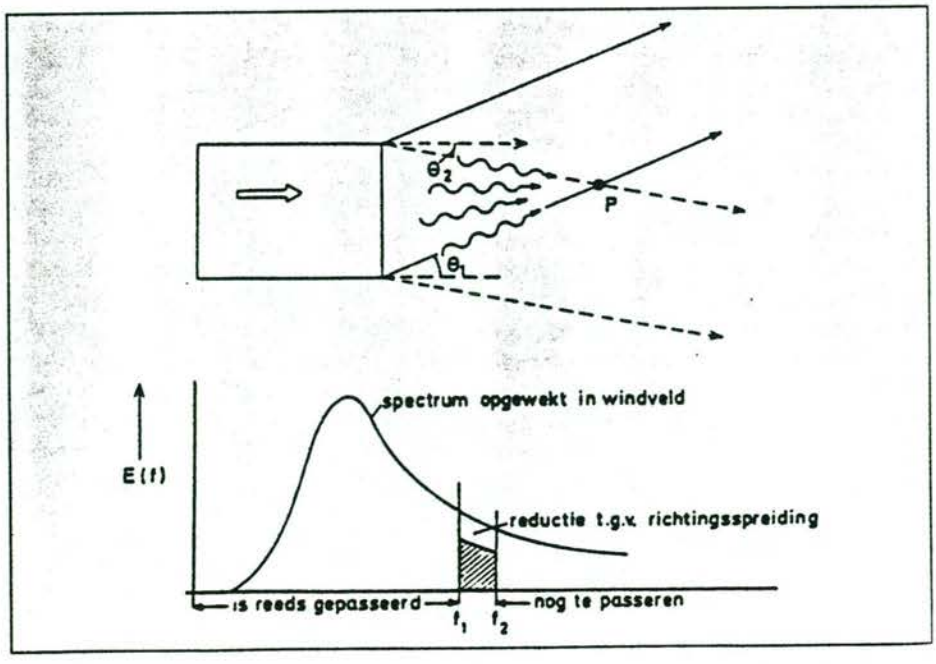

trouwbaar) tot zeer geavanceerd maar alleen bruikbaar op een supercomputer (maar el betrouwbaar).

elaas zijn er van de modellen twee, niet verenigbare, versies. In de eerste versie worden refractie en diffractie berekend zonder dat er goed rekening gehouden kan worden met opwekking en dissipatie van de golven. Deze modellen reconstrueren op verschillende wijzen de feitelijke oppervlakte-uitwijking (waar een ingenieur meestal niet in genteresseerd is). Deze modellen zijn dermate rekenintensief dat ze alleen toepasbaar zijn in kleine gebieden (maximaal enige tientallen golflengten). In de tweede versie kunnen alle effecten van voortplanting, opwekking en dissipatie meegenomen worden, behalve diffractie. Deze modellen beschouwen het energiespectrum van de golven en kunnen op oceanische schaal toegepast worden. Deze laatste modellen gebruiken de energiebalans van de golven zoals die ook gebruikt is in de voorgaande beschrijving van de opwekking en dissipatie van golven. Deze energiebalans kan op twee manieren uitgewerkt worden. De eerste is het volgen van iedere component afzonderlijk over het zee-oppervlak en het bijhouden van de energiebalans van de gevolgde component (een Lagrangian-benadering). Deze methode is tamelijk traditioneel in de kustwaterbouwkunde, waar hij bekend staat als de 'stralenmethode' (men volgt de golfstralen). Daarbij doet zich een aantal klassieke problemen voor, met name daar waar golfstralen elkaar snijden (door het ontbreken van diffractie in dit soort modellen zou de golfhoogte oneindig groot worden). Door middelingsprocedures zijn deze problemen redelijk op te lossen (in feite wordt hiermee diffractie gesimuleerd).

De tweede manier om de energiebalans uit te werken is door (geografisch) lokaal een Eulerse balans op te stellen in een groot aantal roosterpunten (roostermodel). Lokaal worden dan alle genoemde effecten beschouwd (behalve diffractie). Dit is de traditionele methode voor golfmodellen in de oceanografie.

Sinds een paar jaar bestaan er echter ook dit soort modellen voor kusttoepassingen. Ook in deze modellen ontbreekt de diffractie, maar de genoemde klassieke problemen van stralenmodellen doen zich niet voor omdat een middelingsprocedure impliciet in de geografische en spectrale discretisatie van dit soort modellen opgenomen is.

Storm en deining

Een van de meest opvallende verschillen in zeegolven werd in de inleiding al wat poëtisch aangegeven als 'lieflijke deining bij een tropisch strand' enerzijds en 'verwoestende brekers in een storm' anderzijds. Hoe ontstaan deze verschillen?

Om dit duidelijk te maken kan een vrij eenvoudig model gebruikt worden. Veronderstel een oceaan waar een storm is geschematiseerd tot een stationair, rechthoekig geografisch gebied met een constante wind, gericht langs de as van de rechthoek (afbeelding 3). Buiten deze storm heerst windstilte. Veronderstel dat ook in de tijd de wind plotseling begint en eindigt.

Binnen het stormgebied zal na enige tijd een golfveld opgewekt zijn, dat zich kenmerkt door de bekende chaos van hoge en lage golven, brekend en niet brekend, met relatief korte golfkammen, kortom, de golven met 'verwoestende brekers'. Dit beeld is, zoals in het voorgaande aangegeven, redelijk goed te beschrijven met het 'random phase'-model waarin de amplituden gerelateerd zijn aan het energiespectrum van de golven en waarin de fasen volkomen willekeurig gekozen moeten worden. De individuele golfcomponenten verlaten het stormgebied aan de benedenwindse zijde. Deze golfcomponenten zullen zich, na het wegvallen van de wind, over de oceaan verspreiden, zoals in afbeelding 3 aangegeven is.

Er treden nu buiten het stormgebied twee verschijnselen op: frequentiedispersie en richtingdispersie. De lage frequenties planten zich sneller voort dan de hoge frequenties. Hierdoor zullen op een punt dat ver van de storm gelegen is (punt P in de afbeelding), eerst de lage frequenties arriveren (en voorbij trekken) en pas later de hoge frequenties. Daarnaast zorgen de verschillende richtingen van de golfcomponenten in het stormgebied ervoor dat in punt P niet alle energie langskomt. Alleen die componenten waarvan het veld over P heenloopt zullen in P aankomen (en door de frequentiedispersie eerst de lage frequenties en dan pas de hoge frequenties). Op enig tijdstip in P zijn dus van de oorspronkelijke golfcomponenten in de storm slechts die componenten aanwezig die (*a*) uit de richtingen komen waaronder de storm te zien is vanuit P (de gezichtshoek van de storm $\theta_1 \leq \theta \leq \theta_2$, afbeelding 4) en (*b*) bezig zijn het punt P te passeren. Dit zijn in het algemeen niet de laagste frequenties omdat die al voorbij zijn en niet de hoogste frequenties ($f_1 \leq f \leq f_2$, afbeelding 4) omdat die nog moeten aankomen.

Gecombineerd betekent dit dat in punt P slechts een smal spectrum aanwezig is, zowel in de richtingen als in de frequenties. Met andere woorden: de golven zijn tamelijk regelmatig omdat van de aanwezige componenten de frequenties dicht bijeen liggen en de golven zijn tamelijk langkammig omdat de aanwezige componenten uit vrijwel dezelfde richting komen. Bovendien is door dit tweedimensionale filter (in frequentie en richting) slechts een fractie van de oorspronkelijke golfenergie in P aanwezig.

De energie in het stormgebied wordt als het ware 'uitgesmeerd' over de hele oceaan waardoor een 'verdunning' van die energie optreedt. Dissipatie treedt vrijwel niet op in de windstille oceaan, zodat de afname van de golfhoogte buiten het stormgebied vrijwel uitsluitend het gevolg is van deze tweedimensionale dispersie.

Conclusies

Op de oceaan bestaan golfverschijnselen van uiteenlopende aard en schaal. Daarvan zijn de door de wind opgewekte golven wellicht de meest bekende, maar ook getijden zijn op te vatten als golven.

De chaos van windgolven is goed te beschrijven met behulp van het energiespectrum. Met dit spectrum is de fysica van de windgolven goed weer te geven, zowel wat hun voortplanting als hun opwekking en dissipatie betreft. Daar zijn echter een paar uitzonderingen op, waarvan het verschijnsel diffractie het meest opvallende is.

Op basis van de spectrale energiebalans kan voor een gegeven windveld (forecast of hindcast) het bijbehorende golfveld berekend worden. De traditionele methode van de kustwaterbouwkunde om dit te doen met de (Lagrangian) stralenmethode wordt langzaam vervangen door de (Eulerse) methode van een roostermodel dat afkomstig is uit de oceanografie.

Deining ontstaat door een tweedimensionale dispersie van het oorspronkelijke golfveld in een storm. ■

Literatuur

Golfopwekking

[1] Phillips, O.M., On the generation of waves by turbulent wind; in: Journal of Fluid Mechanics, 1957, Vol. 2, No. 5, blz. 417 - 445.

[2] Miles, J.W., On the generation of surface waves by shear flows; in: Journal of Fluid Mechanics, 1975, Vol. 3, No. 2, blz. 185 - 204.

[3] Hasselmann, K, Grundgleichungen der Seegangsvoraussage; in: Schiffstechnik, 1960, Vol. 7, No. 39, blz. 191 - 195.

Golfdissipatie

[4] Komen, G.J., Hasselmann, S., Hasselmann, K., On the existence of a fully developed wind-sea spectrum; in: Journal of Physical Oceanography, 1984, Vol. 14, No. 8, blz. 1271 - 1285.

[5] Battjes, J.A., Jansen, J.P.F.M., Energy loss and set-up due to breaking of random waves; in: Proc. 16th Coastal Engineering Conference, ASCE, 1978, blz. 569 - 587.

Golfvoortplanting

[6] Berkhoff, J.C.W., Computation of combined refraction - diffraction; in: Proc.13th Coastal Engineering Conference, ASCE, 1972, blz. 471 - 490.

[7] Munk, W.H., Miller, G.R., Snodgrass, F.E., Barber, N.F., Directional recording of swell from distant storms; in: Phil. Trans. Royal Soc. London, A 255, 1963, blz. 505 - 584.

Golfmodellen

[8] WAMDI group, The WAM model - A third generation ocean wave prediction model; in: Journal of Physical Oceanography, 1988, Vol. 18, No. 12, blz. 1775 - 181.

Coastal Engineering, 13 (1989) 23–54
Elsevier Science Publishers B.V., Amsterdam — Printed in The Netherlands

A Prediction Model for Stationary, Short-crested Waves in Shallow Water with Ambient Currents

L.H. HOLTHUIJSEN*, N. BOOIJ and T.H.C. HERBERS**

Delft University of Technology, P.O. Box 5048, 2600 GA Delft (The Netherlands)

(Received December 21, 1987; revised and accepted July 22, 1988)

ABSTRACT

Holthuijsen, L.H., Booij, N. and Herbers, T.H.C., 1989. A prediction model for stationary, short-crested waves in shallow water with ambient currents. *Coastal Eng.*, 13: 23–54.

A numerical model for the hindcasting of waves in shallow-water (HISWA) is described and comparisons are made between observations and model results in a realistic field situation. The model is based on a Eulerian presentation of the spectral action balance of the waves rather than on the more conventional (at least in coastal engineering) Lagrangian presentation. Wave propagation is correspondingly computed on a grid rather than along rays. The model accounts for refractive propagation of short-crested waves over arbitrary bottom topography and current fields. The effects of wave growth and dissipation due to wind generation, bottom dissipation and wave breaking (in deep and shallow water) are represented as source terms in the action balance equation. The computational efficiency of the model is enhanced by two simplifications of the basic balance equation. The first one is the removal of time as an independent variable to obtain a stationary model. This is justified by the relatively short travel time of waves in coastal regions. The second simplification is the parameterization of the basic balance equation in terms of a mean frequency and a frequency-integrated action density, both as function of the spectral wave direction. The discrete spectral representation of wave directionality is thus retained. An untuned version of HISWA has been tested in a closed branch of the Rhine estuary where measurements with buoys and a wave gauge are available. In this situation, where wave breaking and short-crestedness dominate, rms-errors in the significant wave height and mean wave period are about 10 and 13% respectively of the observed values.

INTRODUCTION

Coastal engineers are regularly confronted with the task of estimating wave conditions in coastal regions or in inland waters from wave information in deeper water and local wind information. This essentially entails the computation of wave propagation in nearshore regions taking into account the effects

*To whom correspondence should be sent.
**Presently at Scripps Institution of Oceanography, La Jolla, U.S.A.

0378-3839/89/$03.50

of wind, bottom and currents. In this paper we formulate a numerical wave model (called HISWA = HIndcasting Shallow WAter WAves) to carry out such computations for short-crested waves with fairly limited computer capacity and we compare results of this model with observations in the Rhine estuary. The model is of a complexity which places it between models based on monochromatic wave-ray techniques and time-dependent discrete spectral wave models.

Refractive wave propagation in shallow water is sufficiently well described by linear wave theory in many coastal engineering situations. In conventional coastal engineering models this theory is implemented with the wave ray technique, either in a monochromatic approach (e.g. Arthur et al., 1952) or in a discrete spectral approach (e.g. Cavaleri and Malanotte Rizzoli, 1981; Brink-Kjær, 1984; Mathiesen, 1984). These models are of a Lagrangian nature in the sense that the wave development is considered while travelling with the waves along rays. However, this approach is numerically inefficient when nonlinear wave generation and dissipation is to be determined. The reason for this is that to compute such nonlinear phenomena the effects of wave propagation of different spectral components need to be integrated in the spectral domain. This is numerically costly in the wave-ray approach as the relevant information is available only on the wave rays and these are scattered over the area of interest. In an Eulerian approach of wave propagation all wave information is inherently available at the mesh-points of a regular grid. The nonlinear source terms are then readily computed. Such an Eulerian approach is common in models for ocean wave forecasting (e.g. Gelci et al., 1956; Barnett, 1968; Ewing, 1971). In fact some of these models have been extended to include finite depth effects (e.g. Golding, 1983; Janssen et al., 1984; Graber and Madsen, 1985; Young, 1988). Other Eulerian wave models have been designed specifically for shallow water (e.g. Piest, 1965; Battjes, 1968; Karlson, 1969; Chen and Wang, 1983; Sakai et al., 1983; Hirosue and Sakai, 1987).

Ideally one would prefer a fully discrete spectral model accounting for all processes of generation and dissipation and wave-current interactions. However, the very high spatial resolution that is sometimes required in coastal areas would demand excessive computer requirements (e.g. 100×100 gridpoints in an area of 10×10 km for a coastal model as compared to 35×35 gridpoints in an area of 3500×3500 km for an ocean model). Some degree of simplification is therefore needed. One simplification would be to ignore the wave-current interactions. In fact, these interactions are absent in all but one of the above Eulerian models. The exception is the model of Chen and Wang (1983) in which wave-current interactions are accounted for but in which the waves are assumed to be unidirectional at every frequency. We feel that this is unrealistic in many situations, for example when wind waves propagate through strong tidal currents or over very shallow shoals.

We introduce two simplifications to reduce the required computer capacity to manageable proportions. The first one is based on the fact that in coastal situations the travel time of the waves through the area of interest is often short compared to the time scale of the local windfield or the ambient currents. The situation can then be treated as stationary. This simplifies the wave model considerably since it permits the removal of time as an independent variable. The second simplification is to parameterize the balance equation of wave action in the following manner. The action balance equation consists basically of three terms: the local rate of change of the spectral action density (which we removed to make the model stationary); the propagation term (including refraction and shoaling); and the source function which represents the generation and dissipation of wave action due to wind, wave breaking, etc. A full numerical treatment of the source function is not only prohibitively expensive because of the complex nature of nonlinear wave–wave interactions (e.g. Hasselmann and Hasselmann, 1981) but in fact not well possible since the source functions are not well understood in shallow water in the presence of currents. For practical applications some degree of parameterization is therefore needed. Such parameterization can be applied either to the source function alone (notably the nonlinear wave–wave interactions; e.g. Hasselmann et al., 1985) or to the spectral balance equation as a whole (e.g. Günther et al., 1979). The first option, a parameterization of the source function alone is usually sufficient for ocean wave models. However, it is not sufficient for our model as the expected number of gridpoints is potentially one order of magnitude larger than in an ocean wave model. We have therefore chosen for the second option: to parameterize the complete action balance equation. In some presently operating ocean wave models such parameterization is carried out by expressing the wave spectrum and the energy balance equation (action is not used in these models) in terms of a small number of characteristic parameters such as the significant wave height, the mean wave period and a main wave direction (e.g. Günther et al., 1979; Janssen et al., 1984). This implies a considerable reduction of frequency and directional information of the wave field. We feel that for applications in coastal waters such a parameterization is too drastic. In particular the directional details of the wave spectrum should be retained in coastal regions with a complex bathymetry where the occurrence of cross-seas is an essential aspect of the wave field. Therefore, instead of defining integral parameters such as a significant wave height, we define two directional wave functions: the directional action spectrum $A_0(\theta)$ and a mean wave frequency as a function of spectral direction $\omega_0(\theta)$. We accordingly parameterize the propagation terms and the source terms of the spectral action balance equation (the local rate of change has already been removed as indicated). The number of degrees of freedom of the wave model is thus reduced from about 125 per spatial grid point (the number of wave components in a two-dimensional spectrum) to about 25 (the number of directions of A_0 and ω_0) while retaining the

spectral representation of the directionality of the waves. To implement the HISWA model on a computer we have used a finite difference method.

The model has been applied to waves penetrating a closed branch of the Rhine estuary where detailed wave observations are available (Dingemans, 1983; Dingemans et al., 1985) using a priori chosen coefficients from the literature. Experimental computations show that the observed situation is dominated by wave breaking and short-crestedness, suppressing the effects of refraction. Such combination is usually not handled well by other models. We found the rms-error of the model results to be 10.2 and 13.0% respectively of the observed values of the significant wave height (which varied from about 3.0 to about 0.5 m) and of the mean wave period (which varied from about 7.0 to about 2.5 s).

PHYSICAL BACKGROUND

Introduction

Models for hindcasting waves in the absence of currents are usually based on the energy balance equation of the waves in which the wave energy density E, as a function of absolute frequency ω and direction θ, is considered as a slowly varying function in space (x,y) and time t (e.g. Gelci et al., 1956; Hasselmann, 1960; Phillips, 1977). However, in the presence of an ambient current the more relevant wave parameter for modelling purposes is action density A defined as (e.g. Whitham, 1965, 1971):

$$A(\omega,\theta;x,y,t)=E(\omega,\theta;x,y,t)/\sigma \tag{1}$$

with the relative frequency σ defined as:

$$\sigma=\omega-\boldsymbol{k}\cdot\boldsymbol{V} \tag{2}$$

in which $\boldsymbol{k}$ is the wavenumber vector (magnitude k and direction θ) and $\boldsymbol{V}$ is the current velocity vector. The action balance equation, which replaces the more conventional energy balance equation, is then, in the adopted Eulerian approach (dropping the notation for the independent variables from A):

$$\frac{\partial A}{\partial t}+\frac{\partial}{\partial x}(c_x A)+\frac{\partial}{\partial y}(c_y A)+\frac{\partial}{\partial \theta}(c_\theta A)+\frac{\partial}{\partial \omega}(c_\omega A)=T \tag{3}$$

The local rate of change of action density is represented by the first term on the left-hand side of Eq. 3. The other terms on the left-hand side represent the net transport of action in the x-, y-, θ-, and ω-domain respectively. The total effect of generation and dissipation of action (e.g. by wind) is represented by the action source function T. It is also a function of x, y, t, θ and ω.

The propagation speeds c_x and c_y in the balance equation (Eq. 3) are defined

as the x- and y-component respectively of the action propagation speed in (x,y)-space, also called the group velocity $\boldsymbol{c}$. In linear wave theory $\boldsymbol{c}$ is defined as:

$$\boldsymbol{c}=\frac{\partial \sigma}{\partial k}\frac{\boldsymbol{k}}{k}+\boldsymbol{V} \tag{4}$$

It should be noted that in the presence of a current the direction of the group velocity $\boldsymbol{c}$ is in general not equal to the wave direction θ (the direction normal to the wave crest of wave component (θ,ω)).

The propagation speed c_θ, representing refraction (see below), is given by linear wave theory as:

$$c_\theta=-\frac{1}{k}\frac{\partial \sigma}{\partial d}\frac{\partial d}{\partial n}-\frac{\boldsymbol{k}}{k}\cdot\frac{\partial \boldsymbol{V}}{\partial n} \tag{5}$$

in which d is the local water depth and n is the coordinate in (x,y)-space normal to the spectral wave direction θ.

The propagation speed c_ω, which represents the shift of action in the frequency domain induced by time variations in the propagation medium (variations in water depth or current speed and direction) is given by:

$$c_\omega=\boldsymbol{k}\cdot\frac{\partial \boldsymbol{V}}{\partial t}+\frac{\partial \sigma}{\partial d}\frac{\partial d}{\partial t} \tag{6}$$

This representation of wave propagation in the action balance equation (Eq. 3) is unconventional in coastal engineering. The more usual representation is based on wave ray techniques. Fundamentally there is no difference as both approaches represent wave propagation according to the linear theory of surface gravity waves. However, some explanation of the correspondence between the two approaches seems in order. To do this, we consider a situation where the wave field, the bottom topography and the current fields are constant in time. In such a situation the first and fifth term on the left-hand side of the action balance equation (Eq. 3) vanish. This is a situation normally considered when using the wave ray approach. When following the wave energy along a wave ray, the energy is followed across x,y-space with the group velocity with x- and y-component c_x and c_y respectively (the difference between energy and action is not essential for this explanation). This illustrates that the second and third term on the left hand side represent propagation in x,y-space at a given location x,y in a given direction θ. However, in general the direction of the energy propagation is not a constant as wave rays in shallow water are usually not straight lines due to refraction. A curving wave ray implies that the direction of wave propagation changes while travelling along the ray. In other words the energy continually changes direction while travelling through x,y-space. This can be conceived as the energy travelling not only through x,y-space but also (and simultaneously) through θ-space. The travel speed in θ-

space is the rate at which the direction changes as one travels with the group velocity along the (curving) ray. This rate of change is the above speed c_θ. This illustrates that the fourth term on the left hand side represents refraction. The effect of currents is taken into account by including the current speed and direction in the expressions for c_x, c_y and c_θ and by using action density rather than energy density in the formulation (Bretherton and Garrett, 1968).

For the HISWA model we consider precisely such stationary situations as indicated above. The basic equation of our model therefore reduces to:

$$\frac{\partial}{\partial x}(c_x A)+\frac{\partial}{\partial y}(c_y A)+\frac{\partial}{\partial \theta}(c_\theta A)=T \tag{7}$$

with c_x, c_y and c_θ as given above.

However, as indicated in the introduction, this equation is still too complex for a full numerical treatment. We therefore parameterize this equation as a whole with the side-condition that the directional characteristics of the waves should be retained. To this end we have chosen the zero-th and first-order moments of the action spectrum in the frequency domain for the parameterization. The corresponding two wave functions are the one-dimensional directional action spectrum $A_0(\theta)$ and the mean frequency as a function of spectral direction $\omega_0(\theta)$:

$$A_0(\theta)=m_0(\theta) \tag{8}$$

$$\omega_0(\theta)=m_1(\theta)/m_0(\theta) \tag{9}$$

in which the moments m_n of the action density spectrum are defined as:

$$m_n(\theta)=\int_0^\infty \omega^n A(\omega,\theta)\,\mathrm{d}\omega \tag{10}$$

Note that the function $A_0(\theta)$ is a directional spectrum in the sense that it presents the directional distribution of frequency-integrated wave action density. It is not the directional spectrum in the more conventional sense of a two-dimensional wave spectrum, e.g. $A(\omega,\theta)$. The parameterization of the action balance equation is carried out by applying the definition operator used in Eq. 10 with $n=0$ and $n=1$ to the basic balance equation (Eq. 7). This gives two evolution equations: one for $m_0(\theta)$ and one for $m_1(\theta)$. The corresponding equations are (dropping θ from the notation):

$$\frac{\partial}{\partial x}(c^{*}_{0x} m_0)+\frac{\partial}{\partial y}(c^{*}_{0y} m_0)+\frac{\partial}{\partial \theta}(c^{*}_{0\theta} m_0)=T_0 \tag{11}$$

$$\frac{\partial}{\partial x}(c^{**}_{0x} m_1)+\frac{\partial}{\partial y}(c^{**}_{0y} m_1)+\frac{\partial}{\partial \theta}(c^{**}_{0\theta} m_1)=T_1 \tag{12}$$

in which c^{*}_{0x}, c^{*}_{0y} and $c^{*}_{0\theta}$ in Eq. 11 and c^{**}_{0x}, c^{**}_{0y} and $c^{**}_{0\theta}$ in Eq. 12 are the propagation speeds through (x,y,θ)-space of m_0 and m_1 respectively. T_0 and T_1 are the parameterized source functions for m_0 and m_1 respectively. Equations 11 and 12 are implemented in the HISWA model.

The propagation part of these equations (left-hand side) and the generation/dissipation part (right-hand side) are addressed next.

Propagation

In view of other uncertainties in our model (particularly the generation and dissipation of waves in shallow water), the propagation speeds in Eq. 11 and 12 are taken equal to the corresponding speeds at the mean frequency ω_0; c_{0x}, c_{0y} and $c_{0\theta}$. Of these, c_{0x} and c_{0y} are the x- and y-component respectively of the group velocity $\boldsymbol{c}_0$ at frequency ω_0 (see Eq. 4):

$$\boldsymbol{c}_0=\frac{\partial \sigma_0}{\partial k_0}\frac{\boldsymbol{k}_0}{k_0}+\boldsymbol{V} \tag{13}$$

in which $\boldsymbol{k}_0$ is the wavenumber vector corresponding to $\omega_0(\theta)$ (with magnitude k_0 and direction θ) determined from linear wave theory by:

$$\omega_0=\sigma_0+\boldsymbol{k}_0\cdot\boldsymbol{V} \tag{14}$$

and:

$$\sigma_0=\{gk_0\tanh(k_0 d)\}^{1/2} \tag{15}$$

The propagation speed representing refraction at the mean frequency ω_0, $c_{0\theta}$ is, from linear wave theory:

$$c_{0\theta}=-\frac{1}{k_0}\frac{\partial \sigma_0}{\partial d}\frac{\partial d}{\partial n}-\frac{\boldsymbol{k}_0}{k_0}\cdot\frac{\partial \boldsymbol{V}}{\partial n} \tag{16}$$

The source functions T_0 and T_1 are derived below using the above assumptions regarding the propagation speeds.

Generation and dissipation

Formally the source functions T_0 and T_1 can be obtained by parameterizing the action source function T of Eq. 3. However, this function is only partially known and rather complex. Therefore, instead of attempting such a formal parameterization we express T_0 and T_1 in terms of functions which can be estimated more readily, at least to some extent, from information in the literature. To this end we express T_0 and T_1 in terms of the source functions of wave energy (S_E) and the mean frequency of the energy spectrum (S_ω).

If the directional action density $A_0(\theta)$ is approximated by the frequency integrated directional energy density $E_0(\theta)$ $(=\int_0^\infty E(\omega,\theta)d\omega)$ divided by $\sigma_0(\theta)$ then the source function of $m_1(\theta)$, T_1 is the rate at which $E_0\omega_0/\sigma_0$ is generated or dissipated. If we assume that the frequencies ω_0 and σ_0 are approximately equally affected by wave generation and dissipation so that their ratio varies only slowly, then T_1 is related in a simple fashion to S_E, the rate at which $E_0(\theta)$ is generated or dissipated:

$$T_1 \cong \frac{\omega_0}{\sigma_0} S_E \tag{17}$$

S_E will be determined below from information in the literature.

The source function for m_0, T_0 can be readily formulated in terms of S_E and S_ω, the rate of change of the mean frequency $\omega_0(\theta)$. This is achieved by first subtracting Eq. 11 multiplied by ω_0 from Eq. 12. The result of this is:

$$c_{0x}\frac{\partial \omega_0}{\partial x} + c_{0y}\frac{\partial \omega_0}{\partial y} + c_{0\theta}\frac{\partial \omega_0}{\partial \theta} = \frac{1}{A_0}(T_1 - \omega_0 T_0) \tag{18}$$

of which the left-hand side represents the evolution of ω_0 in stationary conditions $(=S_\omega)$. Substituting T_1 from Eq. 17 in Eq. 18, the source function T_0 can be obtained in terms of S_E and S_ω as:

$$T_0 \cong \frac{1}{\sigma_0} S_E - \frac{A_0}{\omega_0} S_\omega \tag{19}$$

The source functions $S_E(\theta)$ and $S_\omega(\theta)$ represent the effects of generation and dissipation. We therefore write them as the sum of their constituent source terms:

$$S_E(\theta) = S_E(\theta)_{\text{wind}} + S_E(\theta)_{\text{bottom}} + S_E(\theta)_{\text{breaking}} + S_E(\theta)_{\text{blocking}} \tag{20}$$

$$S_\omega(\theta) = S_\omega(\theta)_{\text{wind}} + S_\omega(\theta)_{\text{bottom}} + S_\omega(\theta)_{\text{breaking}} + S_\omega(\theta)_{\text{blocking}} \tag{21}$$

The subscripts wind, bottom, breaking and blocking refer to wind generation, bottom friction, wave breaking and current-induced blocking of wave propagation respectively. In the following we formulate these source terms in a fairly pragmatic way. The reasons for this are firstly, that we wish to use rather simple expressions to avoid costly computations and secondly, that detailed information on each of the individual source terms is not available for very shallow water (e.g. the effects of shallow-water wave breaking). In addition the formulations are such that the results of rather basic numerical or physical experiments can be readily incorporated in the model. It should be noted that wind generation is interpreted in the present context to include all processes of wave generation and dissipation in deep water (i.e. wind input, nonlinear

wave–wave interactions and deep-water wave breaking in the absence of currents).

Instead of addressing the source function of the action-averaged frequency $S_\omega(\theta)$ we will address in the following the source function $S_\Omega(\theta)$ of the energy-averaged frequency $\Omega_0(\theta)$:

$$\Omega_0(\theta) = \frac{1}{E_0(\theta)} \int_0^\infty \omega\, E(\omega,\theta)\,\mathrm{d}\omega \tag{22}$$

The reason for this change from $\omega_0(\theta)$ to $\Omega_0(\theta)$ is that information on the energy-averaged frequency $\Omega_0(\theta)$ is more readily available in the literature than on the action-averaged frequency $\omega_0(\theta)$. The ratio of the values of $\omega_0(\theta)$ and $\Omega_0(\theta)$ is usually close to one, in fact, in HISWA we use the value for the mean JONSWAP spectrum ($\omega_0/\Omega_0 = 0.92$; Hasselmann et al., 1973). We correspondingly take $S_\omega = \omega_0/\Omega_0\, S_\Omega$.

To roughly estimate the nature and the magnitude of the source terms we assume in the following a shape of the wave spectrum without implying that the model predicts such a shape. Other assumptions on the spectral shape would probably give roughly the same results. Of course, it would be a simple matter to supplement the output of the model with a standard shape frequency spectrum for each spectral direction (with $E_0(\theta)$ and $\Omega_0(\theta)$ as parameters, e.g. the k^{-3}-spectrum of Eq. 39 or a JONSWAP spectrum (Hasselmann et al., 1973) modified with the Kitaigorodskii scaling, e.g. Bouws et al., 1985).

Generation by wind

The formulation of wave generation by wind is taken from empirical information in an idealized situation. This situation is one in which a stationary, spatially uniform wind with velocity U starts to blow over deep water (no currents, no waves) at time $t=0$. In such a situation, we formulate the evolution in time of the total wave energy E_1 and the overall mean frequency Ω_1 as:

$$E_1 = \int_0^{2\pi} E_0(\theta)\,\mathrm{d}\theta \tag{23}$$

and:

$$\Omega_1 = \frac{1}{E_1} \int_0^{2\pi} \Omega_0(\theta) E_0(\theta)\,\mathrm{d}\theta \tag{24}$$

with the following expressions:

$$\tilde{E}_1 = a\,\tilde{t}^{\,b} \quad \text{for } \tilde{t} < \tilde{t}_m$$
$$\tilde{E}_1 = a\,\tilde{t}_m^{\,b} \quad \text{for } \tilde{t} \geq \tilde{t}_m \qquad (25)$$

and:

$$\tilde{\Omega}_1 = c\,\tilde{t}^{\,d} \quad \text{for } \tilde{t} < \tilde{t}_m$$
$$\tilde{\Omega}_1 = c\,\tilde{t}_m^{\,d} \quad \text{for } \tilde{t} \geq \tilde{t}_m \qquad (26)$$

in which $\tilde{E}_1$, $\tilde{\Omega}_1$ and $\tilde{t}$ are dimensionless representations of E_1, Ω_1 and t based on wind speed U and gravitational acceleration g. Taking the time derivative of Eq. 25 and 26 gives expressions for $S_E(\theta)$ and $S_\Omega(\theta)$ in terms of dimensionless time $\tilde{t}$ provided that we assume the normalized directional energy distribution $D(\theta)$ in this ideal case to be constant in time, so that:

$$E_0(\theta) = E_1\, D_{\text{ideal}}(\theta) \qquad (27)$$

and that $\Omega_0(\theta)$ is constant over θ, so that:

$$\Omega_0(\theta) = \Omega_1 \qquad (28)$$

To determine $S_E(\theta)$ and $S_\Omega(\theta)$ we use a directionally decoupled parametric model the notion of which has been suggested by Seymour (1977). It is based on the assumption that the two-dimensional energy density in direction θ develops independently from the energy densities in other directions (but it does depend on the energy density at other frequencies in the same direction). The validity of these suggestions is supported by Holthuijsen (1983) who observed directional wave spectra with a high directional resolution which in off-shore wind conditions were affected by the shape of the up-wind coast. The observed effects could be reconstructed with a directionally decoupled parameteric model. Observations with similar characteristics were obtained by Donelan et al. (1985). $S_E(\theta)$ and $S_\Omega(\theta)$ are correspondingly taken to be dependent on the equivalent total wave energy $E_1^*(\theta) = E_0(\theta)/D_{\text{ideal}}$ and the equivalent mean wave frequency $\Omega_1^*(\theta) = \Omega_0(\theta)$. During the computations $E_1^*(\theta)$ and $\Omega_1^*(\theta)$ are substituted in Eq. 25 and 26 to obtain equivalent dimensionless durations $\tilde{t}(\theta)$ for $E_1^*(\theta)$ and $\Omega_1^*(\theta)$ respectively which in turn provide the rates of change of $E_1^*(\theta)$ and $\Omega_1^*(\theta)$. The rate of change of $E_1^*(\theta)$ is directionally distributed with D_{ideal} to find $S_E(\theta)$. In HISWA we take $D_{\text{ideal}} = A\cos^n(\theta - \theta_w)$ in which θ_w is the wind direction and n is usually taken 2.0. $S_\Omega(\theta)$ is found by assuming the rate of change of $\Omega_1^*(\theta)$ to be independent of θ. The values of $S_E(\theta)$ and $S_\Omega(\theta)$ are thus determined solely from the values of $E_0(\theta)$ and $\Omega_0(\theta)$ and the wind speed and direction. To obtain results of deep-water wave growth comparable with those of the Shore Protection Manual (CERC, 1973) in another ideal situation (where a constant wind blows perpendicular off a long and straight coast with no currents), we choose the values of the constants in Eq. 25 and 26 as: $a = 1.44\times10^{-8}$; $b = 1.12$; $c = 43.59$; $d = -1/3$; and $\tilde{t}_m = 6.6\times10^4$ (see Fig. 1).

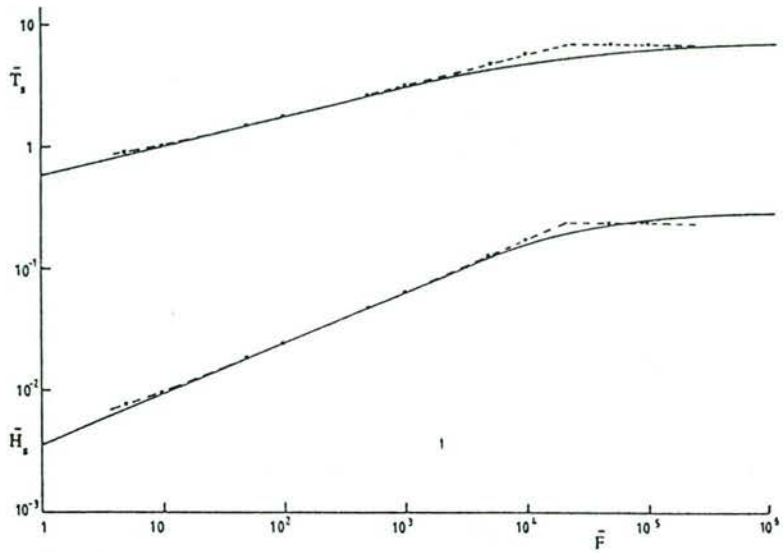

Fig. 1. Growth curves for fetch-limited conditions according to Shore Protection Manual (CERC, 1973, full lines) and HISWA (crosses and dashed lines). Dimensionless significant wave height ($\tilde{H}_s$); wave period ($\tilde{T}_s$; $\tilde{T}_s = 1.2\,\tilde{T}$ assumed); and fetch ($\tilde{F}$) on basis of wind speed (U) and gravitational acceleration (g).

For the evolution of $\Omega_0(\theta)$ in non-ideal situations, we assume that the wind generation forces the value of $\Omega_0(\theta)$ towards the following directional equivalent of the universal relationship $\tilde{\Omega}_1 = e\,\tilde{E}_1^{\,f}$ (e.g. Hasselmann et al., 1976):

$$\tilde{\Omega}_0(\theta) = e\{\tilde{E}_0(\theta)/D_{\text{ideal}}(\theta)\}^f \qquad (29)$$

in which $\tilde{E}_1$, $\tilde{E}_0(\theta)$, $\tilde{\Omega}_1$ and $\tilde{\Omega}_0$ are dimensionless representations of E_1, $E_0(\theta)$, Ω_1 and $\Omega_0(\theta)$ based on wind speed U and gravitational acceleration g. It follows from Eq. 25 and 26 that $e = ca^{-d/b}$ and $f = d/b$. To achieve this behaviour of the model we have chosen the following relaxation formulation:

$$S_\Omega(\theta)_{\text{wind}} = S_{\Omega,\text{ideal}}(\theta)_{\text{wind}}\left(\frac{\tilde{\Omega}_0(\theta)}{e\{\tilde{E}_0(\theta)/D_{\text{ideal}}(\theta)\}^f}\right)^m \qquad (30)$$

thus forcing the value of $\Omega_0(\theta)$ towards the value imposed by Eq. 29. The value of m, governing the rate of relaxation, has been chosen such ($m = 5$) that the model results are similar to those obtained by Günther (1981) (see Fig. 2). This illustration shows the evolution of $\tilde{E}_1$ and $\tilde{\Omega}_1$ in a homogeneous, stationary wind field for various initial values of $\tilde{E}_1$ and $\tilde{\Omega}_1$.

The effect of currents on wave generation is accounted for in the model by taking the wind speed and direction relative to the current.

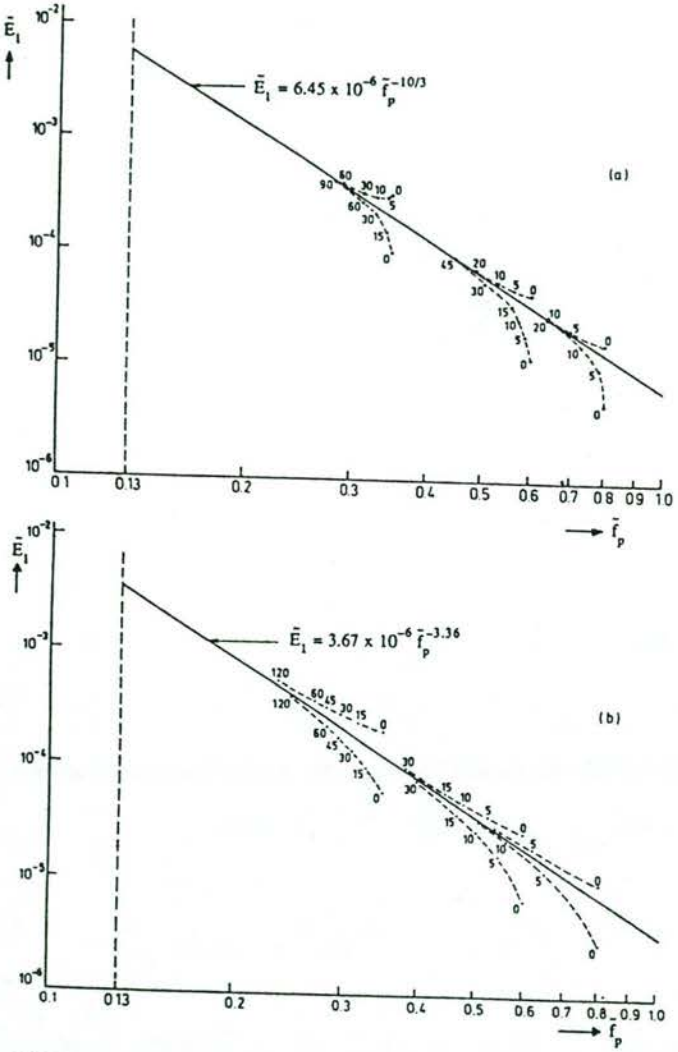

Fig. 2. Relaxation of the dimensionless wave energy ($\tilde{E}_1$) and the dimensionless peak frequency ($\tilde{f}_p$; $\Omega_1 = 0.75\, 2\pi f_p$ assumed) to the universal relationship (full lines); according to Günther (1981, panel a) and HISWA (panel b); time in min.

Bottom dissipation

Bottom dissipation in our model is based on the conventional quadratic friction law to represent bottom shear stress. The corresponding energy dissipation for a harmonic wave with frequency ω and energy $E_1 = \frac{1}{8}H^2$ is (e.g. Putnam and Johnson, 1949):

$$\left(\frac{dE_1}{dt}\right)_{bottom} = \frac{-1}{6\pi}\frac{c_{fw}}{g}\left(\frac{\omega H}{\sinh(kd)}\right)^3 \tag{31}$$

in which c_{fw} is a friction coefficient and H is the wave height. Note that energy is interpreted here and anywhere else in this paper as variance. This expression has been extended by Dingemans (1983) to unidirectional random waves with Rayleigh distributed wave heights, (one single frequency ω):

$$\left(\frac{dE_1}{dt}\right)_{bottom} = \frac{-1}{8\pi^{1/2}}\frac{c_{fw}}{g}\frac{\omega^3}{\sinh^3(kd)}H_{rms}^3 \tag{32}$$

in which H_{rms} is the rms-value of the wave height ($H_{rms} = 2(2E_1)^{1/2}$ if the waves are Rayleigh distributed). Ignoring the negative sign for the moment, this expression may be written as the product of a measure $<\tau>$ of the shear-stress proportional to the orbital velocity squared and a measure $<v>$ of the orbital velocity at the bottom:

$$<\tau> = (8/\pi)^{1/2}\frac{c_{fw}}{g}\frac{\omega^2}{\sinh^2(kd)}E_1 \tag{33}$$

$$<v> = \frac{\omega}{\sinh(kd)}E_1^{1/2} \tag{34}$$

To obtain a simple directional version of this formulation we assume, analogous to the above, that the shear stress is directionally distributed in proportion to the square of the orbital velocity in each direction:

$$<\tau(\theta)> = (8/\pi)^{1/2}\frac{c_{fw}}{g}\frac{\Omega_0^2(\theta)}{\sinh^2\{k_0(\theta)d\}}E_0(\theta) \tag{35}$$

In view of the nonlinear character of the bottom dissipation we assume that the dissipation in each direction is coupled to the other directions through the magnitude of the orbital velocity at the bottom (estimated analogous to Collins, 1972):

$$<v_1> = \left[\int_0^{2\pi}\frac{\Omega_0^2(\theta)E_0(\theta)}{\sinh^2\{k_0(\theta)d\}}d\theta\right]^{1/2} \tag{36}$$

We consequently write the directional distribution of the bottom dissipation as:

$$S_E(\theta)_{bottom} = -<\tau(\theta)><v_1> \tag{37}$$

The effect of a mean current on the bottom dissipation is taken into account

by adding the current component in the θ-direction, V_θ to the characteristic orbital velocity $<v_1>$, with its own friction coefficient c_{fc}, and by replacing the absolute frequency $\Omega_0(\theta)$ by the relative frequency $\sigma_0(\theta)$ in the source term $S_E(\theta)_{\text{bottom}}$ (Eq. 35, 36 and 37):

$$S_E(\theta)_{\text{bottom}} = -(8/\pi)^{1/2} \frac{(c_{fw} <v_1> + c_{fc} V_\theta)}{g} \frac{\sigma_0^2(\theta)}{\sinh^2\{k_0(\theta)d\}} E_0(\theta) \tag{38}$$

in which $V_\theta = V_x \cos\theta + V_y \sin\theta$.

To formulate the effect of bottom dissipation on the mean frequency $\Omega_0(\theta)$ we assume that this dissipation is concentrated at the low frequency side of the wave spectrum because the longest waves are more affected by the bottom than the shorter waves. In addition, the spectrum is assumed to have a universal high-frequency tail if expressed in terms of wavenumber k, in both deep and shallow water (e.g. Kitaigorodskii et al., 1975; Thornton, 1977). Our directional version of this universal spectrum is:

$$\begin{aligned} E(k,\theta) &= \alpha(\theta) k^{-n} \quad \text{for } k \geq k_p \\ E(k,\theta) &= 0 \quad \text{for } k < k_p \end{aligned} \tag{39}$$

in which k_p is the peak wave number and $n=3$ (Kitaigorodskii et al., 1975; Thornton, 1977). The rate of change of the mean frequency $\Omega_0(\theta)$ as induced by this low-frequency bottom dissipation is estimated by first considering the corresponding rate of change of the mean wavenumber $K_0(\theta)$ defined as:

$$K_0(\theta) = \frac{1}{E_0(\theta)} \int_0^\infty k\, E(k,\theta)\, dk \tag{40}$$

It is readily shown that for the assumed spectrum of Eq. 39 with $\alpha(\theta)$ constant in time, the rate of change of $K_0(\theta)$ is directly related to $S_E(\theta)_{\text{bottom}}$ as:

$$\frac{d}{dt}(K_0(\theta)) = \frac{1}{(1-n)} \frac{K_0(\theta)}{E_0(\theta)} S_E(\theta)_{\text{bottom}} \tag{41}$$

If we replace ω_0 and k_0 by $\Omega_0(\theta)$ and $K_0(\theta)$ in Eq. 14 and 15, assuming that these equations hold for $\Omega_0(\theta)$ and $K_0(\theta)$, the rate of change of $\Omega_0(\theta)$ is readily determined from Eq. 41:

$$S_\Omega(\theta)_{\text{bottom}} = \frac{1}{(1-n)} \frac{c_0(\theta) K_0(\theta)}{E_0(\theta)} S_E(\theta)_{\text{bottom}} \tag{42}$$

The effect of a current on the mean frequency is implicit in the formulation of $S_\Omega(\theta)_{\text{bottom}}$ through $S_E(\theta)_{\text{bottom}}$ in Eq. 42, and in the propagation speed $c_0(\theta)$ and the determination of $K_0(\theta)$ from $\Omega_0(\theta)$ with Eq. 14 and 15.

Wave breaking

To account for wave breaking due to a large wave steepness or due to direct bottom effects (e.g. over shoals or on a beach), to the extent that it has not been accounted for implicitly in $S_E(\theta)_{\text{wind}}$ and $S_\Omega(\theta)_{\text{wind}}$, we use the expression of Battjes and Janssen (1979) in our notation:

$$\left(\frac{dE_1}{dt}\right)_{\text{breaking}} = -\alpha_1 Q_b \Omega_1 H_m^2/(8\pi) \tag{43}$$

in which H_m is a maximum wave height, Q_b is the fraction of breaking waves (estimated from the Rayleigh distribution for wave heights and the value of H_m (Battjes and Janssen, 1979) and α_1 is a numerical constant. The value of H_m is taken by Battjes and Janssen (1979) from the criteria of Miche (1944) (wave steepness in deep water and water depth in shallow water):

$$H_m = \gamma_1 k_1^{-1} \tanh(\gamma_2 k_1 d/\gamma_1) \tag{44}$$

with k_1 obtained from Ω_1 with the linear wave theory. We choose the directional distribution of this dissipation such that it does not influence the shape of the directional energy distribution:

$$S_E(\theta)_{\text{breaking}} = -\alpha_1 Q_b \Omega_0(\theta) H_m^2 E_0(\theta)/(8\pi E_1) \tag{45}$$

We have considered to use the values of α_1, γ_1 and γ_2 as used by Battjes and Janssen (1979) (viz. 1.0, 0.88 and 0.8 respectively) but since in our model some deep water breaking is already implicitly accounted for in the wind generation terms, we wished to trigger the above dissipation term at higher values for wave steepness (controlled by γ_1). After some trial and error we choose $\gamma_1 = 1.0$ (wave steepness $H_m/L_1 = 0.16$; where L_1 is $2\pi/k_1$) as a fairly low value (i.e. close to 0.88 or $H_m/L_1 = 0.14$) for which the dissipation modelled by Eq. 45 does not affect deep water wave growth significantly. The values of α_1 and γ_2 in the HISWA model are those used by Battjes and Janssen (1979).

The effect of the above wave breaking mechanism on the mean frequency in shallow water is chosen to be similar to the effect of bottom dissipation (low-frequency dissipation) since in the above model of Battjes and Janssen (1979) only the highest waves (with lowest frequencies) break. We assume that in deep water the mean frequency is not influenced by wave breaking. This behaviour of the model is achieved by using an expression for $S_\Omega(\theta)_{\text{breaking}}$ similar to that of $S_\Omega(\theta)_{\text{bottom}}$ multiplied with a depth dependent reduction factor R the value of which is 0 in deep water and 1 in shallow water:

$$S_\Omega(\theta)_{\text{breaking}} = \frac{R}{1-n} \frac{c_0(\theta) K_0(\theta)}{E_0(\theta)} S_E(\theta)_{\text{breaking}} \tag{46}$$

in which R is:

$$R=1-\{\tanh(\gamma_2 k_1 d)\}^2 \qquad (47)$$

The effect of currents on wave breaking is included in the above source terms to the extent that the propagation speed $c_0(\theta)$ is influenced by the current and to the extent that $K_0(\theta)$ is determined with Eq. 14 and 15.

Wave blocking

In a situation with a strong opposing current some fraction of the wave energy cannot be transported upstream because the group velocity of the highest frequencies in the spectrum is less than the opposing current velocity. This fraction of the wave energy may be dissipated or reflected by the counter current. The lowest frequency above which this phenomenon of wave blocking occurs (the critical frequency ω_c) is the maximum frequency for which a solution exists for the wavenumber k in the dispersion relationship:

$$\omega_c - \boldsymbol{k}\cdot\boldsymbol{U} - [gk\tanh(kd)]^{1/2}=0 \qquad (48)$$

The corresponding wavenumber is the critical wavenumber k_c. To estimate the rates of change of $E_0(\theta)$ and $\Omega_0(\theta)$ induced by wave blocking we again assume that the shape of the wavenumber spectrum is a k^{-n}-tail, (see Eq. 39), except that in this wave blocking situation no wave energy is present above the critical wavenumber:

$$\begin{aligned} &E(k,\theta)=\alpha(\theta)k^{-n} && \text{for } k_p<k<k_c \\ &E(k,\theta)=0 && \text{for } k<k_p \text{ or } k>k_c \end{aligned} \qquad (49)$$

The rate of energy dissipation for this spectrum (with $\alpha(\theta)$ constant in time) is directly related to the current induced rate of change of the critical wavenumber. It follows directly from the time derivative of $E_0(\theta)$ corresponding to Eq. 49 that:

$$S_E(\theta)_{\text{blocking}}=\frac{k_c^{-n}\,(1-n)}{(k_c^{1-n}-k_p^{1-n})}\,E_0(\theta)\,\frac{\mathrm{d}k_c(\theta)}{\mathrm{d}t} \qquad (50)$$

where $\mathrm{d}k_c(\theta)/\mathrm{d}t$ is the current induced rate of change of k_c determined in the model with Eq. 48. The corresponding rate of change of the mean wavenumber $K_0(\theta)$ follows directly from the rate of change of $k_c(\theta)$:

$$\frac{\mathrm{d}}{\mathrm{d}t}\,(K_0(\theta))=\{k_c(\theta)-K_0(\theta)\}S_E(\theta)_{\text{blocking}}/E_0(\theta) \qquad (51)$$

Replacing ω_0 and k_0 by $\Omega_0(\theta)$ and $K_0(\theta)$ in Eq. 14 and 15, and assuming that the equations hold for $\Omega_0(\theta)$ and $K_0(\theta)$, the rate of change of $\Omega_0(\theta)$ is readily determined from Eq. 51:

$$S_\Omega(\theta)_{\text{blocking}}=c_0(\theta)\,\{k_c(\theta)-K_0(\theta)\}\,S_E(\theta)_{\text{blocking}}/E_0(\theta) \qquad (52)$$

The primary effect of the above formulation of blocking is to decrease the mean frequency of the waves $\Omega_0(\theta)$ to a value that is sufficiently low to permit the waves to propagate against the current. The secondary effect is to change the main wave direction of the waves ($\bar{\theta}$, see paragraph on input/output) away from opposing the direction of the current because the more the propagation direction opposes the current direction, the stronger the blocking effect will be. The mean current therefore affects the shape of the directional energy distribution.

Note

It should be noted that the effects of currents on the evolution of the waves in the propagation area are not limited to the above indicated effects on the source terms. The currents also influence the propagation, and therefore the residence time of the waves in the area of interest. The integrated effects of wind generation, bottom dissipation and wave breaking are thus indirectly influenced. Currents also cause a type of shoaling effect which may either increase or decrease the wave energy (which in turn may affect wave breaking).

NUMERICAL BACKGROUND

Numerical method

The evolution equations for $A_0(\theta)$ and for the product $\omega_0(\theta)A_0(\theta)$, Eq. 11 and 12, are partial differential equations of first order with the horizontal coordinates x and y and the spectral direction θ as independent variables. Due to the nature of the equation the state in a point in (x,y,θ)-space (e.g. the value of A_0) is determined by the state upwave from this point (upwave as defined by the propagation speeds c_{0x}, c_{0y} and the directional rate of change $c_{0\theta}$). We have therefore chosen to carry out the computation in a direction roughly parallel to the main wave propagation direction (x-direction in Fig. 3). A consequence of this is that only waves can be represented in the model which make an angle of less than 90° with the computational direction. The computation is carried out using a leap-frog finite difference scheme for propagation in (x,y)-space with user-controlled numerical diffusion added and an upstream finite difference scheme for propagation in θ-space (i.e. refraction). The leap-frog scheme is a diffusion-free second-order scheme, the upstream scheme is a first-order scheme with inherent numerical diffusion (of order $\Delta\theta$). Both schemes are subject to stability conditions, as a consequence of which the angle between wave propagation and computational direction is further restricted. It depends on the mesh sizes; typically the angle is less than 60°. The total directional sector is therefore less than 120°. This seems to be acceptable for most applications of our model since either the waves propagate from deep water to the

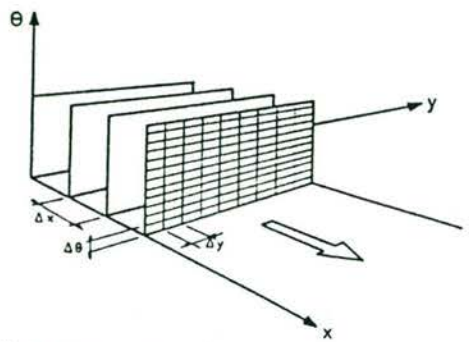

Fig. 3. Diagram of the method of stepwise computation in mean wave direction.

coast with directional changes usually less than 90° or the waves are generated by a local wind within a sector of 90° on both sides of the wind direction. However, this directional restriction implies some limitations on the use of the model. For instance, the propagation of two wave fields crossing each other at large angles is not properly modelled (e.g. locally generated wind sea orthogonal to swell). In such cases one may find an approximate solution by combining the model results obtained separately for each wave field.

Boundary conditions

The boundary conditions for the above partial differential equations are in general the specification of the wave field entering the computation area and the absorption of waves at the boundaries where the waves leave the computation area.

Since we have restricted wave directions to a sector of less than 180° and since wave information along the lateral boundaries in (x,y)-space is usually not available we assume that wave information is given only along the upwave boundary of the model in (x,y)-space (which may or may not be on land). At the other boundaries in (x,y,θ)-space we assume that no waves enter the model. One consequence of these assumptions is that energy which is refracted to outside the directional sector is removed from the model (transported across the boundaries in θ-domain where it is fully absorbed). Another consequence of the above assumptions is that the wave field near the lateral boundaries in (x,y)-space is not well represented in the model since no wave energy enters the area across these boundaries. These boundaries must therefore be chosen far enough from the area of interest. In a nested mode the model accepts wave information along the lateral boundaries in (x,y)-space that is provided by previous computations with the model.

Digitization

Two grids are used in the model: a two-dimensional grid in (x,y)-space to represent the bathymetry and the current field and a three-dimensional grid in (x,y,θ)-space to compute the wave field. Each may have different resolution and orientation in (x,y)-space as long as the wave field grid is covered by the bottom/current grid (wind is constant and therefore needs no grid). The mesh sizes Δx and Δy of the bottom/current grid should be small enough to resolve relevant spatial details in the bathymetry and in the current field. For the three-dimensional wave field grid the spatial resolutions Δx, Δy and $\Delta\theta$ should be sufficient to resolve the relevant spatial variations of the wave field, the horizontal scales of which are roughly equal to those of the bathymetry or of the current field. The value of $\Delta\theta$ depends very much on the width and the smoothness of the functions $A_0(\theta)$ and $\omega_0(\theta)$. For swell, with a narrow directional width of $A_0(\theta)$ (10° on either side of the mean wave direction, say), a relatively high resolution is required (e.g. $\Delta\theta=2°$ or 3°) whereas for a typical wind sea, with a directional width of $(A_0(\theta)$ of about 30° on either side of the wind direction, a directional resolution of about 10° seems to be sufficient. To resolve spatial details, the model can be used in a nested mode.

The values of Δx, Δy and $\Delta\theta$ are normally based on the above physical criteria but the value of Δx should additionally be based on a numerical stability criterion. For our model this criterion can be shown to be (by a Von Neumann stability analysis; e.g. Abbott, 1979):

$$\left|\frac{c_{0y}\Delta x}{c_{0x}\Delta y}\right|+\left|\frac{c_{0\theta}\Delta x}{c_{0x}\Delta\theta}\right|\leq 1 \tag{55}$$

In choosing the values of Δx, Δy and $\Delta\theta$ for a particular application of the HISWA model, we take the value of each of the terms on the left-hand side of Eq. 55 equal to or less than 1/2. From this and the value of $\Delta\theta$, the values of Δx and Δy can be determined as shown below. The smallest of these values and the ones following from the above resolution considerations are to be used.

To estimate the grid size Δx, the ratio of the propagation velocities $c_{0\theta}$ and c_{0x} must be considered. It can be shown that in the absence of currents this ratio is maximal for long waves (phase velocity approximately equal to $(gd)^{1/2}$). Hence the second term on the left-hand side of Eq.55 is always less than or equal to 1/2 if (see Eq. 5):

$$\frac{\Delta x}{\Delta\theta}\leq\cos(\theta)\left[\frac{1}{d}\frac{\partial d}{\partial n}\right]^{-1} \tag{56}$$

Since in the HISWA model the maximum value of $|\theta|$ is typically 60° it follows from Eq. 56 that Δx and $\Delta\theta$ must be chosen such that (replacing the bottom slope normal to θ, $\partial d/\partial n$ by the bottom slope itself, $|\nabla d|$):

$$\frac{\Delta x}{\Delta\theta} \leq \frac{1}{2}\frac{d}{|\nabla d|} \tag{57}$$

To subsequently estimate the grid size Δy consider again a situation without currents. The direction θ is then equal to the direction of propagation so that:

$$\frac{c_{0y}}{c_{0x}} = \tan(\theta) \tag{58}$$

Using this expression one obtains a value of the first term on the left-hand side of Eq. 55 which is less than or equal to 1/2 if the ratio of Δx and Δy is chosen such that:

$$\frac{\Delta y}{\Delta x} \geq 2\tan(\theta) \tag{59}$$

This implies that the maximum value of θ must be less than 90° so that the directional sector of wave propagation in the HISWA model is always less than 180° wide. In fact, the maximum value of θ is usually chosen to be 60° with $\Delta y/\Delta x$ equal to about 3.5.

For very shallow water criterion Eq. 57 often implies a fairly small value of Δx. Such a small value can be avoided if the numerical scheme is unconditionally stable. Work is therefore in progress to replace the upstream scheme for refraction with a fully implicit scheme. The present practice is to use a rather larger value of Δx (determined from the above spatial resolution requirements) and to restrict the refraction speed $c_{0\theta}$ when (occasionally) condition 55 is not met during the computations. Experience has shown that it does not occur very frequently and that it does not greatly affect the model results.

Integration scheme

The integration scheme in the model can be divided into two parts: the propagation of the waves on one hand and the generation and dissipation of the waves on the other. Both parts are briefly described below.

The computational grid (the wave-field grid) is a rectangular grid in (x,y,θ)-space (see Fig. 3) with its x-axis roughly parallel with the mean wave direction in the x,y-plane. The computations start at the upwave boundary at the plane $x=0$ in (x,y,θ)-space where the values of A_0 and ω_0 (and consequently also of c_{0x}, c_{0y} and $c_{0\theta}$) are given for all locations along this boundary and for all spectral directions. The computations proceed step-wise in the x-direction. The values of A_0 and ω_0 for each (y,θ)-value in the plane $x=\Delta x$ in (x,y,θ)-space are computed from the wave information in the first plane ($x=0$). This process of propagation is repeated for each next step, that is, the values of A_0 and ω_0 in the next plane, $x=(j+1)\Delta x$ are determined solely from the wave information on the previous plane $x=j\Delta x$ (see Fig. 3).

The propagation in the model is carried out with the finite difference schemes mentioned in the section on Numerical method which have a first order accuracy in Δx, Δy and $\Delta\theta$ if the option of added numerical diffusion is used.

The modelling of the growth and dissipation from the previous plane $x=j\Delta x$ to the next plane $x=(j+1)\Delta x$ is partially explicit and partially implicit. The fairly smoothly behaving wind generation source terms are evaluated analytically in the model from only the previous wave information (at plane $x=j\Delta x$) to develop the waves from plane $x=j\Delta x$ to plane $x=(j+1)\Delta x$. The other source terms are sometimes highly nonlinear, depending on the geophysical situation. To avoid unstable behaviour of these terms we have chosen an implicit representation of these terms, i.e. the evaluation of these terms in the model includes the (as yet unknown) wave information at the plane $x=(j+1)\Delta x$. This implicit formulation can be combined with the explicit propagation in a simple manner, since it involves only one unknown value, i.e. $A_0(\theta)$.

Input/output

As indicated in the section on Boundary conditions, the model requires wave input at the up-wave boundary (either a discrete spectral representation of $E_0(\theta)$ and $\Omega_0(\theta)$ or a parametric representation, i.e. $E_0(\theta)=E_1 D_{\text{ideal}}(\theta)$. Additional input is limited to only the bottom topography and current field (on a regular grid), the wind speed and direction, grid definitions and output requests. Output of the primary results, $E_0(\theta)$ and $\omega_0(\theta)$ is available on grid points, or lines and locations which are all independent of the computational grid. Integral parameters such as the significant wave height:

$$H_s = 4\,E_1^{1/2} \tag{60}$$

the mean wave period:

$$\bar{T} = 2\pi\,\Omega_1^{-1} \tag{61}$$

and the mean wave direction $\bar{\theta}$ and directional spreading σ_θ (following definitions used for the analysis of pitch-and-roll buoy wave data (e.g. Kuik et al., 1988):

$$\bar{\theta} = \arctan(b/a) \tag{62}$$

$$\sigma_\theta = [2\{1-(a^2+b^2)^{1/2}\}]^{1/2} \tag{63}$$

in which $a=\int_0^{2\pi}\cos(\theta)\,D(\theta)\mathrm{d}\theta$ and $b=\int_0^{2\pi}\sin(\theta)\,D(\theta)\mathrm{d}\theta$ and other secondary output such as the radiation stress gradient for short-crested waves (Battjes, 1972) are also available at the same output grid points, lines or locations.

To assess the behaviour of the model as regards wave propagation, generation and dissipation the model has been successfully applied to rather basic idealized situations for which the results can be compared with analytical solutions or information in the literature (Booij et al., 1988). This is illustrated here for propagation towards a plane beach and in an opposing current. To compare the results with analytical solutions from linear wave theory the waves are taken as fairly long-crested ($\cos^{64}(\theta)$-directional energy distribution) and all source terms have been set at zero (this implies that the mean frequency $\omega_0(\theta)$ remains constant). The waves approach a plane beach (slope 1:120) at an incidence angle in deep water of 30°. In the case of the opposing current (deep water) the waves approach a shear-current (current speed increasing cross-stream from 0 to 2 m s^{-1} over a distance of 1000 m) at an angle of incidence of 60° (30° off the normal to the current direction). The analytical solutions are based on conservation of action and wave number component in the direction normal to the beach or to the current. The results are given in Fig. 4 where it is obvious that the agreement between analytical solutions and numerical results is excellent. Wave growth in a standard situation is addressed in the section on Generation by wind (see Fig. 1).

Tests in laboratory conditions have been described by Booij et al. (1985) and Dingemans et al. (1987). Dingemans et al. (1987) have analyzed their tests quantitatively and in great detail. It concerned a situation with short-crested, random waves propagating around and across a submerged breakwater located in an otherwise flat area. The waves produced a relatively strong current caused by gradients in the wave-induced radiation stresses. These currents were measured and subsequently used as input to the HISWA model so that the test included wave–current interactions which were quite significant. An earlier version of the HISWA model was used which was slightly different from the model described here as regards some numerical and physical aspects. The observed rms-errors are typically about 5% in the significant wave height (H_s), 10–25% in mean period ($\bar{T}$) and about 5° in mean wave direction (% of observed values except directions). Considering the performance of conventional wave models in such situations these results are deemed to be satisfying. A more crucial test is of course the performance of the model in field conditions. The first test of the model under these conditions (no tuning of the model) is presented next.

To test the model in geophysical conditions which are more realistic and complicated than in the academic tests and laboratory tests indicated above, the model has been applied to an area of the Rhine estuary (the Haringvliet, see Fig. 5). This area was chosen because the model results can be compared with the results of a well documented field campaign of the Ministry of Transport and Public Works in the Netherlands (Dingemans, 1983, 1985; Dinge-

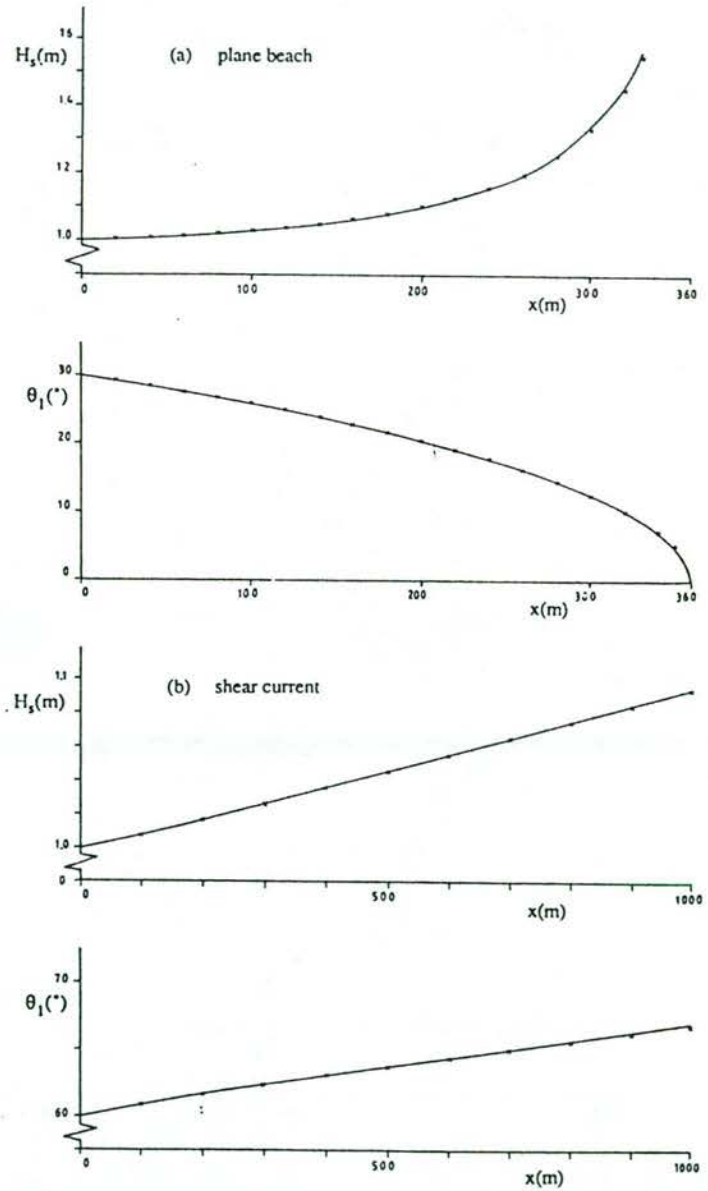

Fig. 4. Analytical solutions from linear wave theory (full lines) and numerical results from HISWA (crosses). Panel (a) for wave propagation towards a plane beach (angle of incidence 30°). Panel (b) for propagation through a shear current (angle of incidence 60°, current speed increasing linearly from 0 to 2 m/s over 1000 m). The waves are fairly long-crested ($\cos^{64}(\theta)$-directional energy distribution) and their (mean) wave period is 5 s.

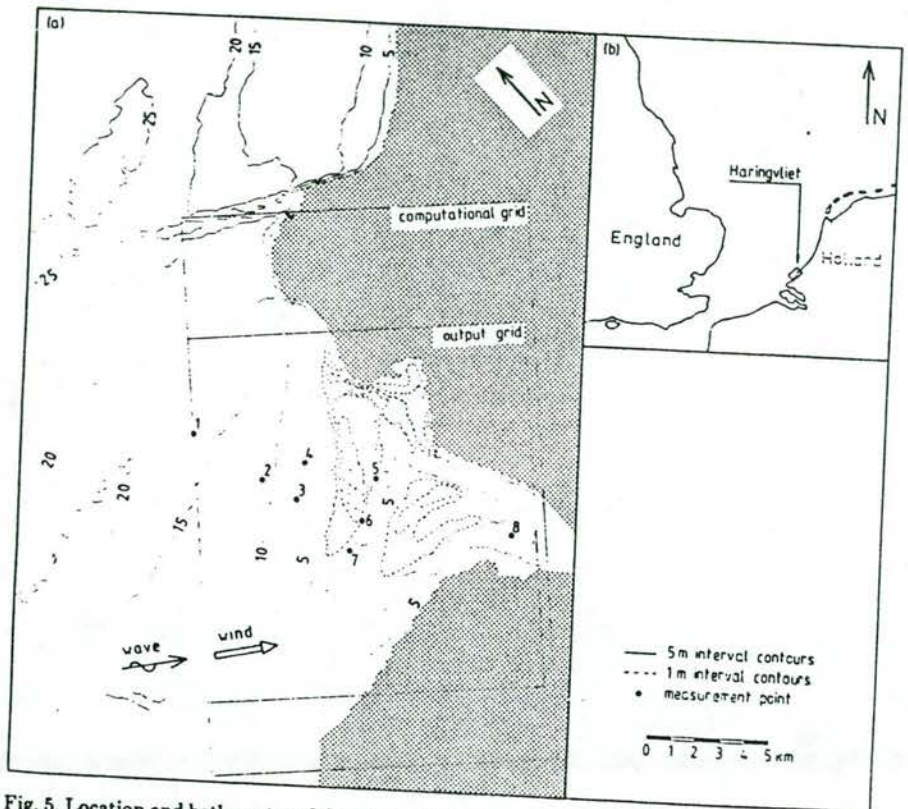

Fig. 5. Location and bathymetry of the Haringvliet estuary and locations of the WAVEC buoy (1), the waverider buoys (2-7) and the wave gauge (8).

mans et al., 1985). This campaign involved the use of one WAVEC pitch-and-roll buoy, one wave gauge and six waverider buoys. The situation can be characterized as non-locally generated waves passing from deeper water into shallow water over a shoal with a regeneration by wind behind the shoal. Currents are practically non-existent in the chosen situation because this particular branch of the Rhine estuary is closed by gates. The location and bathymetry of the study area are indicated in Fig. 5 with the locations of the buoys and the wave gauge. The bathymetry can be roughly characterized as a relatively shallow river mouth, no currents, water depth typically 4–5 m, about 10×10 km in surface area. It is partly protected from the southern North Sea by a shoal of roughly 2×4 km (water depth typically 1–2 m) extending over half the mouth opening.

The computations have been carried out for a situation which occurred on October 14, 1982 at 22.00 h (M.E.T.). The waves are locally generated in the

southern North Sea with a significant wave height of about 3 m and a mean period of about 7 s at the estuary entrance (location 1, Fig. 5). These waves penetrate the area from a northwesterly direction. They break over the shoal with a reduction in wave height from about 2.5 to about 0.5 m over the shoal. The local wind of 16.5 m s^{-1} from a northwesterly direction regenerates the waves to about 0.9 m significant wave height at the wave gauge which is located 5 km behind the shoal (location 8, Fig. 5). Quantitative information is provided in Table 1 (after Dingemans, 1983, 1985). The WAVEC pitch-and-roll buoy in 16 m water depth (location 1, Fig. 5) provides the significant wave height, the peak wave period (the inverse of the peak frequency of the energy spectrum), the mean wave direction and the directional width as input at the up-wave boundary of the model (for parameter values see Table 1). We assume a $\cos^2(\theta)$-directional frequency-integrated energy distribution, commensurate with the directional spreading of $\sigma_\theta = 31°$ as observed by the WAVEC buoy. The waverider buoys and the wave gauge are located at various positions in the area (locations 2–7, Fig. 5) each providing a significant wave height and a mean wave period which can be compared to the results of the model.

The pattern of the model results, shown in Figs. 6 (panel a) and 7 and indicated as "standard" in Table 1, is consistent with the pattern of the observations, e.g. the significant wave height which at the up-wave boundary of the model (16 m water depth) is about 3.4 m, reduces gradually to about 2.5 m at 6 m depth and then very rapidly to about 0.6 m over the shoal. South of the shoal the gradual shoreward decrease in wave height continues. At the location of the wave gauge (about 5 km behind the shoal; location 8 in Fig. 5) the sig-

TABLE 1

Observations and model results at various locations in the Haringvliet of the significant wave height H_s and the mean wave period $\bar{T}$

location	instrument	measurement		HISWA					
				standard		no refraction		no wind	
		H_s (m)	$\bar{T}$ (s)	H_s (m)	$\bar{T}$ (s)	H_s (m)	$\bar{T}$ (s)	H_s (m)	$\bar{T}$ (s)
1	wavec	3.38	7.0*	—	—	—	—	—	—
2	waverider	2.90	6.3	3.27	6.8	3.31	6.8	3.25	6.8
3	waverider	2.58	6.3	2.62	5.9	2.61	5.8	2.62	5.9
4	waverider	2.68	5.9	2.56	5.8	2.54	5.7	2.56	5.8
5	waverider	0.62	2.6	0.68	2.8	0.65	2.9	0.60	2.8
6	waverider	1.05	3.7	1.01	3.4	1.03	3.4	0.76	3.2
7	waverider	1.60	5.1	1.37	3.8	1.36	3.8	1.35	3.7
8	wave gauge	0.95	2.8	0.83	3.4	0.94	3.5	0.64	3.2

*taken as 0.85 T_p where T_p is the observed peak period of 8.3 s.

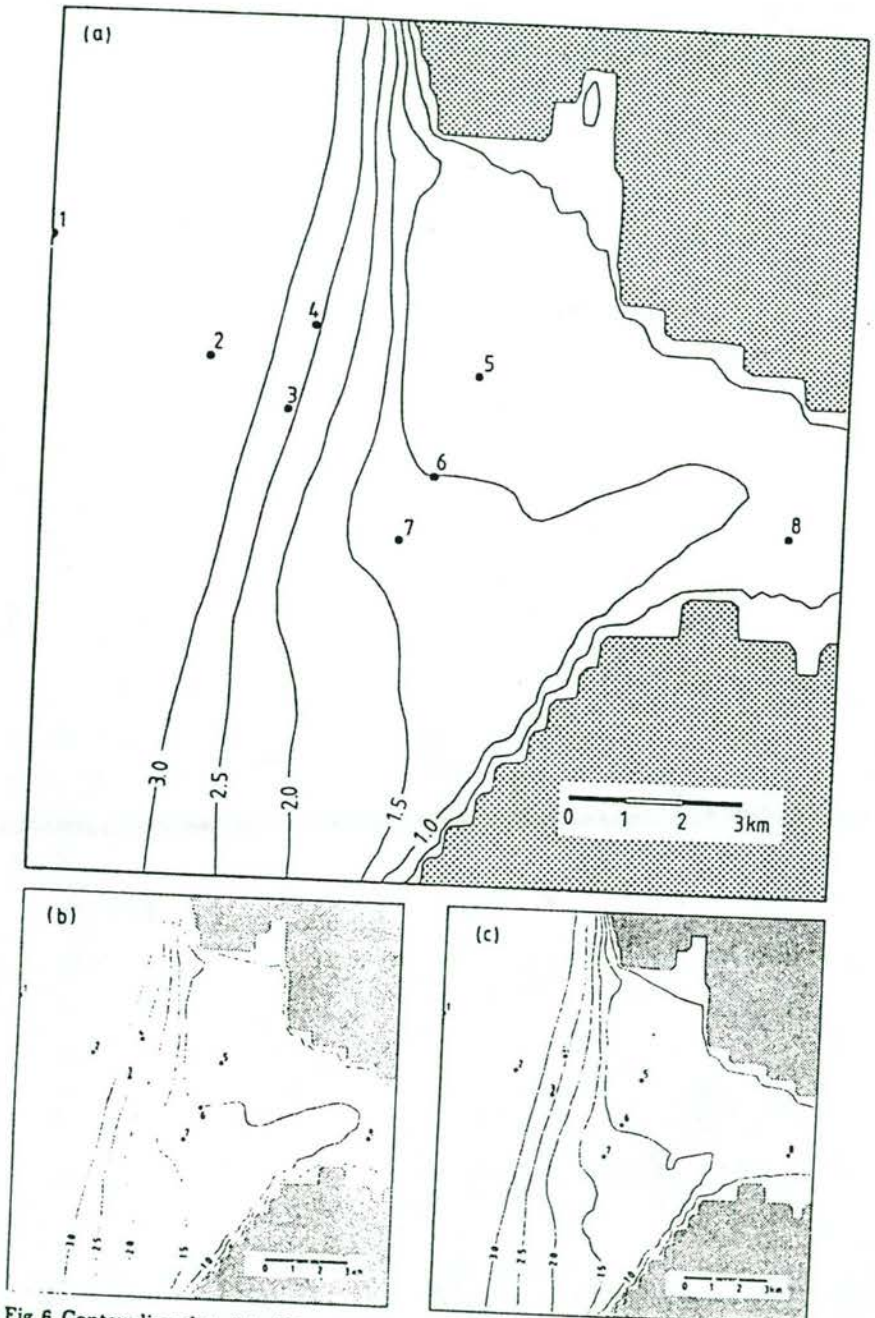

Fig. 6. Contour line plot of significant wave height, contour line interval 0.5 m. Panel (a) standard computations; panel (b) computations without refraction; panel (c) computations without wind.

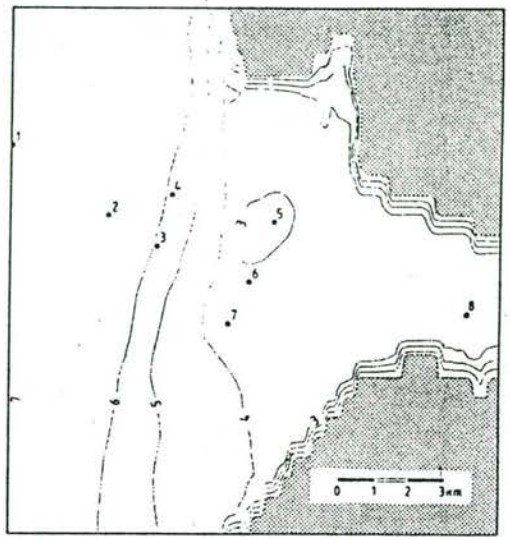

Fig. 7. Contour line plot of mean wave period, contour line interval 1 s (standard computation).

nificant wave height is about 0.8 m. The mean wave period follows roughly the same pattern (Fig. 7).

The initial gradual decrease of wave height is caused by bottom dissipation whereas the rapid decrease near the shoal is caused by wave breaking. The effect of refraction is relatively unimportant as illustrated with the results of a computation in which the refraction term has been set at zero (see Fig. 6, panel b and Table 1). This minor influence of refraction on the spatial wave height distribution is a result of the short-crestedness of the waves. The focussing and defocussing of individual directional components tend to cancel in a short-crested sea. Such short-crestedness can in principle also be properly accounted for in models based on the wave-ray technique (although it would be uneconomical to add wave generation and dissipation, see Introduction) but only in a discrete spectral manner. In the conventional monochromatic, unidirectional wave-ray approach unrealistic results are obtained in this case, in particular behind the shoal (see Fig. 8; with the same (mean) wave period and (mean) wave direction at the upwave boundary). Behind the shoal the waves are regenerated by the wind. This is illustrated by applying the model to the same situation (including refraction) but without wind (Fig. 6, panel c and Table 1).

The differences (rms-errors) between the observations and the model results (labelled "standard" in Table 1, i.e. computations including refraction and wind generation) are 0.18 m and 0.6 s for the significant wave height and the mean wave period respectively. This is 10.2 and 13.0% respectively of the

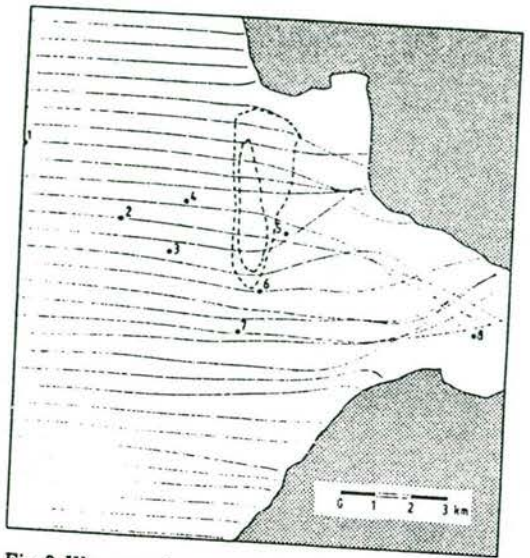

Fig. 8. Wave rays for 7 s period monochromatic, unidirectional waves.

mean observed values. The mean errors for the significant wave height and mean period are small (less than 0.01 m and 0.1 s respectively).

The above rms-errors are partly based on data from locations near the upwave boundary where any reasonable model will produce small errors since little happens to the waves anyway. On the other hand, some data are from locations where the waves have been modified considerably (e.g. a factor five in significant wave height at location 5). A good model should reproduce such large changes. Such a quality however is not properly expressed by rms-errors. For instance, the field tests of the model of Resio (1987, 1988) show a small rms-error in the significant wave height (0.16 m which is only 7.1% of the observed mean value) but the observed change in significant wave height is also small (0.41 m rms-value). A more suitable measure for the model performance, in which the boundary situation cannot dominate, is therefore defined as the performance of a perfect model (unity) minus the performance of the model relative to the observed changes (from the upwave boundary):

$$\text{performance rate} = 1 - \frac{\text{rms (error)}}{\text{rms (observed changes)}} \qquad (64)$$

For the above tests with the HISWA model the rms-value of the changes in significant wave height is 1.83 m and in mean wave period 2.4 s. With the above rms-errors, the performance rates for the HISWA model are then 0.91 and 0.76

respectively for the significant wave height and the mean wave period. This compares favourably with 0.61 for the significant wave height in the field tests of the model of Resio (1987, 1988; model wave periods not available).

CONCLUSIONS

The wave prediction model HISWA presented here is a stationary, directionally decoupled parametric model for predicting short-crested waves in shallow water with arbitrary bottom topography and current patterns. The phenomena accounted for are shoaling, refraction, wind generation, wave breaking (surfzone inclusive), bottom dissipation and wave blocking including the influence of currents on these phenomena. The basis of the model is the prediction of two directional wave functions: the one-dimensional directional action spectrum and the average frequency as a function of spectral direction. From these functions (in each of a large number of grid points in the geographical prediction area), the model determines integral functions such as the significant wave height, the average wave period and the mean wave direction and other functions such as the radiation stress gradient. For reasons of computing efficiency the computations are carried out on a regular grid rather than along wave rays.

The model is stationary, i.e. the environment (depth, wind and current) is not allowed to vary in time and the predicted wave functions are also constant in time. This is normally not a serious restriction for wave computations in coastal regions because the travel time of the waves in such regions is usually small compared to the time scales of variations in depth, wind and currents. If such slow variations are to be taken into account then the wave model should be applied in a sequence of stationary situations which approximate the non-stationary situation.

After passing a number of academic tests the model has been applied to a fairly complex situation in the mouth of the river Rhine in which wave breaking and short-crestedness dominate other effects such as refraction. The rms-errors for the significant wave height and the mean wave period for this situation are about 10 and 13% of the mean observed values respectively. This implies that in this situation HISWA correctly reproduces about 90% of the observed changes in the significant wave height and about 75% of the observed changes in the mean wave period.

ACKNOWLEDGEMENTS

The HISWA model has been developed under contract with the Department of Transport and Public Works in the Netherlands. We greatly appreciate the support of and discussions with our colleagues A.J. Kuik and J.A. Vogel of this Department and with M.W. Dingemans of Delft Hydraulics. We thank J.A.

Battjes of the Delft University of Technology for his comments on early drafts of this paper and J. Dekker for assisting us in the computations.

REFERENCES

Abbott, M.B., 1979. Computational Hydraulics. Pitman, London, 324 pp.

Arthur, R.S., Munk, W.H. and Isaacs, J.D., 1952. The direct construction of wave rays. Trans. Am. Geoph. Union, 33: 855-865.

Barnett, T.P., 1968. On the generation, dissipation and prediction of ocean wind waves. J. Geophys. Res., 73: 513-534.

Battjes, J.A., 1968. Refraction of water waves. ASCE J. Waterw. Harbors Div., 94, WW4 (Nov.): 437-451.

Battjes, J.A., 1972. Radiation stresses in short-crested waves. J. Mar. Res., 30: 56-64.

Battjes, J.A. and Janssen, J.P.F.M., 1979. Energy loss and set-up due to breaking of random waves. In: Proc. 16th Int. Coastal Engineering Conference, 1978, Hamburg. ASCE, New York, N.Y., pp. 569-587.

Booij, N., Holthuijsen, L.H. and Herbers, T.H.C., 1985. A numerical model for wave boundary conditions in port design. In: J.H. Pounsford (Editors), Proc. Int. Conf. Numerical and Hydraulic Modelling of Ports and Harbours, Birmingham, pp. 263-268.

Booij, N., Holthuijsen, L.H., Dekker, J. and Schoonbeek, R., 1988. Standard tests for the shallow water wave model HISWA. Delft Univ. Technol., Dep. Civ. Eng., Group Hydraul. Geotech. Eng., Rep. No. 6-88, 42 pp.

Bouws, E., Günther, H., Rosenthal, W. and Vincent, C.L., 1985. Similarity of the wind wave spectrum in finite depth water: 1. Spectral form. J. Geophys. Res., 90: 975-986.

Bretherton, F.P. and Garrett, G.J.R., 1968. Wavetrains in inhomogeneous moving media. Proc. R. Soc. London, A302: 529-554.

Brink-Kjær, O., 1984. Depth-current refraction of wave spectra. In: Proc. Symp. Description and Modelling of Directional Seas, 1984, Copenhagen. Pap. C-7. Tech. Univ. Denmark, Copenhagen, 12 pp.

Cavaleri, L. and Malanotte Rizzoli, P., 1981. Wind wave prediction in shallow water: theory and applications. J. Geophys. Res., 86: 10961-10973.

CERC, 1973. Shore Protection Manual. U.S. Army Coastal Eng. Res. Center, Corps Engineers. 1145 pp.

Chen, Y. and Wang, H., 1983. Numerical model for nonstationary shallow water wave spectral transformations. J. Geophys. Res., 88: 9851-9863.

Collins, J.I., 1972. Prediction of shallow water spectra. J. Geophys. Res., 77: 2693-2707.

Dingemans, M.W., 1983. Verification of numerical wave equation models with field measurements, CREDIZ verification Haringvliet. Delft Hydraulics Lab., Rep. No. W488, Delft, 137 pp.

Dingemans, M.W., 1985. Surface wave propagation over an uneven bottom, Evaluation of two-dimensional horizontal wave propagation models. Delft Hydraulics Lab., Rep. No. W301, part 5, Delft, 117 pp.

Dingemans, M.W., Stive, M.J.F., Kuik, A.J., Radder, A.C. and Booij, N., 1985. Field and laboratory verification of the wave propagation model CREDIZ. In: B.L. Edge (Editor), Proc. 19th Int. Coastal Eng. Conf., 1984, Houston. ASCE, New York, N.Y., pp. 1178-1191.

Dingemans, M.W., Stive, M.J.F., Bosma, J., De Vriend, H.J. and Vogel, J.A., 1987. Directional nearshore wave propagation and induced currents. In: B.L. Edge (Editor), Proc. 20th Int. Coastal Eng. Conf. (Nov. 1986), Taipei. ASCE, New York, N.Y., pp. 1092-1106.

Donelan, M.A., Hamilton, J. and Hui, W.H., 1985. Directional spectra of wind-generated waves. Philos. Trans. R. Soc. London, A315: 509-562.

Ewing, J.A., 1971. A numerical wave prediction method for the North Atlantic Ocean. Dtsch. Hydrogr. Z., 24: 241-261.

Gelci, R., Cazale, H. and Vassal, J., 1956. Utilisation des diagrammes de propagation à la prévision énergétique de la houle. Bulletin d'information du Comité central d'océanographie et d'études des côtes, 8: 169-197.

Golding, B., 1983. A wave prediction system for real-time sea state forecasting. Q. J. Met. Soc., 109: 393-416.

Graber, H.C. and Madsen, O.S., 1985. A parametric wind wave model for arbitrary water depths. In: Y. Toba and H. Mitsuyasu (Editors), The Ocean Surface. D. Reidel, Dordrecht, pp. 193-199.

Günther, H., 1981. A parametric surface wave model and the statistics of the prediction parameters. Ph.D. thesis. Hamburger Geophysikalische Einzelschriften, A55, 90 pp.

Günther, H., Rosenthal, W. and Richter, K., 1979. A hybrid parametrical wave prediction model. J. Geophys. Res., 84: 5727-5738.

Hasselmann, K., 1960. Grundgleichungen der Seegangsvoraussage. Schiffstechnik, Vol. 7, No. 39: 191-195.

Hasselmann, S. and Hasselmann, K., 1981. A symmetrical method of computing the nonlinear transfer in a gravity wave spectrum. Hamburger Geophysikalische Einzelschriften, Max-Planck-Institut für Meteorologie, A52, 177 pp.

Hasselmann, K., Barnett, T.P., Bouws, E., Carlson, H., Cartwright, D.E., Enke, K., Ewing, J.A., Gienapp, H., Hasselmann, D.E., Kruseman, P., Meerburg, A., Müller, P., Olbers, D.J., Richter, K., Sell, W. and Walden, H., 1973. Measurements of wind-wave growth and swell decay during the Joint North Sea Wave Project (JONSWAP). Dtsch. Hydrogr. Z., A8, No. 12, 95 pp.

Hasselmann, K., Ross, D.B., Müller, P. and Sell, W., 1976. A parametric wave prediction model. J. Phys. Oceanogr., 6: 200-228.

Hasselmann, S., Hasselmann, K., Allender, J.H. and Barnett, T.P., 1985. Computations and parameterizations of the nonlinear energy transfer in a gravity-wave spectrum. Part II: Parameterizations of the nonlinear energy transfer for applications in wave models. J. Phys. Oceanogr., 15: 1378-1391.

Hirosue, F. and Sakai, T., 1987. Directional spectra in current-depth refraction. In: B.L. Edge (Editor), Proc. 20th Int. Coastal Eng. Conf. (Nov. 1986), Taipei. ASCE, New York, N.Y., pp. 247-260.

Holthuijsen, L.H., 1983. Observations of the directional distribution of ocean-wave energy in fetch-limited conditions. J. Phys. Oceanogr., 13: 191-207.

Janssen, P.A.E.M., Komen, G.J. and De Voogt, W.J.P., 1984. An operational coupled hybrid wave prediction model. J. Geophys. Res., 89: 3635-3654.

Karlson, T., 1969. Refraction of continuous ocean wave spectra. Proc. ASCE J. Waterw. Harbors Div., Vol. 95, No. WW4: 437-448.

Kitaigorodskii, S.A., Krasitskii, V.O. and Zaslavskii, M.M., 1975. On Phillips' theory of equilibrium range in the spectra of wind-generated gravity waves. J. Phys. Oceanogr., 5: 410-420.

Kuik, A.J., Van Vledder, G.Ph. and Holthuijsen, L.H., 1988. A method for the routine analysis of pitch and roll buoy wave data. J. Phys. Oceanogr., 18: 1020-1034.

Mathiesen, M., 1984. Current-depth refraction of directional wave spectra. In: Symp. Description and Modelling of Directional Seas, 1984, Copenhagen. Pap. No. C-6. Tech. Univ. Denmark, Copenhagen, 8 pp.

Miche, R., 1944. Mouvements ondulatoires de la mer en profondeur constante ou décroissante. Ann. Ponts Chausées, 114: 369-406.

Phillips, O.M., 1977. The dynamics of the Upper Ocean. Cambridge University Press, 336 pp.

Pierson, W.J. and Moskowitz, L., 1964. A proposed spectral form for fully developed wind seas based on the similarity theory of S.A. Kitaigorodskii. J. Geophys. Res., 69: 5181-5190.

Piest, J., 1965. Seegangsbestimmung und Seegangsrefraktion in einem Meer mit nicht-ebenem Boden - eine theoretische Untersuchung. Dtsch. Hydrogr. Z., 18: 67-74.

Putnam, J.A. and Johnson, J.W., 1949. The dissipation of wave energy by bottom friction. Trans. Am. Geoph. Union, 30: 67–74.
Resio, D.T., 1987. Shallow-water waves. I: Theory. Proc. ASCE J. Waterw., Ports Coastal Ocean Eng., 113: 264–281.
Resio, D.T., 1988. Shallow-water waves II: Data comparisons. Proc. ASCE J. Waterw., Ports Coastal Ocean Eng., 114: 50–65.
Sakai, T., Kosecki, M. and Iwagaki, Y., 1983. Irregular wave refraction due to current. J. Hydraul. Eng., ASCE, 109: 1203–1215.
Seymour, R.J., 1977. Estimating wave generation on restricted fetches. Proc. ASCE, J. Waterw., Port Coastal Ocean Div., 103, No. WW2: 251–264.
Thornton, E.B., 1977. Rederivation of the saturation range in the frequency spectrum of wind-generated gravity waves. J. Phys. Oceanogr., 7: 137–140.
Whitham, G.B., 1965. A general approach to linear and nonlinear dispersive waves using a Lagrangian. J. Fluid Mech., 22: 273–284.
Whitham, G.B., 1971. Dispersive waves and variational principles. In: A.H. Tahb (Editor), Studies of Applied Mathematics, 7: 181–212.
Young, I.R., 1988. A shallow water spectral wave model. J. Geophys. Res., 93: 5113–5129.

CHAPTER 30

Verification of numerical wave propagation models in tidal inlets

J.A. VOGEL, A.C. RADDER AND J.H. DE REUS*

The performance of two numerical wave propagation models has been investigated by comparison with field data. The first model is a refraction-diffraction model based on the parabolic equation method. The second is a refraction model based on the wave action equation, using a regular grid. Two field situations, viz. a tidal inlet and a river estuary along the Dutch coast, were used to determine the influence of the local wind on waves behind an island and a breaker zone. It may be concluded from the results of the computations and measurements that a much better agreement is obtained when wave growth due to wind is properly accounted for in the numerical models. In complicated coastal areas the models perform well for both engineering and research purposes.

1. INTRODUCTION

Sea waves approaching coastal regions can be influenced by a number of physical processes: shoaling, refraction by depth and current variations, diffraction, nonlinear effects, energy dissipation by wave breaking and bottom friction, and wave growth due to wind. In order to estimate inshore wave conditions from wave data available offshore, shallow water wave models should be able to account for these effects. Usually, numerical 2D shallow water wave propagation models include propagation and dissipation processes, while the influence of the local wind is often neglected (see e.g. Martin et al., 1987; Vincent and Carrie, 1988). For regions behind an island (c.q. peninsula) or a breaker zone the input from the local wind may be appreciable, and this effect cannot be accounted for by, e.g., taking a lower value of the friction factor. The purpose of this study is to verify two numerical models in this respect, with wave measurements in two field situations.

*senior researchers, Rijkswaterstaat, Tidal Waters Division, P.O.Box 20904, 2500 EX The Hague, The Netherlands

2. SHALLOW WATER WAVE MODELS

The performance of two shallow water wave models has been investigated:

- The model CREDIZ, which is based on the parabolic approximation of the mild-slope equation (Radder, 1979; Dingemans et al., 1984; Dingemans 1985).
- the model HISWA, which is based on refraction computations using a regular grid (Holthuijsen and Booij, 1986; Holthuijsen et al., 1988)

A mathematical formulation of these models is given below.

2.1 The model Crediz

The parabolic model CREDIZ describes the propagation of waves in coastal areas with non-uniform depth and current, in particular where both refraction and diffraction effects are important. The model is based on the following equation for monochromatic wave motion (for more details, see Dingemans, 1985):

$$\nabla \cdot (cc_g \nabla \varphi) + (k^2 cc_g + i\sigma(W + \nabla \cdot \vec{U}))\varphi = 0 \tag{1}$$

where $\vec{U}$ is the (steady) current-velocity vector, ∇ is the horizontal gradient operator $(\partial/\partial x,\ \partial/\partial y)$, $\varphi(x,y)$ is the complex wave potential function, k the wave number, c and c_g the phase- and group velocity, σ the relative angular frequency, $i = \sqrt{-1}$ the imaginary unit, and W a dissipation coëfficient, to be specified later on.

The absolute (ω) and relative (σ) frequencies are related by:

$$\omega = \sigma + \vec{k} \cdot \vec{U} \tag{2}$$

where σ is given by the linear dispersion relation:

$$\sigma^2 = gk \tanh kh \tag{3}$$

with g the acceleration of gravity and h the local depth.

In the parabolic approximation the assumption is made that the waves propagate mainly into a specific direction, say x.

Defining the operator M by $M = \frac{\partial}{\partial y}(\beta \frac{\partial}{\partial y})$ with $\beta = cc_g$

the parabolic approximation to equation (1) is given by:

$$\frac{\partial}{\partial x}(\sqrt{\beta k}\,\varphi + \frac{p_1}{k\sqrt{\beta k}} M\varphi) - i(k\sqrt{\beta k}\,\varphi + \frac{p_2}{\sqrt{\beta k}} M\varphi) + \frac{\sigma}{2\sqrt{\beta k}}(W + \nabla \cdot \vec{U})\varphi = 0 \tag{4}$$

The coefficients p_1 and p_2 result from the approximation of pseudo-operators by differential operators and are related by:

$$p_2 = p_1 + \frac{1}{2}, \qquad 0 \le p_1 \le \frac{1}{2} \quad (\text{optimal} : p_1 = \frac{1}{4}) \tag{5}$$

As the wave-number vector $\vec{k}$ in (2) is not exactly known beforehand, the relative frequency σ is approximated by:

$$\sigma = \omega - r\,k\,U_x$$

in which r is a reduction factor expressing the fact that the waves do not exactly follow the x-direction ($0 \le r \le 1$; standard value: $r = 0.9$).

The energy-dissipation term $W\varphi$ in equation (4) accounts for the effects of wave breaking, bottom friction and wave growth due to wind:

$$W\varphi = (W_b + W_f + W_g)\,\varphi \tag{6}$$

The dissipation function W_b due to wave breaking is computed according to the method of Battjes and Janssen (1978); see also Battjes and Stive (1985). For the dissipation function W_f due to bottom friction the method of Putnam and Johnson (1949) is used.

The effect of wave growth by wind is simulated by the (negative) dissipation term W_g :

$$W_g = -\frac{2c_g}{H_s}\frac{dH_s}{dx} \tag{7}$$

where $H_s = 2a$ is the significant wave height and a the wave amplitude. To compute the gradient dH_s/dx in (7), the growth curve of Krylov/Wilson is used (cf. Holthuijsen, 1980; Krylov et al.,1976; Wilson, 1965):

$$\tilde{H}_s = \beta\,[1 - 1/(1 + \alpha\sqrt{\tilde{x}})^2\,] \tag{8}$$

with $\tilde{H}_s = gH_s/V_x^2$, $\tilde{x} = gx/V_x^2$,
V_x = component of wind speed in x-direction,
α, β = coefficients ($\alpha \approx 0.006$, $\beta \approx 0.256$).

It is noted that the growth curve (8) is based on a parametric description of the wave spectrum; the effect of wave growth is assumed to be local, while

the period of the waves (due to the restriction to mc ·romatic waves) is ssumed to be constant, equal to the peak period of the rum. Therefore, a spectral decomposition is not allowed when (8) is used.

The influence of the wave amplitude a on the propagation velocity is taken into account by setting the local depth h in the dispersion relation (3) equal to: $h = d + p_v a$ where d is the actual mean water depth and p_v is an adjustable parameter (standard value: 1). In the shallow water limit the celerity c of a solitary wave is obtained for $p_v = 1$, while in the deep water limit the linear expression for c is recovered.

The parabolic differential equation (4) can be solved in finite difference form, using a two-level, implicit numerical scheme on a rectangular grid. When dissipative physical effects are included (through the term $W\varphi$), the difference equations are linearized in a special way to ensure stability: in the case of $W < 0$, a positive diffusion is introduced in the (fully implicit) numerical scheme, in order to prevent non-linear instabilities in the early stage of wave growth due to wind. In practice, fairly accurate solutions have been obtained for values of grid spacings Δx and Δy according to: $\Delta x/L \leq 1/4$; $\Delta y/L \leq 1/6$, where $L = 2\pi/k$ is the local wave length.

The solution of equation (4) requires as initial conditions the amplitude, period and direction of the incident wave field; along the lateral bounderies, the wave field is generally not known, and an approximate boundary condition (reflecting or partially absorbing) may be applied. However, for instance in case of strong wave-current interactions, these conditions give not the right description; therefore, the computational grid should be chosen sufficiently large, to avoid disturbances of the wave field in the region of interest.

2.2 The model HISWA

The model HISWA accounts for refractive propagation of shortcrested waves over arbitrary bottom topography and current fields. The model is based on the action balance equation:

$$\frac{\partial A}{\partial t} + \dot{x}_i \frac{\partial A}{\partial x_i} + \dot{k}_i \frac{\partial A}{\partial k_i} = T \tag{9}$$

where $A(\vec{k}, \vec{x}, t)$ denotes the wave action density, $\dot{x}_i \equiv \frac{dx_i}{dt} = \frac{\partial \Omega}{\partial k_i}$ is the group velocity and $\dot{k}_i \equiv \frac{dk_i}{dt} = -\frac{\partial \Omega}{\partial x_i}$ is the rate of change of wave number due to refraction. The right hand side denotes the local change of action density, e.g. by dissipation. The dispersion relation is given as $\omega = \Omega(\vec{k}, \vec{x}, t)$, see (2) and (3). For simplicity we assume in this derivation that there is no ambient current; see Dingemans et al. (1986) for the current case. In the model the simplifying assumption of stationarity, i.e. no explicit dependence on time, is made. Then

Ω is a Hamiltc for the vectorfield $(\dot{x}_i, \dot{k}_i)$. Transforming from $(\vec{k}, \vec{x})$-spa to the $(\vec{x}, \omega, \vartheta)$-. e with ϑ the wave direction and introducing the absolu. energy density $\tilde{E}$ by $\tilde{E} = A\omega$, one obtains after integration over ω between 0 and ∞:

$$\frac{\partial}{\partial x}[\omega^A \cdot A^{(o)} \cdot \bar{c}_g \cos\vartheta] + \frac{\partial}{\partial y}[\omega^A \cdot A^{(o)} \cdot \bar{c}_g \sin\vartheta] + \frac{\partial}{\partial \vartheta}[\omega^A \cdot A^{(o)} \cdot \bar{c}_\vartheta] = T_1 \tag{10}$$

where the mean quantities ω^A, $A^{(o)}$, $\bar{c}_g$ and $\bar{c}_\vartheta$ are defined by:
$A^{(o)}(x,y,\vartheta) = \int_0^\infty A(x,y,\omega,\vartheta)d\omega$; $\omega^A(x,y,\vartheta) = \frac{1}{A^{(o)}}\int_0^\infty \omega A d\omega$;
$E^{(o)} = \omega^A \cdot A^{(o)}$; $\bar{c}_g = \frac{1}{E^{(o)}}\int_0^\infty \tilde{E} \cdot c_g d\omega$; $\bar{c}_\vartheta = \frac{-1}{E^{(o)}}\int_0^\infty \tilde{E}(c_g - \frac{c}{2})\frac{1}{h}\frac{\partial h}{\partial n} d\omega$;
$T_1 = \int_0^\infty \omega T d\omega$; $c_g = \frac{\partial \Omega}{\partial k}$; $c = \frac{\omega}{k}$; $\vec{n} = (-\sin\vartheta, \cos\vartheta)$.

Using Leibniz' rule and rewriting the result, a second equation is obtained:

$$\frac{\partial}{\partial x}[A^{(o)} \cdot \bar{c}_g \cos\vartheta] + \frac{\partial}{\partial y}[A^{(o)} \cdot \bar{c}_g \sin\vartheta] + \frac{\partial}{\partial \vartheta}[A^{(o)} \cdot \bar{c}_\vartheta] = \frac{1}{\omega^A}[T_1 - A^{(o)} \cdot \bar{c}_{g,i} \cdot \frac{\partial \omega^A}{\partial x_i}] \tag{11}$$

Equation (10) and (11) are the basic equations for HISWA. The source term T_1 is implemented as $(\omega^A/\sigma^A) \cdot S^{(o)}$, where $S^{(o)}$ denotes the local chance of energy and $\bar{c}_{g,i} \cdot \frac{\partial \omega^A}{\partial x_i}$ is interpreted as the change of the frequency ω^A, which is prescribed as a function S_ω of the local data.

The source terms $S^{(o)}$ and S_ω represent the effects of wave breaking, bottom friction, wind wave generation, and wave blocking on an opposing current. The dissipation due to wave breaking and bottom friction is modelled by the same methods as used in the CREDIZ model. The formulation is extended to random waves with directional distribution by assuming that the dissipation per direction is proportional to the energy density at that direction.
The formulation of the source term for wave generation by wind is based on available expressions giving the total energy and the frequency averaged over the whole spectrum, as functions of fetch and wind speed. Details can be found in Holthuijsen et al. (1988).

The first order partial differential equations (10, 11) can be solved on a regular grid in (x,y,ϑ)-space, with the x-direction parallel to the main direction of the wave field. In the present version of the model, a leapfrog finite difference scheme is used, together with appropriate boundary conditions. As initial conditions, the wave height, period, direction and spreading (or the directional spectrum) of the incident wave field are required.

3. COMPARISON WITH FIELD MEASU ''MENTS

The present verification study concerns two field situat. .:
- the tidal inlet of Texel,
- the estuary of Haringvliet.

Results of the comparison are presented below.

3.1 The tidal inlet of Texel.

This is a strait connecting an ebb tidal delta at the North Sea side with the area of interest, the Wadden Sea, at the other side (see fig. 1). The entrance of the inlet is sheltered by a shoal, which is flooded only during very high tide. The effect of the local wind is thus dominant, while the influence of the tidal current is of secondary importance.

Wave data are available from five locations, of which we used three in this paper:
EIERLAND, located offshore in the North Sea, to provide the input wave conditions for the models;
BOLLEN and MALZWIN, located in the Wadden Sea, to verify the numerical models.
Apart from the wavestaff at MALZWIN, waverider buoys were employed at the measurement locations. Measurements were selected from the period 11 October 1981 to 11 March 1982, using the criteria:
- wind direction ranging from 220° to 300° (± SW to NW);
- wind speed higher than 6 m/s.

In table 1 thirteen selected cases are shown which provide the input wave parameters measured at the offshore buoy. In each case, the tidal current is represented by one of four characteristic stages: maximum ebb, slack tide ebb-flood, maximum flood, slack tide flood-ebb (see figs. 2 - 5). The wave direction of the incident wave field is assumed to be equal to the wind direction, given in table 1.

The bottom topography is represented by a depth array of 136 x 104 grid points, with a spacing of 250 m. At the same grid points, the components of the current velocities are given. Further details can be found in: den Adel (1988). The results of the computations of the models are compared with the measurements in table 1, and a scatter plot is given in fig. 10.
From the computations we draw the conclusions:
- the influence of the local wind is most important in this area: when wave growth due to wind is not accounted for, the computed wave height reduces to values less than a few percent of the incident wave height. This is mainly due to -besides breaking on the shoal- diffraction of wave energy in the Wadden Sea: swell decays here rapidly.
- the influence of the tidal current (with velocities up to 1.5 m/s) can be appreciable: differences of more than 50% may be found, comparing cases with and w ut current; in the maximum-ebb case nr. 13, a tunneling of waves does ((see figs. 6, 7 and 8, 9).
- the influence of the waves on the North Sea is very small; only during maximum-ebb-flow and if the waves come from the South-East more than a few percent of the input wave height remains at the Wadden Sea.
- the change in significant wave period plays a role: at lower periods, the wave-current interaction is stronger, while refraction by depth and bottom friction are weaker. This partially explains the differences in the results of the model computations.

Remarks
1. The present version of the model HISWA does not perform well in case of very small directional distribution; therefore, the model should be used with care when swell-components are present in the wave field.
2. The model CREDIZ shows a sensitive dependence of the side-boundary conditions of the computational grid, in case of strong tidal currents crossing these boundaries; care should be taken that the wave field in the area of interest is not disturbed, by choosing the computational grid sufficiently large.

3.2 The estuary of Haringvliet.

This area is characterized by a shoal called Hinderplaat which falls partly dry during low tide, a region with nearly straight isobaths offshore the shoal, and a complicated bottom geometry inshore (see fig. 11). In the vicinity of the shoal, wave breaking is the predominant physical process; after this breaking, the wind may enhance the wave height appreciably along a distance of a few miles behind the shoal.
Wave data are available from a measurement campaign during the autumn of 1982 (for details, see Dingemans, 1983; Dingemans et al. 1984). Recently, this data set has been used extensively to test the performance of numerical shallow water wave models (Martin et al. 1987; Vincent and Carrie, 1988). However, energy input from the wind is not included in these models.
In order to test the effect of the local wind, the storm situation of 14 - 15 October 1982 was selected. For a fair comparison with previous CREDIZ results, the same cases as described by Dingemans (1983) were used, with the same input parameters (e.g. the 1981 - bottom topography, consisting of 88 x 117 grid points with spacing of 250 m, and a bottom friction factor f = 0.005 instead of the more appropriate 0.01). Further input conditions were:
- wind direction ranging from 300° to 320°;
- wind speed ranging from 12.9 to 16.5 m/s;
- peak period ranging from 7.1 to 8.3 s (at the Wavec buoy).

The results of the computations are shown in table 2, where the relative error δ is defined by $\delta = (H_s - H_{sm})/H_{sm}$. For each of the six cases, the bias b and the rms-deviation ϵ_{rms} are given in table 3.

By definition, $b = \sum(H_s - H_{sm})/\sum H_{sm}$;

$$\epsilon_{rms} = [n^{-1}\sum(H_s - H_{sm})^2]^{1/2}/[n^{-1}\sum H_{sm}].$$

The following conclusions may be inferred:

- the model CREDIZ (and, to a lesser extent, also HISWA) performs much better when wave growth due to wind is properly accounted for, especially at low water levels.
- while HISWA performs well at E-75, the wave-staff far behind the shoal, CREDIZ still gives too low values of H_s there; this is probably due to the effect of directional spreading of the wave field, and the transfer of energy between spectral components, resulting in a lowering of the significant wave period, and less dissipation due to bottom friction.
- the computed wave height at WR4, just behind the Hinderplaat, is still too low for low water levels; this is probably due to (local) set-up of the mean water level by waves, which effect is not included in the models.
- at the other locations (mainly at WR5 and WR6), the process of spectral saturation (white-capping) is of importance. This process is simulated in the models by the dissipation method of Battjes and Janssen (1978) for random breaking waves, where breaking is caused also by exceedence of steepness.

4. CONCLUSIONS

A verification study of two wave propagation models has been made, using field data in which the influence of the local wind is significant. In spite of the distinct differences between the models (e.g. CREDIZ is a monochromatic model including diffractive effects, while HISWA is a variable frequency model with directional spreading effects), both models perform equally well in complicated coastal areas. (For specific conclusions, see §3.1 and §3.2).
There remains the problem to describe in a more fundamental way changes in wave frequency, especially in shallow water (for instance, by the undular bore model; see Dingemans and Battjes, these Proceedings). This is important when the models are used in sediment transport studies.

Acknowledgements.

The authors would like to thank J.D. den Adel, J. Hoekema, A.W. Hokke, D. Knoester, T. Louters and A.M. Walburg for assistance in the computations, R.C.M. Ariaans and A.P. Roskam for supplying the field data.

Table 1. Comparison of significant wave heights and periods, Texel.

case nr.	water level (m)	tidal stage	wind speed (m/s)	wind direction (o)	incident wave EIERLAND Hs(m)	Ts(m)	wave height (m) meas.	CREDIZ	HISWA	wave period (s) meas.	HISWA	location
1	0.49	ebb-flood	8	250	1.38	6.1	0.15	0.26	0.23	3.7	3.6	BOLLEN
2	0.20	,,	18	270	4.41	10.0	0.86	0.55	0.84	3.8	3.9	,,
3	0.50	,,	18	270	4.41	10.0	0.88	0.74	0.82	3.5	4.0	,,
4	0.52	max. flood	7	280	1.92	9.1	0.14	0.19	0.15	3.6	4.5	,,
5	1.00	,,	9	240	1.35	6.0	0.20	0.27	0.21	4.0	4.0	,,
6	0.87	flood-ebb	7	230	1.12	6.4	0.15	0.15	0.30	3.7	2.6	,,
7	0.12	,,	8	280	1.81	8.2	0.27	0.29	0.26	3.4	2.9	,,
8	1.73	,,	15	280	4.24	9.6	0.64	0.52	0.33	3.6	4.8	MALZWIN
9	1.49	,,	15	280	4.24	9.6	0.55	0.51	0.33	4.2	4.6	,,
10	-0.18	max. ebb	6	290	1.01	6.2	0.30	0.17	0.15	2.8	3.3	BOLLEN
11	-0.62	,,	9	300	1.69	7.7	0.21	0.29	0.35	3.4	2.6	,,
12	-0.48	,,	9	220	2.28	7.0	0.51	0.28	0.32	3.3	5.3	,,
13	-0.3	,,	11	230	2.24	7.7	0.36	0.38	0.38	4.7	4.7	,,

Table 2. Continued

date and time	water level	location	measurement Hsm	CREDIZ (new) Hs	CREDIZ (new) δ(%)	HISWA (new) Hs	HISWA (new) δ(%)
82 10 14 23.00	1.70	Wa	3.54	3.54	0	3.54	0
		WR1	3.10	3.40	+10	3.54	+14
		WR2	2.63	3.11	+18	3.16	+20
		WR3	2.72	3.04	+12	3.11	+14
		WR4	0.72	0.79	+10	0.99	+38
		WR5	1.45	1.50	+ 3	1.53	+ 6
		WR6	1.86	1.88	+ 1	1.88	+ 1
		E-75	1.08	0.99	- 8	1.10	+ 2
82 10 15 02.00	1.50	Wa	2.89	2.89		2.89	0
		WR1	2.68	2.82	+ 5	2.86	+ 7
		WR2	2.75	2.70	- 2	2.83	+ 3
		WR3	2.68	2.74	+ 2	2.81	+ 5
		WR4	0.70	0.76	+ 9	0.88	+26
		WR5	1.15	1.39	+21	1.40	+22
		WR6	1.95	1.63	-16	1.75	-10
		E-75	0.88	0.46	-48	1.05	+19
82 10 15 04.00	0.45	Wa	2.72	2.72	0	2.72	0
		WR1	2.49	2.63	+ 6	2.72	+ 9
		WR2	2.41	2.43	+ 1	2.53	+ 5
		WR3	2.56	2.44	- 5	2.49	- 3
		WR4	0.44	0.30	-32	0.44	0
		WR5	0.70	0.99	+41	1.05	+50
		WR6	1.35	1.32	- 2	1.40	+ 4
		E-75	0.63	0.50	-21	0.72	+14

Table 2. Comparison of significant wave heights, Haringvliet.

date and time	water level	location	measurement Hsm	CREDIZ (new) Hs	CREDIZ (new) δ(%)	HISWA (new) Hs	HISWA (new) δ(%)
82 10 14 17.00	-0.10	Wa	2.58	2.58	0	2.58	0
		WR1	2.34	2.55	+ 9	2.58	+10
		WR2	2.21	2.31	+ 5	2.34	+ 6
		WR3	2.21	2.23	+ 1	2.30	+ 4
		WR4	0.40	0.29	-27	0.28	-30
		WR5	0.66	0.76	+15	0.89	+35
		WR6	1.16	1.29	+11	1.22	+ 5
		E-75	0.61	0.52	-15	0.58	- 5
82 10 14 20.00	0.20	Wa	3.06	3.06	0	3.06	0
		WR1	2.65	2.98	+12	3.05	+15
		WR2	2.38	2.57	+ 8	2.56	+ 8
		WR3	2.45	2.48	+ 1	2.50	+ 2
		WR4	0.48	0.33	-31	0.36	-25
		WR5	0.75	0.89	+19	1.00	+33
		WR6	1.20	1.39	+16	1.32	+10
		E-75	0.74	0.46	-38	0.64	-14
82 10 14 22.00	0.85	Wa	3.23	3.23	0	3.23	0
		WR1	2.90	3.18	+10	3.24	+12
		WR2	2.53	2.85	+13	2.83	+12
		WR3	2.70	2.74	+ 1	2.77	+ 3
		WR4	0.62	0.52	-16	0.65	+ 5
		WR5	1.05	1.17	+11	1.21	+15
		WR6	1.60	1.61	+ 1	1.56	- 3
		E-75	0.94	0.78	-17	0.86	- 9

Table 3. Bias and rms-deviation (%); Haringvliet.

time	water level (m)	CREDIZ, old *) b	CREDIZ, old *) ϵ_{rms}	CREDIZ, new b	CREDIZ, new ϵ_{rms}	HISWA, new b	HISWA, new ϵ_{rms}
17.00	- 0.10	- 1.5	19.2	+ 3.8	8.8	+ 6.3	10.8
20.00	0.20	- 2.4	26.1	+ 4.2	13.7	+ 7.3	13.5
22.00	0.85	+ 1.9	16.5	+ 4.1	10.3	+ 6.3	10.6
23.00	1.70	+ 6.9	12.4	+ 8.5	12.9	+12.9	16.4
02.00	1.50	- 3.2	15.3	- 2.3	12.5	+ 6.2	9.7
04.00	0.45	+ 0.5	13.4	+ 0.3	9.9	+ 7.3	11.3

*) Cf. Dingemans et al. (1984)

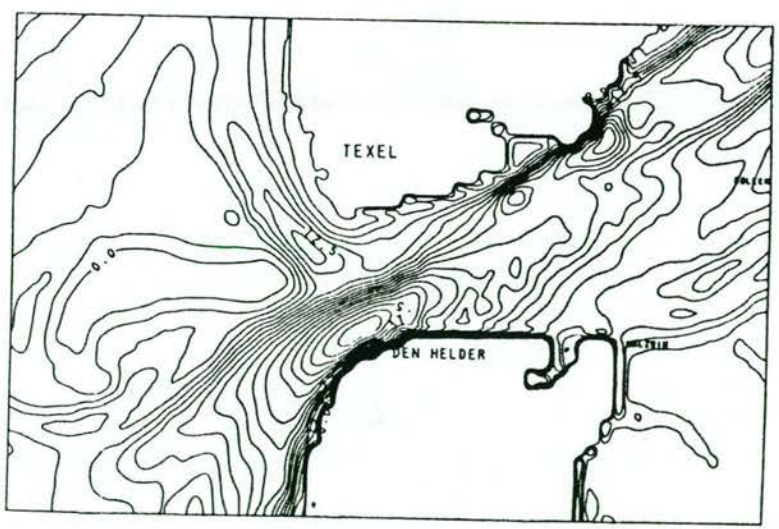

Fig. 1 Bottom contours, tidal inlet of Texel.

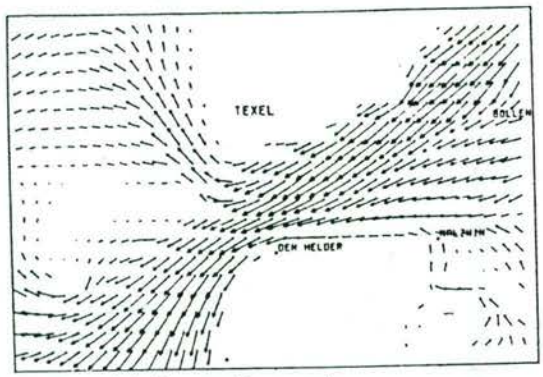

Fig. 2 Maximum ebb current.

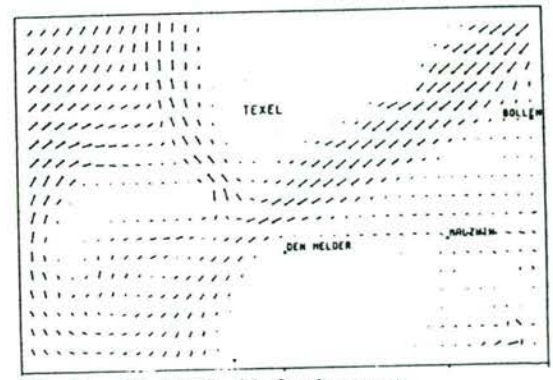

Fig. 3 Slack tide ebb-flood current.

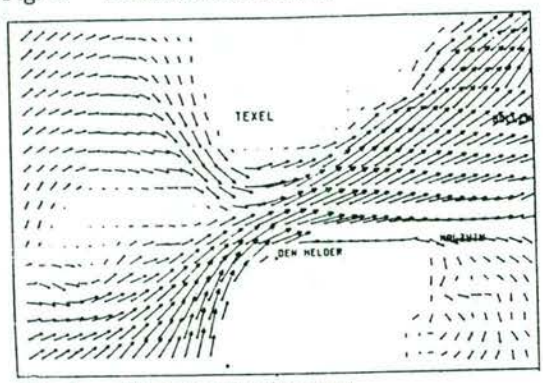

Fig. 4 Maximum flood current.

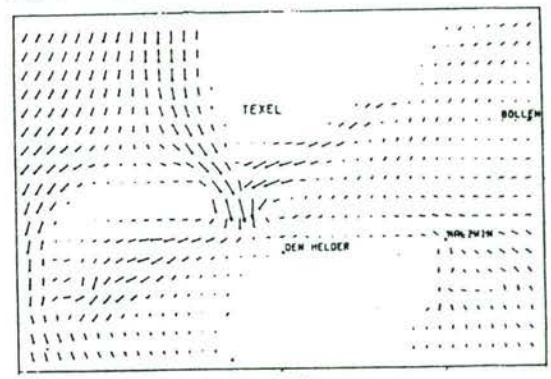

Fig. 5 Slack tide flood-ebb current.

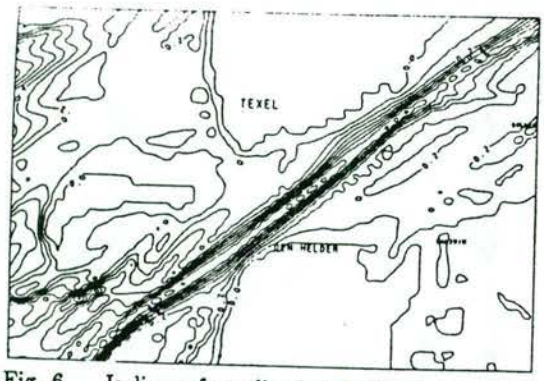

Fig. 6 Isolines of amplitude (CREDIZ), max. ebb current.

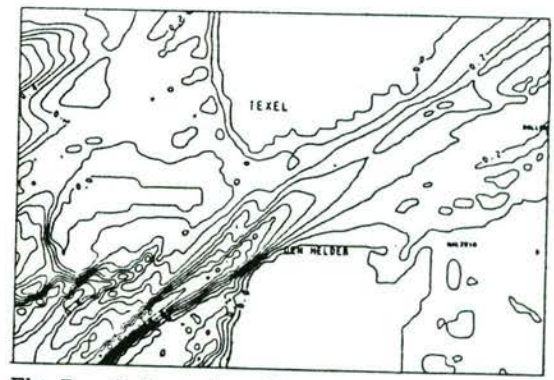

Fig. 7 Isolines of amplitude (CREDIZ), no current.

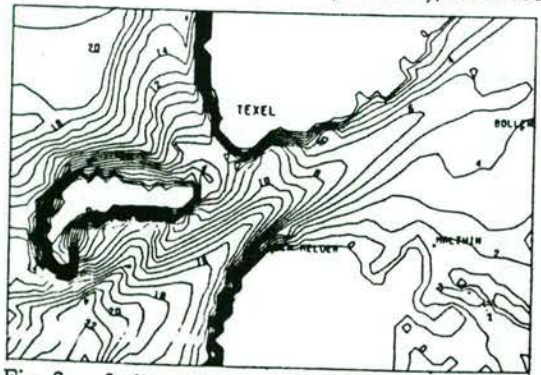

Fig. 8 Isolines of wave height (HISWA), max. ebb current.

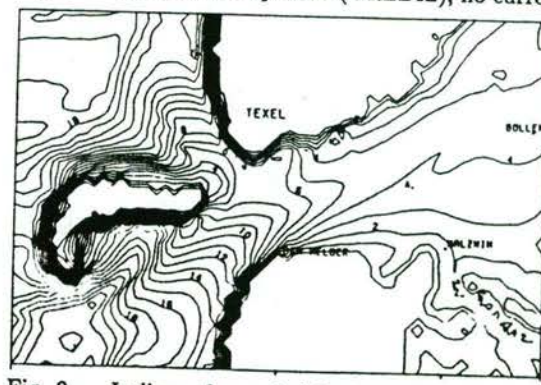

Fig. 9 Isolines of wave height (HISWA), no current.

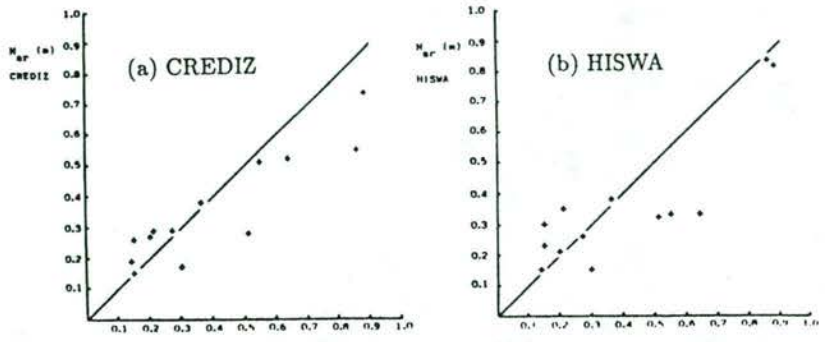

fig. 10 Comparison of measured and computed wave heights.

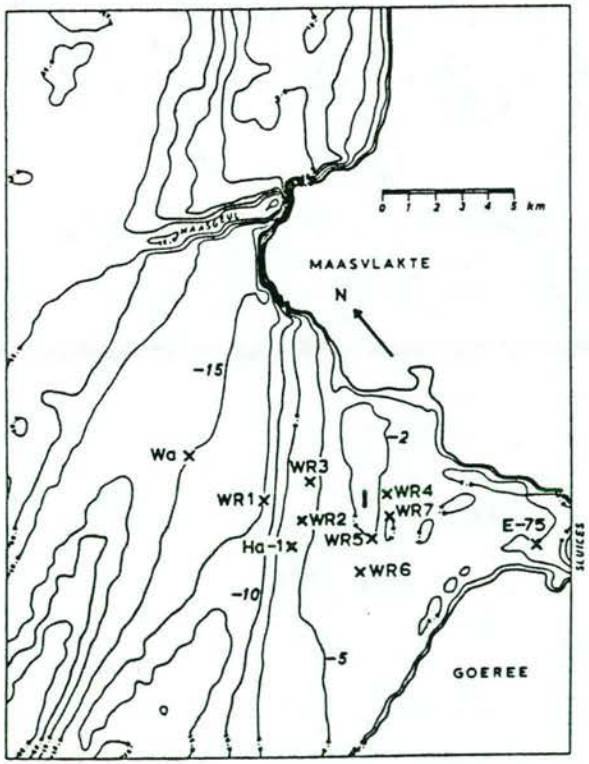

Fig. 11 Bottom contours, estuary of Haringvliet.

REFERENCES

Adel, J.D. den, *Verificatie van de numerieke golfvoortplantingsmodellen CREDIZ en HISWA bij het zeegat van Tezel*, Rijkswaterstaat, Report GWAO 88.044 (in Dutch) (1988).

Battjes, J.A. and Janssen, J.P.F.M., *Energy loss and set-up due to breaking of random waves*, Proc. 16th Coastal Eng. Conf. ASCE, Hamburg, 569 - 587 (1978).

Battjes, J.A. and Stive, M.J.F., *Calibration and verification of a dissipation model for random breaking waves*, J. Geophys. Res. 90 (C5), 9159 - 9167 (1985).

Dingemans, M.W., *Verification of numerical wave propagation models with field measurements. CREDIZ verification Haringvliet*, Delft Hydraulics Lab., Report W 488 (1983).

Dingemans, M.W., *Surface wave propagation over an uneven bottom. Evaluation of two-dimensional horizontal wave propagation models*, Delft Hydraulics Lab., Report W 301, part 5 (1985).

Dingemans, M.W.; Stive, M.J.F.; Kuik, A.J.; Radder, A.C. and Booij, N., *Field and Laboratory verification of the wave propagation model CREDIZ*, Proc. 19th Coastal Eng. Conf. ASCE, Houston, 1178 - 1191 (1984).

Dingemans, M.W.; Stive, M.J.F.; Bosman, J.; De Vriend, H.J. and Vogel, J.A., *Directional nearshore wave propagation and induced currents*, Proc. 20th Coastal Eng. Conf. ASCE, Taipei, 1092 - 1106 (1986).

Holthuijsen, L.H., *Methoden voor golfvoorspelling (in Dutch)*, Technische Adviescommissie voor de Waterkeringen (1980).

Holthuijsen, L.H. and Booij, N., *A grid model for shallow water waves*, Proc. 20th Coastal Eng. Conf. ASCE, Taipei, 261 - 270 (1986).

Holthuijsen, L.H.; Booij, N. and Herbers, T.H.C., *A prediction model for stationary, short-crested waves in shallow water with ambient currents*, Coastal Engineering, in preparation (1988).

Krylov, Yu.M. Strekalov, S.S. and Tsyplukhin, V.F., *Vetrovye volug i ich vozdejstvie na sooruzewija (wind waves and their impact on structures). In Russian*, Hydrometeoizdat, Leningrad (1976).

Martin, C.J.; Dalrymple, R.A. and Miller, M.C., *A verification procedure for wave propagation models*, Modelling the Offshore Environment, Proc. of an international conference, Society for Underwater Technology, London. Chap. 13, 181 - 202 (1987).

Putnam, J.A. and Johnson, J.W., *The dissipation of wave energy by bottom friction*, Transactions Am. Geophys. Union, 30, 67 - 74 (1949).

Radder, A.C., *On the parabolic equation method for water wave propagation*, J. Fluid Mech. 95, 159 - 176 (1979).

Vincent, C.E. and Carrie, A., *Evaluation of an energy propagation wave refraction model*, Continental Shelf Res. 8 (3), 287 - 305 (1988).

Wilson, B.W., *Numerical prediction of ocean waves in the North Atlantic for December, 1959*, Deutsche Hydrographische Zeitschrift, 18 (3), 114 - 130 (1965).

International Conference on
Numerical and Hydraulic Modelling of Ports and Harbours
Birmingham, England: 23-25 April 1985

PAPER J3

A NUMERICAL MODEL FOR WAVE BOUNDARY CONDITIONS IN PORT DESIGN

N. Booij, L.H. Holthuijsen and T.H.C. Herbers
Scientific officers at the Delft University of Technology, Department of Civil Engineering, the Netherlands

Synopsis

This paper describes a numerical model to compute the propagation, generation and dissipation of irregular waves in coastal regions with uneven bottom topography and arbitrary current patterns. This model is based on the energy (or action) balance of the waves including the effects of refraction, growth by wind and decay by bottom friction and surf breaking. The wave spectrum is represented as discrete spectral over the directions and parametric over the frequencies, i.e. for each spectral direction the model determines the wave energy density and the mean wave frequency.
Test computations for the approach area of San Ciprian (Spain) are compared with observations in a laboratory with emphasis on the effects of refraction and short-crestedness.
The model is part of a comprehensive package for the computation of waves, currents and water levels from meteorological and topographical data in the marine environment.

Introduction

For the practice of predicting waves in coastal regions and harbours it is convenient to distinguish a sequence of stages in the development of the waves: wave generation and propagation in open sea, propagation and decay in coastal regions and penetration into a harbour. In view of the large variation in scale and in physical processes during these stages it is practical to use a different type of model for each of these stages.

At the Delft University of Technology a comprehensive program package called Ocean Pack is being developed which contains the above three types of wave models. These models are supplemented with a storm surge/tide model to account for the potentially strong effect of currents on the waves in coastal regions (e.g. tidal flats, estuaries). A relation diagram for the models is given in fig. 1.
The deep water wave model is a non-stationary directionally decoupled hybrid model to compute the development of sea and swell along straight rays pointing towards a chosen hindcast location for arbitrary wind fields. This model provides boundary conditions to the shallow water model. This shallow water model computes stationary wave conditions for an arbitrary bottom topography and current pattern for a constant wind. It provides boundary conditions to the model for wave penetration in harbours (diffraction). The harbour penetration model is based on the boundary element method, implying stationary wave conditions. The stationarity condition for both the shallow water model and the harbour penetration model is acceptable in most cases inview of the relatively short travel time of the waves through the coastal areas of interest. If a significant influence of currents or water levels on the waves is expected e.g. in tidal areas or estuaries, the non-stationary storm surge/tide model in the package provides the required data to the shallow water model. The storm surge/tide model can also be used independently from the wave models.

The present paper is concentrated on the shallow water model (HISWA = HIndcasting Shallow WAter waves). The wave conditions are computed in this model from the local balance of wave quantities taking into account wave growth and decay. This approach is fairly conventional for open sea wave models but HISWA differs from presently operating models in that the energy (or action) balance equation considered contains wave-current interaction terms, and in that the energy density of the waves is evaluated over a grid (rather than along wave rays) with the inclusion of surf breaking.

In most models currently used in coastal or harbour engineering, wave propagation in coastal regions is computed with the so-called ray method for refraction, either in a monochromatic approach (e.g. Wiegel, 1964) or in a discrete spectral approach (e.g. Piest, 1965 , Cavaleri and Malanotte Rizzoli, 1981). Recently Sakai (1983) developed a shallow water propagation model using a grid rather than rays based on the work of Karlsson (1969). It considers the propagation of spectral wave components from discrete spectral directions at one fixed frequency. The HISWA model can in this respect be considered to be a further development of the propagation model bij Sakai (1983) in the sense that for each spectral wave direction one frequency is used but that in the HISWA model this frequency (and the associated energy density) can change under the influence of wind, current and bottom. The alternative choice of having many frequencies each with its energy concentrated in one direction has been implemented by Cheng and Wang (1983).

Diffraction may affect the propagation of waves in regions with high spatial gradients of wave energy. Ideally, a mathematically well formulated model should be used to combine refraction and diffraction. Examples of such models are the mild-slope equation of Berkhoff (1976) or the parabolic version of this equation by Radder (1979) and Booij (1981). However, computations with numerical models based on these equations are prohibitively expensive for many applications as the grid of these models has a very high spatial resolution (mesh-size is a small fraction of the wave length). Diffraction is therefore only crudely approximated in the HISWA model by means of a diffusion term.

Held at Birmingham University. Organised and sponsored by BHRA, The Fluid Engineering Centre in conjunction with the Department of Civil Engineering of Birmingham University. Co-sponsored by the International Association for Hydraulic Research.

The development of wave energy in the HISWA model is conventional in the sense that the modelling of each relevant physical process is taken from literature. The development of the wave period as affected by the various physical processes is not always available in the literature. Ad hoc assumptions are therefore made which still need to be verified with observations in the field.

The paper consists of the following sections: section 2 in which the mathematical formulation of the HISWA model is given; section 3 in which a test case relevant to harbour design is described and section 4 in which we formulate our conclusions.

The HISWA-model

Spectral models for wave prediction are usually applied in situations without current. These models can therefore be based on the spectral balance equation of the waves (e.g. Gelci et al., 1956; Hasselmann, 1960):

$$\frac{D}{Dt} E(\omega,\theta;\underline{x},t) = S \qquad (1)$$

in which E is the spectral energy density which is a function of frequency ω, direction θ, horizontal location $\underline{x}$ and time t. The rate of change of E in a system moving with the energy, DE/Dt is equal to the net result of all processes of wave generation and dissipation, denoted by S. For the definition of D/Dt we refer the reader to the Appendix. But, the HISWA model described here, is to be applied also in situations with current. It is therefore based on the action balance equation instead of the energy balance equation because wave action is conserved in the presence of a mean current whereas wave energy is not (Bretherton and Garrett, 1969):

$$\frac{D}{Dt} A(\omega,\theta;\underline{x},t) = T \qquad (2)$$

The action density A is defined as

$$A = E/\sigma \qquad (3)$$

in which σ is the frequency relative to the current

$$\sigma = \omega - \underline{k}.\underline{U} \qquad (4)$$

in which $\underline{k}$ is the wavenumber vector and $\underline{U}$ is the current vector. The source function for wave action is denoted with T. It is possible to integrate the action balance equation over $\underline{x}$-space for each combination of frequency and direction to obtain in each point of the area of interest the two-dimensional action density spectrum. This action density spectrum is readily transformed to the energy density spectrum with the local relative frequency σ. Such a discrete spectral approach would be extremely expensive in many cases due to the nonlinear character of the energy source term S (e.g. Hasselmann et al., 1973) and hence also for the action source term T. Some degree of parameterization is therefore called for. Two alternatives are available: (a) parameterize the source term and evaluate the balance equation for each spectral component (so-called discrete spectral wave models) and (b) parameterize the wave spectrum and reformulate the balance equation to obtain a small number of prognostic equations (so-called parametric models). These alternatives represent either a very large degree of freedom (discrete spectral models have typically 100-200 spectral components, e.g. Gelci et al., 1956; Ewing, 1971; Barnett, 1968) or a very limited degree of freedom (parametric models have typically 2-5 prognostic parameters, e.g. Wilson, 1965; Sanders, 1976; Günther, 1981). We consider here another alternative as a compromise between the above two types of models: a model which is parametric in frequencies but discrete spectral in the directions. That is, the model predicts two prognostic parameters for each of the chosen discrete spectral directions (a parametric, directionally decoupled model). We choose for the prognostic variables the directional ~~energy~~ action density A_o and the mean action frequency ω_o, defined as

$$A_o(\theta) = \int_0^\infty A(\omega,\theta)d\theta \qquad (5)$$

and

$$\omega_o(\theta) = \int_0^\infty \omega\, A(\omega,\theta)d\omega/A_o \qquad (6)$$

The prognostic equations for A_o and ω_o are obtained basically by applying the definition operators in equations (5) and (6) to the balance equation. The result for the prognostic equation for A_o is simply

$$\frac{D}{Dt} A_o(\theta) = T_o(\theta) \qquad (7)$$

in which

$$T_o(\theta) = \int_0^\infty T(\omega,\theta)d\omega \qquad (8)$$

The result for the prognostic equation for ω_o is initially

$$\frac{D}{Dt} (\omega_o(\theta)A_o(\theta) = \int_0^\infty \omega T(\omega,\theta)d\theta \qquad (9)$$

but this equation can be reformulated with the help of equation (7) to give (dropping θ from the notation)

$$\frac{D}{Dt} (\omega_o A_o) = \omega_o T_o + A_o \frac{d\omega_o}{dt} \qquad (10)$$

The definition of the operator d/dt is given in the Appendix. The prognostic equations (7) and (10) contain two source terms which need to be elaborated. The first is $d(\omega_o)/dt$ which is the rate of change of ω_o due to dissipative and energy generating processes. It will be estimated from information in the literature or from ad-hoc assumptions. The second source term is T_o which we will express in terms of the rate of change of the total wave energy in the absence of current as follows. Eventually it will also be estimated from information in the literature or from ad-hoc assumptions.

If we assume that the normalized growth rate of the total wave energy $E_o(\theta) = \int E(\omega,\theta)d\theta$ is large compared with the normalized development rate of ω_o/σ_o,

$$\frac{1}{E_o}\frac{DE_o}{Dt} >> \frac{1}{(\omega_o/\sigma_o)}\frac{d(\omega_o/\sigma_o)}{dt} \qquad (11)$$

then we may write for each spectral direction

$$\frac{D}{Dt} (\omega_o A_o) = \frac{\omega_o}{\sigma_o}\frac{DE_o}{Dt} \qquad (12)$$

in which

$$\sigma_o \equiv \int_0^\infty \sigma A \, d\omega / A_o \qquad (13)$$

and

$$E_o \equiv \int_0^\infty E \, d\omega \qquad (14)$$

Substitution of (12) in (7) and (10) gives the final expressions for the prognostic equation for A_o and ω_o:

$$\frac{DA_o}{Dt} = \frac{1}{\sigma_o}\frac{DE_o}{Dt} - \frac{A_o}{\omega_o}\frac{d\omega_o}{dt} \qquad (15)$$

$$\frac{D}{Dt}(\omega_o A_o) = \frac{\omega_o}{\sigma_o}\frac{DE_o}{Dt} \qquad (16)$$

in which DE_o/Dt and $d\omega_o/dt$ will be taken from literature as far as possible.

The above expressions (15) and (17) are Lagrangian in nature. The HISWA-model is implemented on a grid which requires an Eulerian formulation. The Eulerian equivalent of equations (15) and (17) is therefore used in the HISWA model (stationary situation):

$$\frac{\partial}{\partial x}(c_{x_o} A_o) + \frac{\partial}{\partial y}(c_{y_o} A_o) + \frac{\partial}{\partial \theta}(c_{\theta_o} A_o) = = \frac{1}{\sigma_o}\frac{DE_o}{Dt} - \frac{A_o}{\omega_o}\frac{d\omega_o}{dt} \qquad (17)$$

$$\frac{\partial}{\partial x}(c_{x_o} \omega_o A_o) + \frac{\partial}{\partial y}(c_{y_o} \omega_o A_o) + \frac{\partial}{\partial \theta}(c_{\theta_o} \omega_o A_o) = = \frac{\omega_o}{\sigma_o}\frac{DE_o}{Dt} \qquad (18)$$

in which

$$\begin{aligned} c_{x_o} &= c_g \cos\theta + U_x \\ c_{y_o} &= c_g \sin\theta + U_y \\ c_{\theta_o} &= -\frac{1}{k}\frac{\partial \sigma}{\partial d}\frac{\partial d}{\partial n} - \frac{\underline{k}}{k}\cdot\frac{\partial \underline{U}}{\partial n} \end{aligned} \qquad (19)$$

c_g being the group velocity relative to the current, and n the direction in space normal to θ. $\underline{U}$ is the current velocity.

The value of DE_o/Dt, i.e. the growth of wave energy density $E_o(\theta)$ is taken equal to its growth in the ideal situation of a limitless ocean with a homogeneous and stationary wind field. The results of the SWAMP study (Allender et al., 1981) were used to express DE_o/Dt in terms of E_o assuming a $\cos^2(\theta)$- directional distribution. The effect of a mean current is taken into account by using the wind relative to the current instead of the actual wind. The development of the mean action frequency $\omega_o(\theta)$ is assumed to be directly related to the growth of $E_o(\theta)$. The formulation in HISWA is based on an assumed universal relationship between the total wave energy and the mean frequency. When the wave field does not conform to this universal relationship (e.g. due to changes in the bottom or current pattern or through arbitrarily chosen boundary wave conditions), the evolution of ω_o is adapted to force the wave field towards this relationship (similar to the results of Günther, 1981, his fig. 14).

The decay of the waves is modelled for three processes: bottom friction, surf dissipation and wave-current interaction. The bottom dissipation is based on a fairly conventional nonlinear bottom friction model which includes the effects of currents on the dissipation (quadratic friction law ,Putnam and Johnson, 1949). The change in the mean frequency $\omega_o(\theta)$ is directly related to the energy dissipation with a simple ad-hoc formulation assuming that the spectrum conforms to a k^{-3} shape (k is wavenumber, see Kitaigorodskii et al., 1975). Surf dissipation is modelled in the HISWA model to dissipate energy in breaking waves. The formulation is from Battjes and Jansen (1978) which is based on a bore model applied to a given highest fraction of the waves in a random wave field. The corresponding change in mean wave frequency is directly related to the energy dissipation by a simple ad-hoc formulation. In addition to this dissipation (which relates to breaking on a beach and to breaking on an opposing current) another dissipation mechanism for opposing currents is modelled in the HISWA model. This is the loss of wave energy which is carried by frequencies (spectral frequencies) which cannot travel up-stream. A simple relaxation model is used to remove this high-frequency energy from the wave field.

Numerical background

The conventional method of computing wave propagation in shallow water is based on a solution with characteristics (the so-called ray technique, e.g. Cavaleri and Malanotte Rizzoli, 1981). However, if nonlinear source terms (e.g. bottom dissipation or wave breaking) are to be incorporated in the model this ray technique is relatively inefficient due to the large number of information transfers between the rays. To avoid this we have chosen to perform all computations on a grid (see also Sakai et al., 1983). The three independent dimensions in the model are x and y for location and θ for spectral direction, the grid is therefore three-dimensional. The computations are performed in downwave direction as in the parabolic model of Radder (1979) and Booij (1981). The direction in which the computation progresses is equal to the positive x-axis of the grid sothat this axis needs to be chosen parallel to the main wave direction in the area.

The method of computation is an explicit finite difference method which can be considered as an iterative approximation of the Crank-Nicholson scheme (Abbott, 1979; Richtmyer and Morton, 1967). As with any other explicit method this scheme is subject to stability constraints, viz.,

$$\frac{\Delta x}{\Delta y} \leq \frac{c_x}{c_y} \qquad (20a)$$

and

$$\frac{\Delta x}{\Delta \theta} \leq \frac{c_x}{c_\theta} \qquad (20b)$$

in which Δx, Δy and $\Delta\theta$ are the increments in location and direction. In absence of currents inequality (20a) can be rewritten as

$$\frac{\Delta x}{\Delta y} \leq \operatorname{cotg}\theta \qquad (21)$$

where θ is the spectral propagation direction measured counterclockwise from the positive

x-axis. When Δx and Δy are chosen, it follows that θ must remain within a certain sector:

$$-\theta_o \leq \theta \leq \theta_o \qquad (22)$$

The value of θ_o is always less than 90°. All waves outside the sector defined by (22) are neglected in the HISWA model. A wave field which refracted so far from the x-axis that part of the waves travel outside this directional sector will induce a non-physical loss of energy in the model.

A test

We demonstrate here the performance of the model as far as refraction is concerned. The test area is the approach to San Ciprian harbour (Spain). This area was also used by Stive and Dingemans (1983) to test the parabolic model mentioned earlier (Radder, 1979; Booij, 1981). The computational results are compared with observations in a laboratory with emphasis on the effect of short-crestedness.

In the test area considered the dominant effect on the wave field is refraction. The influence of directional spreading of the incident wave field on the distribution of wave energy is demonstrated.

In the study of Stive and Dingemans (1983) a physical model has been used to investigate the wave conditions along a projected breakwater at the entrance of the harbour of San Ciprian (see fig. 2). The present test is therefore concentrated on the wave height distribution along this breakwater. The waves are uni-directional in the physical model since they were generated by means of a rigid wave board. The HISWA model, which accomodates finite directional spreading is therefore used with a very narrow direction distibution. The directional distribution of the incident waves was accordingly modelled as $D_1(\theta) = A_1 \cos^{64}(\theta-\theta_i)$ in which θ_i = mean direction of the incoming wave field and A_1 is a normalisation coefficient.
The influence of wind and dissipation due to bottom friction has been taken equal to zero in the computation, which corresponds to the situation in the physical model. Dissipation due to surf breaking was also taken into account, but it was assumed that breaking has no effect on the average frequency.

To demonstrate the effect of short-crestedness (increased directional energy spreading), the computations were also carried out with a wider directional distribution $D_2 = A_2 \cos^2(\theta-\theta_i)$ in which A_2 is a normalization factor. This distribution is more characteristic for waves in a storm than the long-crested waves in the physical model (or in the $\cos^{64}$ distribution) which are more typical for swell. For both computations with the HISWA model the wave height and wave period at the northern boundary of the model were 5.5 m and 12 s respectively while the main wave direction at this boundary was 180° (nautical convention).

The spatial wave height distribution obtained with the computations for the long-crested waves (fig. 3) indicates a concentration of energy due to the focussing effect of the "hillock" in the sea bottom located at about 1500 m north of the seaward end of the breakwater. A fairly narrow beam of wave energy is directed towards the end of the breakwater. This is also seen in the wave height distribution along the breakwater (fig. 4) where the maximum wave height is considerably higher than the incoming wave height. The computation results agree fairly well with the observations in the physical model.

The effect of short-crestedness is to smooth the spatial wave height distribution (fig. 5). The distribution along the breakwater shows (fig. 2) that the maximum wave height is greatly reduced compared with the long-crested wave situation. It is apparently essential to consider in the design of this breakwater to what extent the design conditions are those of a swell or of a local storm.

Summary and conclusions

A description has been given of a numerical model to compute wave conditions in coastal regions taking into account wind-, bottom- and current effects. In addition to the primary wave parameters significant wave height, average frequency and main wave direction, the model also predicts the frequency integrated directional energy distribution of the waves and an average wave frequency for each spectral direction. These quantities are computed on a regular grid which permits a ready determination of derived quantities such as radiation stress gradient at each gridpoint in the area.

Results of computations of refractive wave propagation for long-crested waves which approach a projected breakwater off San Ciprian (Spain) agree fairly well with observations in a physical model. For these long-crested waves a considerable energy concentration occurs on the breakwater. It is shown with additional computations that introducing short-crestedness in the wave field reduces this concentration considerably.

Acknowledgements

The development of the HISWA model has been commissioned by the Ministry of Public Works in the Netherlands. We appreciate the permission of this Ministry to publish the above material. We thank M.J.F. Stive of the Delft Hydraulic Laboratory for providing us with information that supplemented reference Stive and Dingemans (1983).

Appendix

The operators D/Dt and d/dt are defined as follows

$$\frac{D}{Dt} Q = \frac{\partial Q}{\partial t} + \frac{\partial}{\partial x}(c_x Q) + \frac{\partial}{\partial y}(c_y Q) + \frac{\partial}{\partial \theta}(c_\theta Q) + \frac{\partial}{\partial \omega}(c_\omega Q),$$

and

$$\frac{d}{dt} Q = \frac{\partial Q}{\partial t} + c_x \frac{\partial Q}{\partial x} + c_y \frac{\partial Q}{\partial y} + c_\theta \frac{\partial Q}{\partial \theta} + c_\omega \frac{\partial Q}{\partial \omega},$$

in which Q is the quantity to be transported and c_x, c_y, c_θ and c_ω are propagation speeds in respectively x-, y-, θ- and ω-domain.

The fact that the model is stationary means that $\partial Q/\partial t = 0$, not $dQ/dt = 0$ or $DQ/Dt = 0$.

References

Abbott, M.B., (1979), "Computational Hydraulics", Pitman, London.

Allender, J. et al., (1981), "Sea Wave Modelling Project (SWAMP)",Proceedings Conference on Turbulent Fluxes through the Sea Surface, Wave Dynamics and Prediction, Miami, 1981, NATO Conference series V, Plenum Press.

Barnett, T.P., (1968), "On the generation, dissipation and prediction of ocean wind waves", Journal of Geophysical Research, Vol. 73, No. 2, pp. 513-534.

Battjes, J.A. and J.P.F.M. Jansen, (1978), "Energy loss and set-up due to breaking of random waves", Proceedings 16th Coastal Engineering Conference, Hamburg, ASCE, New York, pp. 569-587.

Berkhoff, J.C.W. (1976), "Mathematical models for simple harmonic linear water waves; wave diffraction and refraction". Delft Hydr. Lab., Publ. No. 163.

Booij, N., (1981), "Gravity waves on water with non-uniform depth and current". Dissertation, Delft Univ. Techn., Dept. of Civil Engineering.

Bretherton, F.P. and G.J.R. Garrett (1969), "Wavetrains in inhomogeneous moving media". Proc. Roy. Soc., A, vol. 302, pp. 529-554.

Cavaleri, L. and P. Malanotte Rizzoli, (1981), "Wind wave prediction in shallow water: theory and applications", Journal of Geophysical Research, Vol. 86, No. C11, pp. 10961-10973.

Chen, Y. and Wang, H., (1983), "Numerical model for Nonstationary Shallow Water Wave Spectral Transformations", Journal of Geophysical Research, Vol. 88, No. C14, pp. 9851-9863.

Ewing, J.A., (1971), "A numerical wave prediction model for the North Atlantic Ocean", Deutsche Hydrographische Zeitschrift, Vol. 24, No. 6, pp. 241-261.

Gelci, R., H. Cazale and J. Vassal, (1956), "Utilization des diagrammes de propagation à la prévision énergétique de la houle", Bulletin d'information du Comité central d'oceanographie et d'études des côtes, Vol. 8, No. 4, pp. 169-197.

Günther, H. et al.,(1979), "A hybrid parametrical wave prediction model", Journal of Geophysical Research, Vol. 84, C9, pp. 5727-5738.

Günther, H., (1981), "A parametric surface wave model and the statistics of the prediction parameters", Hamburger Geophysikalische Einzelschriften, Universität Hamburg und Max-Planck-Institute für Meterologie, Reihe A Heft 55.

Hasselmann, K., (1960), "Grundgleichungen der Seegangsvoraussage", Schiffstechnik, Vol. 7, Heft 39, pp. 191-195.

Hasselmann, K. et al., (1973), "Measurements of wind-wave growth and swell decay during the Joint North Sea Wave Project (JONSWAP)", Ergänzungsheft zur Deutschen Hydrographischen Zeitschrift, Reihe A(8), No. 12.

Karlsson, T., (1969), "Refraction of continuous ocean wave spectra", Journal of the Waterways and Harbour Division, ASCE, Vol. 95, No. WW4, pp. 437-448.

Kitaigorodskii, S.A., et al., (1975), "On Phillips theory of equilibrium range in the spectra of wind-generated gravity waves", Journal of Physical Oceanography, Vol. 5, pp. 410-420.

Piest, J., (1965), "Seegangsbestimmung und Seegangsrefraktion in einem Meer mit nicht-ebene Boden - eine theoretische Untersuchung", Deutsche Hydrographische Zeitschrift, Vol. 18, No. 6, pp. 253-260.

Putnam, J.A. and J.W. Johnson, (1949), "The dissipation of wave energy by bottom friction", Trans. Am. Geophys. Union, Vol. 30, No. 1, pp. 67-74.

Radder, A.C., (1979), "On the parabolic equation method for water wave propagation". J. Fluid Mech., Vol. 95, pp. 159-176.

Richtmyer, R.D. and K.W. Morton, (1967), "Difference methods for initial value problems", Interscience publ., New York.

Sakai, T., M. Kosecki and Y. Iwagaki, (1983), "Irregular wave refraction due to current", Journal of Hydraulic Engineering ASCE, Vol. 109, No. 9, paper no. 18233, pp. 1203-1215.

Sanders, J.W., (1976), "A growth-stage scaling model for the wind-driven sea", Deutsche Hydrographische Zeitschrift, Vol. 29, No. 4, pp. 136-161.

Stive, M.J.F. and M.W. Dingemans, (1983), "Verification of the refraction-diffraction wave propagation model CREDIZ in a realistic laboratory situation; report on investigation", Delft Hydraulics Lab., December 1983, no. S 581.

Wiegel, R.L., (1964), "Oceanographical Engineering", Fluid Mechanics Series Prentice-Hall.

Wilson, B.W., (1965), "Numerical prediction of ocean waves in the North Atlantic for December 1959", Deutsche Hydrographysche Zeitschrift, Vol. 18, No. 3, pp. 114-130.

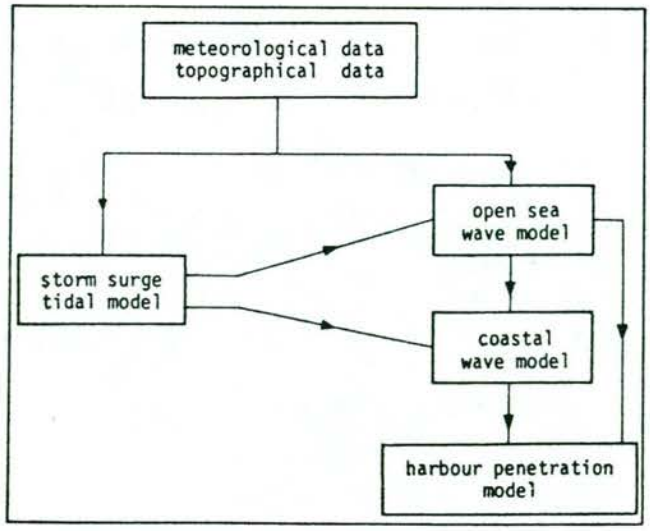

Fig. 1 Relation diagram for Ocean Pack.

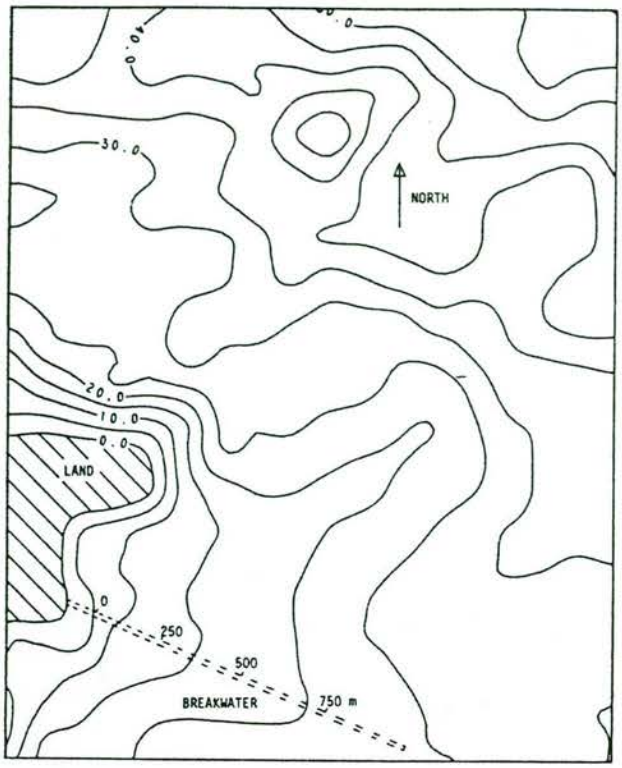

Fig. 2 Bathymetry in area off San Ciprian, contourline interval is 5.0 m. Projected breakwater is indicated with dashed lines.

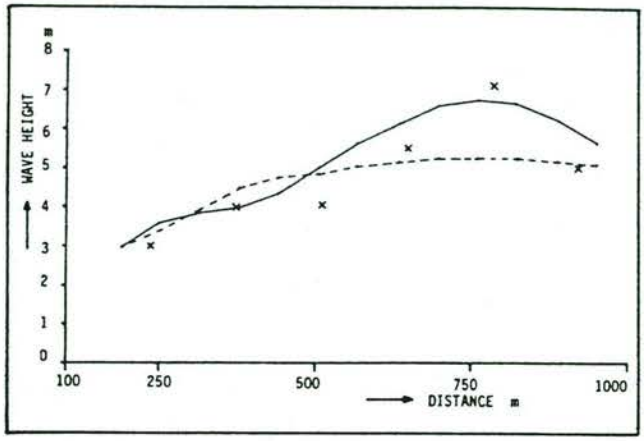

Fig. 4 Observed and computed wave height distribution along projected breakwater. Crosses indicate the observations, drawn line indicates long-crested waves computations, dashed line indicates short-crested waves computations.

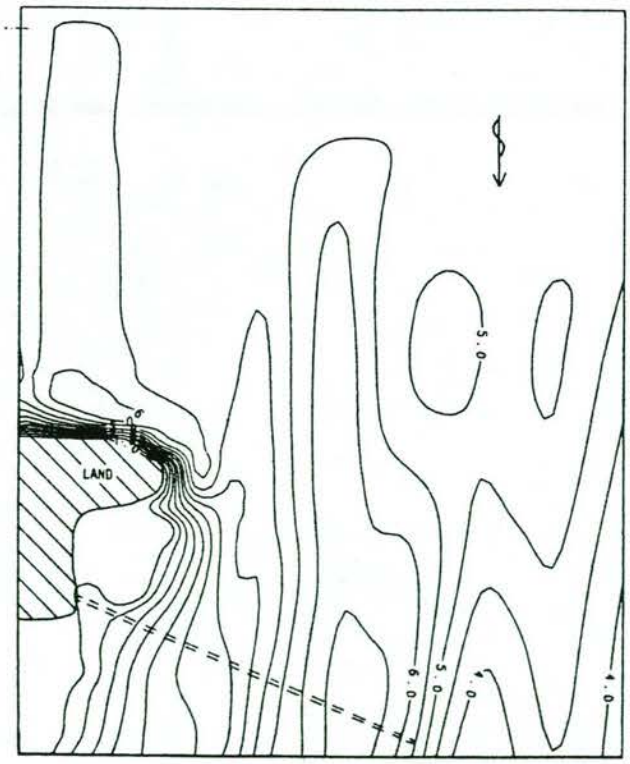

Fig. 3 Computed wave height distribution in area of projected breakwater for long-crested waves approaching from North. Contourline interval is 0.5 m.

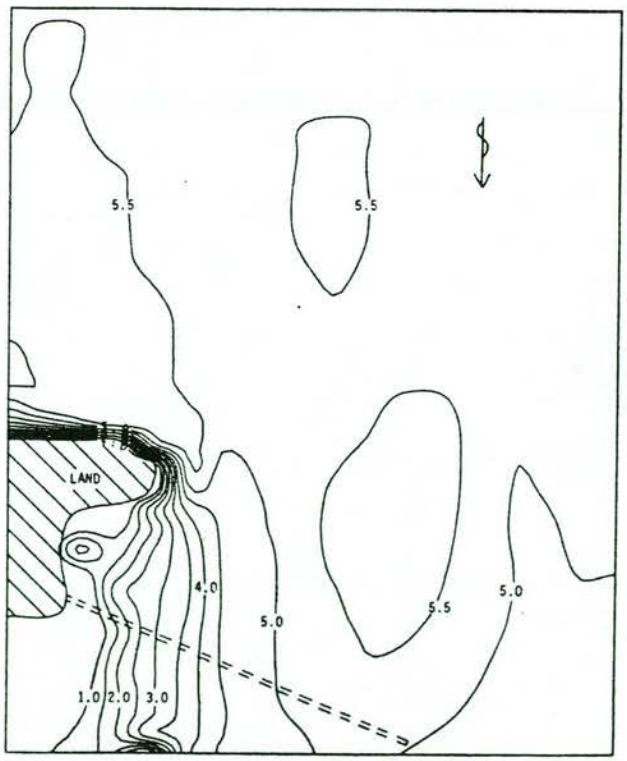

Fig. 5 Computed wave height distribution in area of projected breakwater for short-crested waves approaching from North. Contourline interval is 0.5 m.

Coastal Engineering Conference, Taiwan, 1986

CHAPTER 20

A GRID MODEL FOR SHALLOW WATER WAVES

Leo H. Holthuijsen
and Nico Booij *)

1. INTRODUCTION

Waves in coastal regions can be affected by the bottom, by currents and by the local wind. The traditional approach in numerical modelling of these waves is to compute the wave propagation with so-called wave rays for mono-chromatic waves (one constant period and one deep water direction) and to supplement this with computations of bottom dissipation. This approach has two important disadvantages. Firstly, spectral computations, e.g. to determine a varying mean wave period or varying short-crestedness, would be rather inefficient in this approach. Secondly, interpretation of the results of the refraction computations is usually cumbersome because of crossing wave rays. The model presented here has been designed to correct these shortcomings: the computations are carried out efficiently for a large number of wave components and the effects of currents, bottom friction, local wind and wave breaking are added. This requires the exploitation of the concept of the spectral action balance equation and numerical wave propagation on a grid rather than along wave rays.

The model has been in operation for problems varying from locally generated waves over tidal flats to swell penetration into Norwegian fjords. A comparison with extensive measurements is described for young swell under high wind penetrating the Rhine estuary.

2. THE MODEL

2.1 Introduction

The representation of the wave spectrum in the model is parametric in frequency and discrete spectral in directions, that is, for each spectral direction two prognostic variables are defined: a directional energy density and a mean frequency. The model treats the

*) scientific officers, Delft University of Technology, Stevinweg 1, Delft, the Netherlands.

action balance of the waves for each spectral direction separately (the action balance is used to accommodate current effects). It is therefore a directionally decoupled parametric model.

Propagation of waves in the model is based on the linear theory for bottom and current refraction, while wave generation and dissipation is taken mostly from the literature. The balance equations for the basic wave parameters are integrated with a finite difference method on a regular grid in the study area. This approach avoids the classical problem of crossing rays and caustics frequently occurring in the more conventional wave ray technique. The computations are performed in downwave direction as in the parabolic wave propagation of Radder (1979).

2.2 Equations

Wave hindcasting models are usually based on the energy balance equation of the waves (e.g. Gelci et al., 1956; Hasselmann, 1960). However, in the presence of a mean current it is wave action that is conserved (e.g. Bretherton and Garrett, 1968). Since we wish to include in our model the influence of currents, we base our model on the action balance equation. Wave action in this balance equation is a function of time (t), space (x,y), direction (θ) and frequency (ω). Since in coastal regions a high spatial resolution is required, in view of the scale of the bottom irregularities, some parameterization of the balance equation is necessary to reduce the computer effort. In such a parameterization the directional details of the wave spectrum should be retained since the occurrence of cross-seas is an essential aspect of the wave field in coastal regions. We have therefore parameterized the action balance equation in the frequency domain only, while we retained the discrete spectral direction as independent variable. We have chosen the zero-th and first moment of the action spectrum in the frequency domain as the quantities appearing in the parameterized balance equations. The corresponding two basic wave parameters are the directional action density $A_0(\theta)$ and the mean frequency per direction $\omega_0(\theta)$:

$$A_0(\theta;x,y,t) = \int_0^{\infty} A(\omega,\theta;x,y,t)d\omega \qquad (1)$$

$$\omega_0(\theta;x,y,t) = \frac{1}{A_0}\int_0^{\infty} \omega A(\omega,\theta;x,y,t)d\omega \qquad (2)$$

The conservation equations for the zero-th moment $A_0(\theta)$ and for the first moment $\omega_0(\theta)A_0(\theta)$ are derived essentially by applying the definition operators (1) and (2) to the action balance equation of the waves. With some assumptions added, the results are

(Booij and Holthuijsen, 1987):

$$\frac{\partial A_0}{\partial t} + \frac{\partial}{\partial x}(c_{0x}A_0) + \frac{\partial}{\partial y}(c_{0y}A_0) + \frac{\partial}{\partial \theta}(c_{0\theta}A_0) = \frac{1}{\sigma_0}S_E - \frac{A_0}{\omega_0}S_\omega \qquad (3)$$

$$\frac{\partial}{\partial t}(\omega_0 A_0) + \frac{\partial}{\partial x}(c_{0x}\omega_0 A_0) + \frac{\partial}{\partial y}(c_{0y}\omega_0 A_0) + \frac{\partial}{\partial \theta}(c_{0\theta}\omega_0 A_0) = \frac{\omega_0}{\sigma_0}S_E \qquad (4)$$

in which c_{0x} and c_{0y} are the x- and y-components respectively of the propagation velocity c_0 at frequency ω_0 in direction θ and $c_{0\theta}$ is the rate of directional change of A_0 (i.e. refraction). $S_E(\theta)$ is the rate of change of the directional energy density $E_0(\theta)$ and $S_\omega(\theta)$ is the rate of change of the direction dependent mean wave frequency $\omega_0(\theta)$. $E_0(\theta)$ is taken to be equal to $A_0(\theta)\,.\,\sigma_0(\theta)$, σ_0 being the average frequency relative to the mean current. The advantage of expressing the developments of $A_0(\theta)$ and $\omega_0(\theta)A_0(\theta)$ in terms of the (direction dependent) source terms $S_E(\theta)$ and $S_\omega(\theta)$ is that these source terms can be estimated, at least to a large extent, from information in the literature.

2.3 Propagation

The conventional approach for computing refractive propagation in shallow water is to use solutions along characteristics (wave rays). However, in such an approach, which is of a Lagrangian nature, the determination of nonlinear wave generation or dissipation would require extensive numerical interactions between different wave rays. This is numerically rather inefficient since a large number of spatial interpolations between the spatially scattered wave rays would be needed. We have therefore chosen for the above Eulerian formulation of propagation i.e. refraction computations on a regular grid (e.g. Karlson, 1969; Sakai et al., 1983). All wave information required for the evaluation of nonlinear source terms is then intrinsically available at each grid point.

For coastal waters and inland waters the travel time of the waves through the area of interest is usually small compared with the time scales of wind and current (e.g. tides). The situation may then be considered as stationary so that the terms with $\partial/\partial t$ vanish from equations (3) and (4).

In the absence of currents the second and third terms on the left-hand side of equation (3) or (4) represent propagation at the group velocity of the waves along straight lines which in varying water depths accounts for the phenomenon of "shoaling". In the presence of currents this propagation is corrected by adding the current velocity to the group velocity:

$$c_{0x} = c_0 \cos\theta + V_x \tag{5}$$

$$c_{0y} = c_0 \sin\theta + V_y \tag{6}$$

in which c_0 is the propagation speed (group velocity) at frequency ω_0 from linear wave theory relative to the mean current (V_x,V_y). The fourth term on the left-hand side of equation (3) represents the change of direction of the action transport, i.e. refraction, induced by bottom- and current variations. From linear wave theory we find the rate of directional change $c_{0\theta}$:

$$c_{0\theta} = -\frac{1}{k_0}\left(\frac{\partial\sigma}{\partial d}\right)_0 \frac{\partial d}{\partial n} - \frac{k_0}{k_0}\cdot\frac{\partial V}{\partial n} \tag{7}$$

in which n is the coordinate in (x,y)-space normal to the spectral wave direction θ, $\underline{V}$ is the mean current vector (V_x,V_y), $\underline{k}_0$ is the wave number vector corresponding to ω_0 with magnitude k_0 and direction θ and $(\partial\sigma/\partial d)_0$ is the depth derivative of σ for $k=k_0$.

2.4 Generation and dissipation

The generation and dissipation of the waves in the conservation equations (3) and (4) is expressed in terms of the direction dependent source terms $S_E(\theta)$ and $S_\omega(\theta)$. These source terms can be interpreted as the rates of change of $E_0(\theta)$ and $\omega_0(\theta)$ in a homogeneous situation. Each is the sum of the effects of wind wave generation, bottom dissipation, wave breaking and wave blocking on an opposing current. We therefore write the source functions $S_E(\theta)$ and $S_\omega(\theta)$ as the sum of constituent source terms.

The formulation of the source term for wave generation by wind is taken from empirical information in an idealized situation (CERC, 1973). This situation is one in which a homogeneous, stationary wind U blows over deep water perpendicularly off a long and straight coastline. Expressions are available in the literature giving the total energy and the frequency averaged over the whole spectrum as functions of fetch and wind speed. In order to obtain the source terms of wind growth as function of θ, it is assumed that in the above idealized case the energy distribution over θ is of the form $\cos^2(\theta)$, and that the averaged frequency in the idealized situation is independent of direction.

Bottom dissipation in our model is based on the conventional quadratic friction law to represent bottom shear stress. The corresponding energy dissipation for a harmonic wave

with height H and frequency ω (e.g. Putnam and Johnson, 1949) has been extended by Dingemans (1983) to random waves. The form of this expression can be seen as a measure for the orbital velocity multiplied with a measure for the bottom shear stress. The required directional version of this expression is obtained by multiplying a measure for the total orbital velocity with an expression for the shear stress based on the directional energy density and the directional mean frequency. To formulate the source term for the average frequency change due to bottom dissipation we assume a simple spectral shape and a concentration of the dissipation at the lower frequency side of this spectrum. The assumed shape of the spectrum is: zero for frequencies below the peak frequency and a ω^{-m}-tail for frequencies above the peak frequency. The result is an expression relating the source term of the bottom induced frequency change to that of the bottom induced energy change.

The source term for energy dissipation due to wave breaking caused by exceedence of steepness or exceedence of a wave height to depth ratio, is modeled after Battjes and Janssen (1978). Dissipation in this model is based on a bore model. As in the case of bottom friction, only total dissipation is obtained this way. The corresponding directional distribution of dissipation is obtained by assuming that the dissipation per direction is proportional to the energy density at that direction. The frequency change induced by breaking due to steepness is assumed to be zero. For the frequency change due to depth breaking a similar expression is used as described above for bottom friction.

In a situation with a strong opposing current some fraction of the wave energy cannot be transported upstream because the group velocity of the highest frequencies in the spectrum is less than the opposing current velocity. The lowest frequency above which this phenomenon of wave blocking occurs (the critical frequency ω_c) is the maximum frequency for which a solution exists for the wavenumber in the dispersion relationship from linear wave theory (including a mean current). In the model the "blocked" energy is dissipated with a simple relaxation model in which the total wave energy reduces eventually to the "unblocked" energy. The average frequency is similarly reduced to the average frequency of the "unblocked" energy.

3. NUMERICAL BACKGROUND

The prognostic equations for $A_0(\theta)$ and for the product $\omega_0(\theta)A_0(\theta)$, equations (3) and (4), are partial differential equations of first order with the horizontal coordinates x and y and the spectral direction θ as independent variables. Due to the nature of the equation the state in a point in (x,y,θ)-space (e.g. the value of A_0) is determined by the state upwave

from this point (upwave as defined by the propagation speeds c_{0x}, c_{0y} and the directional rate of change $c_{0\theta}$). We have therefore chosen for an upstream finite difference scheme.

The boundary conditions for these partial differential equations are in general that the incoming wave field should be given at the boundaries and that the outgoing wave field is fully absorbed by the boundaries. To fully exploit the stationarity of the wave field in our model we restrict wave directions to a constant directional sector of less than 180° (typically 120°). This seems to be acceptable for most applications of our model since waves propagate from deep water to the coast with directional changes usually less than 90° or the waves are generated by a local wind within a sector of 90° on either side of the wind direction. Since we have restricted wave directions to a sector of less than 180° and since wave information along the lateral boundaries in (x,y)-space is usually not available we assume that wave information is given only along an upwave boundary of the model in (x,y)-space (which may or may not be on land). At the other boundaries in (x,y,θ)-space we assume that no waves enter the model.

4. FIELD AND LABORATORY TESTS

Results of wave propagation in the model have been compared with observations in a large laboratory wave tank simulating swell propagation off San Ciprian (Spain), see Booij et al. (1985), and in an irregular-wave tank containing a submerged bar, see Dingemans et al. (1986). To test the model in geophysical conditions which are more realistic and complicated than in these laboratory tests, the model has been applied in an area of the Rhine estuary. This area was chosen because the model results can be compared with the results of a well documented field campaign of the Ministry of Public Works and Transport in the Netherlands (Dingemans, 1983, 1985). This campaign involved the use of 1 pitch-and-roll buoy, 1 wave gauge and 6 waverider buoys. The situation can be characterized as non-locally generated waves passing from deeper water into shallow water over a shoal with a regeneration by wind behind the shoal. Currents are practically non-existent in the chosen situation.

The bathymetry is given in fig. 1 with the location of the buoys and the wave gauge indicated. This bathymetry can be roughly characterized as a relatively shallow estuary (water depth typically 4 m – 5 m), about 10 km x 10 km in surface area. It is partly protected from the southern North Sea by a shoal of roughly 2 km x 4 km (water depth typically 1 m – 2 m) extending over half of its opening.

The computations have been carried out for a situation which occurred on October 14, 1982 at 22.00 hours (M.E.T.). The waves are locally generated in the southern North Sea with a significant wave height of about 3 m and a mean period of about 7 s at the estuary

entrance. These waves penetrate the area from north-westerly direction. They break over the shoal with a reduction in wave height to about 0.5 m over the shoal. The local wind of 16.5 m/s regenerates the waves to about 0.9 m significant wave height at the wave gauge which is located 5 km behind the shoal (see table 1).

The pitch-and-roll buoy in 16 m water depth (point 1 fig. 1) provided not only the significant wave height and the mean wave period as input at the up-wave boundary of the model (for parameter values see table 1), it also provided the mean wave direction and the directional spreading as input for that boundary. The waverider buoys and the wave gauge located at various locations in the area (points 2 to 7 in fig. 1) provided each a significant wave height and a mean wave period which can be compared with the results of the model. In fig. 2 it is shown that the pattern of the model results is consistent with the pattern of the observations (table 1; Dingemans, 1985; Dingemans, 1983), e.g. the significant wave height which at the up-wave boundary of the model (16 m water depth) is about 3.4 m, reduces gradually to about 2.5 m at 6 m depth and then very rapidly to about 0.6 m over the shoal. South of the shoal the gradual decrease in wave height continues. At the location of the wave gauge (about 5 km behind the shoal) the significant wave height is about 0.9 m. The mean wave period follows roughly the same pattern. A quantitative comparison with the observations is given in table 1.

These results are satisfactory considering that no tuning of the model is used in this complex geophysical situation. Further improvement may be expected from tuning the present model (e.g. high-frequency regeneration of waves behind a shoal should decrease the mean wave period rather than increase it as presently modelled).

Table 1
Observations and model results in the Haringvliet

location	observation		model result	
	H_s (m)	T_{mean}(s)	H_s (m)	T_{mean}(s)
1. pitch-roll buoy	3.38	7.0	3.27	7.0
2. waverider	2.90	6.3	3.19	6.8
3. waverider	2.58	6.3	2.59	6.2
4. waverider	2.68	5.9	2.54	6.1
5. waverider	0.62	2.6	0.60	4.4
6. waverider	1.05	3.7	1.14	4.5
7. waverider	1.60	5.1	1.42	4.7
8. wave gauge	0.95	2.8	0.87	3.8

5 CONCLUSIONS

The model presented here is conceptually different from the traditional approach in shallow water wave models. It is a finite difference approximation of a directionally decoupled action balance equation. Because of the finite difference approximation, classical problems of ray refraction computations are avoided and the effects of wind, currents, bottom dissipation and surf breaking are efficiently computed.

The results of the (untuned) model applied to an observed situation in the Rhine estuary showed an rms-error of about 8.3% in the significant wave height and an rms-error of about 18.7% in the mean wave period.

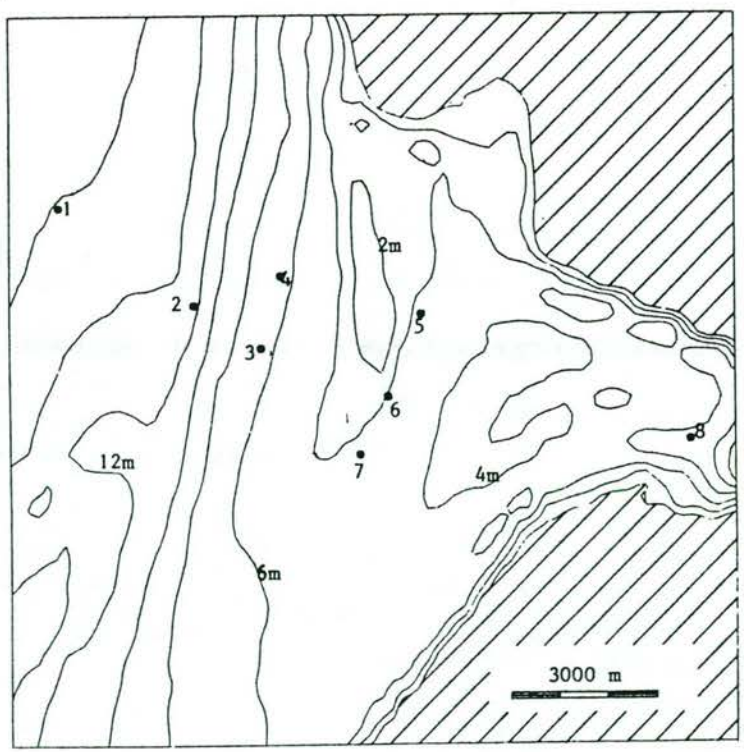

Fig. 1 Bathymetry of the Haringvliet area
in the south-west of the Netherlands.
Circles indicate locations of observation.

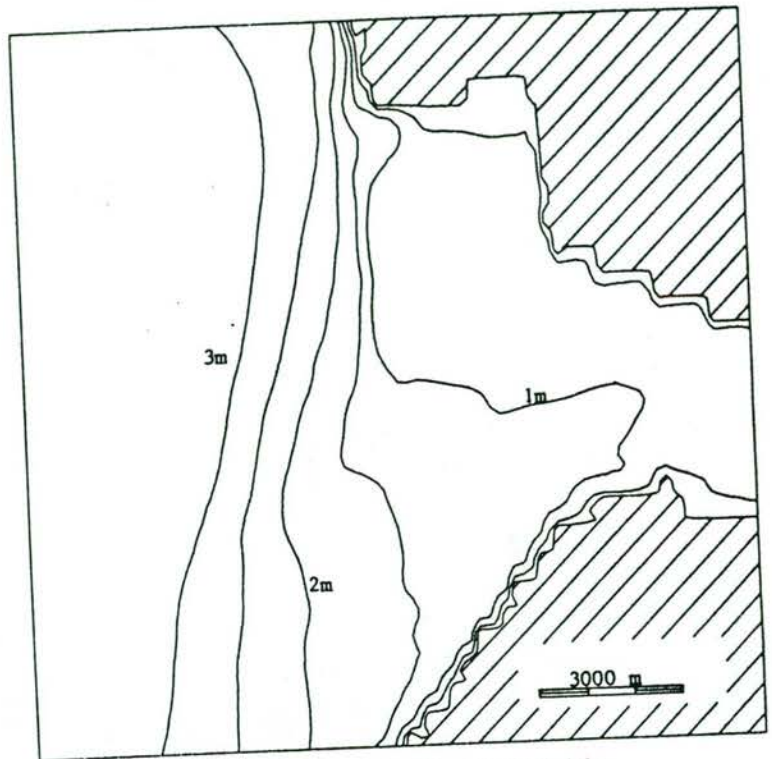

Fig. 2. Iso-lines of significant wave height.
Hatched area is land.

References

Battjes, J.A. and J.P.F.M. Janssen, 1978. Energy loss and set-up due to breaking of random waves, Proc. 16th Intl. Coastal Engineering Conference, Hamburg, ASCE, New York, pp. 569–587.

Booij, N., L.H. Holthuijsen and T.H.C. Herbers, 1985. A numerical model for wave boundary conditions in port design, International Conference on Numerical and Hydraulic Modelling of Ports and Harbours, Birmingham, 23-25 April, 1985, pp. 263–268.

Booij, N. and L.H. Holthuijsen, 1987. The directionally decoupled shallow water model HISWA, Delft University of Technology, in preparation.

Bretherton, F.P. and G.J.R. Garrett, 1968, Wavetrains in homogeneous moving media, Proc. R. Soc. London, A302, pp. 529–554.

CERC; Shore Protection Manual, 1973. U.S. Army Coastal Engineering Research Center, Corps of Engineers.

Dingemans, M.W., 1983. Verification of numerical wave equation models with field measurements, CREDIZ verification Haringvliet, Delft Hydraulics Laboratory, Rep. No. W488.

Dingemans, M.W., 1985. Surface wave propagation over an uneven bottom, Evaluation of two-dimensional horizontal wave propagation models, Delft Hydraulics Laboratory, Rep. No. W301, part 5.

Dingemans, M.W., M.J.F. Stive, J. Bosma, H.J. de Vriend and J.A. Vogel, 1986, Directional nearshore wave propagation and induced currents, Proc. 20th Intl. Coastal Engineering Conference, Taipei, ASCE, New York.

Gelci, R., H. Cazale and J. Vassal, 1956. Utilization des diagrammes de propagation à la prévision energetique de la houle, Bulletin d'information du Comité central d'oceanographie et d'études des côtes, Vol. 8, No. 4, pp. 169–197.

Hasselmann, K., 1960. Grundgleichungen der Seegangsvoraussage, Schiffstechnik, Vol. 7, No. 39, pp. 191–195.

Karlson, T., 1969. Refraction of continuous ocean wave spectra, Journal of the Waterways and Harbour Division, ASCE, Vol. 95, No. WW4, pp. 437–448.

Putnam, J.A. and J.W. Johnson, 1949. The dissipation of wave energy by bottom friction, Trans. Am. Geoph. Union, Vol. 30, No. 1, pp. 67–74.

Radder, A.C., 1979. On the parabolic equation method for water wave propagation, Journal of Fluid Mechanics, Vol. 95, pp. 159-176.

Sakai, T., M. Kosecki and Y. Iwagaki, 1983. Irregular wave refraction due to current, Journal of Hydraulic Engineering, ASCE, Vol. 109, No. 9, Paper no. 18233, pp. 1203–1215.

Coastal Engineering Conference, Taiwan, 1986

CHAPTER 81

Recently, a depth and current refraction model has been developed for the computation of directionally spread, random wave propagation in coastal regions (Booij et al., 1985). For the verification of the performance of this model laboratory measurements in a directional, shallow water wave basin were conducted. Specific attention was given to the verification of the new features of the numerical model, viz. the effects of directional spreading and ambient current field on the wave propagation and transformation process, and the change of characteristic spectral wave frequency due to wave dissipation processes.

1.0 INTRODUCTION

Since the late seventies it has become a policy in the Netherlands to verify the performance of nearshore wave propagation models (see e.g. Dingemans et al., 1984). Recently, the Delft Technical University has devised a depth and current refraction model on a grid including directional characteristics, HISWA, see also Holthuijsen and Booij (1986) in these proceedings. In contrast to the now generally accepted parabolic refraction-diffraction models, for this model it was chosen to disregard the diffraction part in order to include directional spreading of the wave field. Moreover, also the change of characteristic wave period has been modelled. Because from the previous verification studies only scarce information on directional spread is available, a special laboratory experiment has been set up in a new wave basin, equiped to generate directional, shallow water waves (Mynett et al., 1984).

The primary purpose of this study is the verification of the wave heights and the wave periods, including the effect of directional spread on the wave characteristics. A geometry consisting of a semi-cylindrical bank on a horizontal bottom has been chosen, so that these effects may be studied.
In order to separate the two-dimensional effects around the tip of the bank, refraction and diffraction, from the one-dimensional effects due to shoaling and wave breaking, also the case of the fully cylindrical bar has been included. Moreover, to obtain information on the variability of the wave field in the basin, also the case of constant depth is considered.
Here a first, concise report is given of the verification of HISWA against the laboratory measurements. A full report will appear elsewhere.

1) Delft Hydraulics, Delft, the Netherlands
2) Rijkswaterstaat - DGW, den Haag, the Netherlands

2.0 MATHEMATICAL FORMULATION OF HISWA

It is well known that the evolution of random wave fields can be described by

$$\frac{\partial A}{\partial t} + \dot{x}_i \frac{\partial A}{\partial x_i} + \dot{k}_i \frac{\partial A}{\partial k_i} = S, \qquad (1)$$

where $A(\vec{k},\vec{x},t)$ denotes the wave action density, $\dot{x}_i = dx_i/dt = \partial\Omega/\partial k_i$ is the group velocity, v_i, and $\dot{k}_i = dk_i/dt = -\partial\Omega/\partial x_i$ is the rate of change of wave number due to refraction. Notice that the summation convention has been used with $i = 1,2$. The dispersion relation is given as $\omega = \Omega(\vec{k},\vec{x},t)$. When the medium in which the waves propagate does not depend on time explicitly, one has $\omega = \Omega(\vec{k},\vec{x})$, which case is taken here; in that case Ω is a Hamiltonian for the vector field $(\dot{x}_i,\dot{k}_i)$. In the case of an ambient current field $\vec{U}(\vec{x})$ one has

$$\Omega = \omega_r + k_i U_i , \qquad \omega_r = [gk\cdot\tanh kh]^{\frac{1}{2}}, \qquad k = |\vec{k}| ,$$

where $h(\vec{x})$ is the waterdepth. Then one has $v_i = c_{gi} + U_i$ and $c_{gi} = \partial\omega_r/\partial x_i$. Transforming from (k,x) space to the space (x,ω,θ), with θ the wave direction, and introducing the absolute energy density $\tilde{E}$ by $\tilde{E} = A\omega$, one obtains for the transport of energy along the vector field defined by the Hamiltonian Ω,

$$\frac{\partial\tilde{E}}{\partial t} + \frac{\partial}{\partial x_i}[\tilde{E}v_i] - \frac{\partial}{\partial\theta}\left[\tilde{E}\left\{(c_g - \tfrac{c}{2})\frac{1}{h}\frac{\partial h}{\partial n} + \cos\theta\frac{\partial U_1}{\partial n} + \sin\theta\frac{\partial U_2}{\partial n}\right\}\right] = \omega S, \qquad (2)$$

where $c = \omega_r/k$ and n is the direction in space normal to θ.
This equation for the absolute energy becomes, after assuming time-independency ($\partial\tilde{E}/\partial t \equiv 0$, and thus stationary wave fields) and integration over ω between 0 and ∞ :

$$\frac{\partial}{\partial x_i}[\omega^{(A)}\cdot A^{(o)}\cdot\bar{v}_i] + \frac{\partial}{\partial\theta}[\omega^{(A)}\cdot A^{(o)}\cdot\bar{C}_\theta] = S_1, \qquad (3)$$

where the mean quantities $\omega^{(A)}$, $A^{(o)}$, $\bar{v}_i$ and $\bar{C}_\theta$ are defined by

$$A^{(o)}(\vec{x},\theta) = \int_o^\infty A(\vec{x},\omega,\theta)d\omega , \qquad \omega^{(A)}(\vec{x},\theta) = A_o^{-1}\int_o^\infty \omega A d\omega$$

$$E^{(o)} = \omega^{(A)} A^{(o)} , \qquad \bar{v}_i = (1/E^{(o)})\int_o^\infty \tilde{E}\, v_i\, d\omega,$$

$$\bar{C}_\theta = -(1/E^{(o)})\int_o^\infty \tilde{E}\,(c_g - \tfrac{c}{2})\frac{1}{h}\frac{\partial h}{\partial n}\,d\omega + \cos\theta\frac{\partial U_1}{\partial n} + \sin\theta\frac{\partial U_2}{\partial n} , \qquad S_1 = \int_o^\infty \omega S d\omega.$$

Using Leibniz' rule and rewriting the result, a second equation is obtained:

$$\frac{\partial}{\partial x_i}[A^{(o)}\bar{v}_i] + \frac{\partial}{\partial\theta}(A^{(o)}\bar{C}_\theta) = \frac{1}{\omega^{(A)}}\left[S_1 - A^{(o)}\bar{v}_i\frac{\partial\omega^{(A)}}{\partial x_i}\right]. \qquad (4)$$

Equations (3) and (4) are the basic equations for HISWA. The source term S_1 is implemented as $(\omega^{(A)}/\sigma^{(A)})S^{(o)}$, where $S^{(o)}$ denotes the change of energy and $\bar{v}_i\,\partial\omega^{(A)}/\partial x_i$ is interpreted as the change of the frequency

$\omega(A)$ and is prescribed as a function S_ω of the local data. For the inclusion of source terms $S^{(o)}$ and the numerical solution technique is referred to Holthuijsen and Booij (1986).

3.0 EXPERIMENTS

Wave basin

In a wave basin of 26.40 m width and 34 m length a wave generator is available, consisting of 80 flaps which can be driven independently of each other, with a total length of 26.40 m, see Fig. 1. After considering several geometries by numerical investigation, a geometry consisting of a submerged, semi-cylindrical bar on an otherwise horizontal bottom has been chosen, see Fig 1. As a check and for comparison, measurements have also been performed for the case of a submerged, fully cylindrical bar (extending over the whole width of the basin) and for the horizontal bottom situation. The unperturbed water depth is 40 cm. Opposite to the wave generator a wave absorbing gravel beach was made, with a slope of 1:7 and with the waterline at 30 m from the wave board.

Input wave conditions

The input conditions are varied according to the properties of the two-dimensional spectrum $S(f,\theta)$:

- the width of $S(f,\theta)$ in f;
- the width of $S(f,\theta)$ in θ
- the wave height HmO;
- the incident wave direction, θ_o.

We have :

$$S(f,\theta) = E(f).D(\theta;f),$$

where we took JONSWAP-type spectra E(f) and a $\cos^m(\theta)$-type directional distribution:

$$E(f) = A_o \tilde{S}(\nu) \quad , \quad \tilde{S}(\nu) = \nu^{-5} \exp\left[-\frac{5}{4}\nu^{-4}\right] \gamma(\nu)$$

$$\gamma(\nu) = \gamma_o \exp\left[-\frac{(\nu-1)^2}{2\sigma^2}\right] \quad , \quad \nu = f/fm,$$

$$A_o = \alpha_o g^2 (2\pi)^{-4} f_m^{-5}; \qquad \sigma = 0.07, \ \nu < 1; \qquad \sigma = 0.09, \ \nu > 1$$

and

$$D(\theta;f) = B_2 \cos^m(\theta-\theta_o); \quad -\frac{\pi}{2} \leq \theta-\theta_o \leq \frac{\pi}{2}$$

$$= 0 \quad ; \text{ elsewhere.} \qquad B_2 = \frac{1}{\sqrt{\pi}} \cdot \frac{\Gamma(\frac{1}{2}m+1)}{\Gamma(\frac{1}{2}m+\frac{1}{2})}.$$

Here γ_0 is the peak-enhancement factor and m is the exponent of the $\cos^m\theta$ directional distribution.

The input wave conditions, selected in such a way, that some of them are also useful for testing other wave propagation models, are chosen to be

case	Hs [cm]	Tp [s]	γ_o	m	θ_o [deg]	current meas.
1	5	1.25	7	20	0	-
2	10	1.25	7	20	0	-
3	10	1.25	7	4	0	-
4	10	1.25	1	4	0	-
5	10	1.25	3.3	4	0	+
6	10	1.25	7	20	20	-
7	10	1.25	3.3	4	20	-
8	10	1.25	3.3		0	+

Table 3.1 Input conditions.

Measuring devices

The water surface elevation was measured with a resistance type, temperature corrected wave gauge. The relationship between the depth of immersion of the vertical conductor and the output voltage is approximately linear. The deviation from linearity is less than 1% (relative error).
In order to detect the wave directionality, Delft Hydraulics has developed a wave direction meter in which a wave gauge as described above is combined with point measurement of two orbital velocity components in the horizontal plane. The device is a button-type instrument containing two orthogonal electro-magnetic velocity meters (Fig. 2). The measurement range is from -50 to + 50 cm/s. The stability is approximately 1 cm/s, the noise is better than 1 cm/s and the linearity deviation is less than 1% (relative error). The direction of the two velocity components was +45° and -45° to the orthogonal line from the wave generator.

Measurements

At 26 sites, as depicted in Fig. 3, wave height measurements are taken. At seven of these sites directional information is obtained from measurements of the two horizontal velocity components. Because of the large amount of information, and the fact that only three directional measuring devices were available, two repetitions of each run with a diffe rent lay-out of the instruments were necessary. The instruments at sites 10 and 15 were kept in place so that the reproducibility of the experiments could be assessed.

Current measurements have been performed for the semi-cylindrical bank situation for the cases 5 and 8, at 81 measuring sites located in a square grid pattern at intervals of 3 m. Three wave direction meters have been used for this purpose, which had to be replaced 26 times so as to cover all positions. At all positions the velocities were measured at half water depth. For three positions the velocities were measured at five different levels so as to obtain some information concerning the vertical structure of the velocity field. Moreover, two wave gauges have been used, which remained at the same place during all tests. At the toe

of the wave damping talus the mean water level was measured at ten dif ferent positions by means of a narrow connection tube and gauge-glass.

All cases as given in Table 3.1 have been run for the three different bottom topographies, except the current measurements which have only been performed for the semi-cylindrical bank configuration.

The various measurements are denoted by mexy, where x = 1, 2, or 3 indi cates the geometry (empty basin, cylindrical bank and semi-cylindrical bank respectively) and y gives the measurement condition (1-8) as listed in Table 3.1.

As an example of resulting spectra for me35 the spectra E(f) at site 10, close to the wave board and site 28, behind the bar are shown in Figures 4 and 5, together with the target (JONSWAP) spectra, scaled with the spectral peak and the peak frequency. The principal part of the spectrum closely follows the shape of the target spectrum. It is noted, however, that behind the bar a considerable second harmonic spectral peak in E(f) is observed, due to wave breaking over the bar. The variance of this second harmonic peak in the spectrum has been analyzed for seven sites. To characterize this peak we calculated the variance above the frequency f = 1.4 Hz, m0d2. For the measurements me35, me25 and mel5 the rate m0d2/m0 has been given in the next Table, and m0 is the total variance.

$$m0d2 = \int_{1.4}^{3.125} E(f)df, \qquad m0 = \int_{0}^{3.125} E(f)df.$$

	site	semi-cyl. me35	cyl. me25	empty basin mel5
in front	19	20.8	19.9	18.5
of	10	20.0	18.5	17.7
bank	18	21.2	20.8	20.5
on bank	38	21.2	20.8	20.5
behind	39	37.1	51.5	17.6
bank	29	43.1	52.1	18.3
	28	60.9	51.0	17.8

Table 4.1 Values m0d2/m0 in %.

Inspection of the tabulated results, especially for mel5, indicates that the contribution of the second spectral part is approximately 20% in the target spectra, which remains unaffected as the wave field propagates over the horizontal bottom. In the nearly one-dimensional case of wave breaking over the cylindrical bank the second spectral part grows relative to the primary spectral part; the energy densities become approximately equal. In the case of wave breaking over the semi-cylindrical bank the growth of the second spectral part relative to the primary spectral part varies with its position relative to the bank. These results indicate that the concept of one characteristic mean frequency is doubtful in such situations.

5.0 VERIFICATIONS

Boundary conditions and computations

Computations have been performed for all cases in Table 3.1 for both the semi-cylindrical and cylindrical bank geometry. The boundary conditions used as input in the numerical model have been determined from the corresponding measurement series. For the wave height the height Hm0 at site 10 has been taken ($Hm0 = 4\sqrt{m_0}$) and for the wave period T the average wave period, T_{m-10}, has been taken, defined as

$$T_{m-10} = m_{-1}/m_0, \qquad m_j = \int_0^\infty f^j E(f)\, df$$

The moments m_j have been determined from the measured spectrum.

As the computed wave height behind the bar depends critically on the wave breaking parameter γ, the value for γ has been determined according to the algorithm as given by Battjes and Stive (1985), using T_{m-10} for the wave period. The bottom friction coefficient fw has been set at 0.01, a reasonable standard value.

Because the sidewards boundaries in the mathematical model are dissipative, the wave field close to these boundaries is distorted. Following Dingemans et al. (1984) for the parabolic wave model, a region with an apex of 20 degrees is taken to be a possibly distorted area; this followed also from initial computations with an empty basin. The computational region is now taken to be 50 m wide, instead of 26.40 m, the actual width of the wave basin.

Method of comparison

A relatively large amount of data has been collected, especially since we are dealing with measurements on a grid. The measurement parameters are the wave height Hm0, the wave period T_{m-10}, the main wave direction teta and the directional spread σ_θ. In addition to a graphical comparison between measurements and computations, a more objective measure of correspondence was sought. To that end the approach of Willmott (1981, 1984) was adopted, in which a set of statistical measures is used. For all parameters mentioned the following procedure was followed; as an example it is elaborated here for the wave height.

The wave height field as obtained from the measurements mexy is to be compared with that from the corresponding computations; this is done at 26 sites where the wave height is compared with the computed wave height H at that site. In fact, from the computations output is generated in a square of 50 by 50 cm with midpoint the site in question, where 25 wave heights are given (see Sketch 1 below). For the comparison the mean value over the middle 9 points is used; the standard deviations are also computed, but are so low that in fact the wave height at the site alone could equally well have been taken.

```
x x x x x
x x x x x
x x o x x
x x x x x
x x x x x
```

Sketch 1

A direct comparison of the HmO and the H values is given by means of a scatter plot, which gives visual information on the correspondence. The statistical parameters recommended by Willmott (1981, 1984) are defined in the following way.

Consider a set of observations $\{O_i\}$ and predictions $\{P_i\}$, i=1,...,n. Then the mean absolute error, mae, and the root mean square error, rmse, are given by, with $\langle\cdot\rangle$ denoting the averaging operator,

$$\text{mae} = \langle|P_i - O_i|\rangle \qquad \text{and} \qquad \text{rmse} = [\langle(P_i - O_i)^2\rangle]^{\frac{1}{2}}.$$

With an ordinary least square regression $\hat{P}_i = a + bO_i$ the systematic and unsystematic part of the rms error, rmses and rmseu, can than be obtained as

$$\text{rmses} = [\langle(\hat{P}_i - O_i)^2\rangle]^{\frac{1}{2}} \qquad \text{and} \qquad \text{rmseu} = [\langle(P_i - \hat{P}_i)^2\rangle]^{\frac{1}{2}}.$$

The potential variance, PE, is given by

$$PE = \sum_i [|P_i - \langle O_i\rangle| + |O_i - \langle O_i\rangle|]^2$$

and an index of agreement, d, is given as

$$d = 1 - \frac{n \cdot \text{rmse}^2}{PE}; \qquad 0 \le d \le 1.$$

For d = 1 one has perfect agreement and for d = 0 none at all.

The parameters $\langle O_i\rangle$, $\langle P_i\rangle$, $s(O_i)$, $s(P_i)$, a, b mae, rmse, rmses, rmseu and d form a complete set for comparison purposes. Other variables can be derived from this set, see Willmott (1981, 1984). The bias for instance, is given by $(\langle P_i\rangle - \langle O_i\rangle)/\langle O_i\rangle$. It has to be stressed that a single parameter is in most cases not suited for model validation. Notice that these parameters are not scaled, apart from d.

Due to space limitations in the following the attention is restricted to case 5, for the semi-cylindrical bank. This particular choice is motivated by the fact that the conditions of case 5 come close to situations observed in nature and this case is one of the two primary cases around which the parameters are varied (the other one is case 2).

Wave heights

For case 5 a number of numerical model computations was made. One of the initial computations, ve35b, has been performed with starting values H = 10.42 cm and T = 1.17 s and wave breaking parameter γ = 0.84. The value of the latter parameter is determined according to the algorithm of Battjes and Stive (1985), so that the model may be considered untuned. The resulting wave heights H at the 26 sites are compared with the corresponding measured HmO values. A scatter plot of these values is given in Figure 6. Notice that the computed wave height values lie mostly below the measured ones; the bias is approximately -7%.

As can be expected in case of the semi-cylindrical bank geometry, a considerable current field is generated by the waves, especially due to wave breaking on the bar. Because the mathematical model also gives the

driving forces (in fact the gradients of the radiation stress components) for subsequent use in current models, such a wave driven current computation has been carried out and the resulting current field has been used in a second computation, ve35bs, in order to account for effects of current refraction on the wave field. The current field of a closely related computation, ve35a, where γ = .80 instead of .84 in ve35b, has been given in Fig. 7 and the stream function is given in Fig. 8. The resulting scatter plot of the pairs of wave heights at the sites is shown in Fig. 9. It is clear upon comparison of Figures 6 and 9 that inclusion of wave driven currents gives a closer correspondence between computed and measured wave heights. The bias has been reduced from approximately -7% to approximately -2%.

Because the wave generated current field has also been measured for case 5 for the semi-cylindrical bank geometry in 81 points 3 m apart, see Fig. 10, the measured current field can also be used for the wave propagation computations. The result of such a computation, ve35s1, has been given in the scatter plot of Fig. 11.

The statistical parameters for the computations ve35b, ve35bs and ve35s1 are given in the Table 5.1 below. For comparison the results for the fully cylindrical bank, computation ve25 (H = 10.23 cm, T = 1.17 s, γ = 0.83), are also included; H_c denotes the computed wave heights.

		ve35b	ve35bs	ve35s1	ve25
<HmO>	[cm]	8.79	8.79	8.79	6.97
<Hc>	[cm]	8.22	8.65	8.55	6.91
s(HmO)	[cm]	1.76	1.76	1.76	2.52
s(Hc)	[cm]	2.01	1.76	1.79	2.52
a	[cm]	-1.14	0.48	-0.09	-0.03
b	-	1.06	0.93	0.98	1.00
mae	[cm]	0.72	0.53	0.36	0.22
rmse	[cm]	0.92	0.66	0.50	0.28
rmses	[cm]	0.59	0.19	0.24	0.06
rmseu	[cm]	0.71	0.63	0.43	0.27
d	-	0.94	0.96	0.98	1.00

Table 5.1 Statistical parameters for wave height, over 26 sites.

These figures show that the correspondence between computed and measured wave heights becomes better with increasing accuracy of the current field. Concentrating on the mae and rmse deviation measures a continuous reduction is seen to occur from left to right in the Table. Whereas the accuracy of the wave height prediction in case ve35b (no current refraction) is already satisfactory (bias -6.6% and rmse = 10.5%), a large part of these deviations is due to the neglect of the wave-induced current field.

Taking the measured current field into account in the wave propagation computation, one has bias = -2.8% and rmse = 5.7%; as scaling parameter the value <HmO> has been used. Considering the systematic part of the rmse deviation, rmses, it is seen that tuning is possible for better correspondence because the contribution to the mean square error due to systematic deviations is still 24% of the total mean square error; in

The values of the statistical parameters for the wave direction θ are:

	ve35b	ve35bs	ve35s1
$\langle\theta_m\rangle$	-4.6	-4.6	-4.6
$\langle\theta_c\rangle$	-13.7	-0.1	-3.5
$s(\theta_m)$	5.7	5.7	5.7
$s(\theta_c)$	13.6	2.8	5.1
a	-7.9	-1.3	-1.6
b	1.3	-0.3	0.4
rmse	14.0	8.5	5.4
rmses	9.2	8.2	3.4
rmseu	10.6	2.2	4.4
d	0.53	0.33	0.69

Table 5.5 Statistical parameters for wave directions.

It is seen from Tables 5.4 and 5.5 that value of the index of agreement d is quite low in all cases, as also follows from the linear regression coefficient b.

6.0 CONCLUSIONS

For wave height prediction the numerical model performs well: without taking the wave-generated current field into account the bias is -6.6% and the rms error is 10.5%. Taking the current field into account these values are -2.8% and 5.7% respectively. Notice that these values are obtained without any tuning of the model, i.e. the parameters are chosen beforehand according to known prescriptions, derived from other model investigations, where, moreover, a fixed frequency was chosen. Especially for the wave breaking parameter γ there are indications, also obtained from other models, that it should be chosen somewhat higher; this would result in a smaller negative, or positive, bias. As the figures are based on all 26 values, and values in front of the bank are of course much better, the accuracy is somewhat less than apparent from the given figures. Taking into account the 17 sites lying on and behind the bank, the result is bias = -7.8 versus -3.2% and rmse = 11.1 versus 5.1%.

For a good prediction of the principal wave direction the inclusion of the wave-generated current field is essential. The prediction of the wave period is less satisfactory, the decrease in T is too fast. The modelling of the change in frequency is too simple; a very schematized spectral shape is assumed and, moreover, the assumed similarity of spectral shapes is seen not to be valid in strong dissipation zones. The effect of wave breaking on the spectral shape is the loss of energy on the low frequency part and the generation of higher harmonics in the spectrum, see Figures 4 and 5. It can also happen that wave breaking is so strong that the wave energy in the original frequency band has totally disappeared and that only the higher harmonic peak in the spectrum remains; an example of this behaviour has been given in Figures 17 and 18 of Dingemans et al. (1984) for field measurements in the Haringvliet region, in the Rhine-Meuse estuary. It is necessary to model the transfer of energy to higher harmonics in the spectrum in order to be able to obtain a good prediction of characteristic wave period due to breaking of waves in shallow water.

The wave-induced current field prediction is quite good. Inclusion of such current fields has been shown to be necessary in some situation so as to obtain more accurate wave height predictions in shallow water regions. The modelling of wave and current fields, possible via an iterative computation procedure, needs further investigation. This may be important for coastal models with waves and tides, especially where the interaction between bottom changes and waves and currents is a very sensative process.

7.0 REFERENCES

Battjes, J.A. and **M.J.F. Stive**, (1985). Calibration and verification of a dissipation model for random breaking waves. J. Geophysical Res. 90 (C5), Sept. 1985 pp. 9159-9167.

Booij, N., L.H. Holthuijsen and **T.H. Herbers**, (1985). A numerical model for wave boundary conditions in port design. Int. Conf. on Numerical and Hydraulic Modelling of Ports and Harbours, Birmingham, England, April 1985, pp. 263-268.

Dingemans, M.W., M.J.F. Stive, A.J. Kuik, A.C. Radder and **N. Booij**, (1984). Field and laboratory verification of the wave propagation model CREDIZ. Proc. 19th Conf. on Coastal Engng, Houston, 1984 pp. 1178-1191.

Holthuijsen, L.H. and **N. Booij**, (1986). A grid model for shallow water waves. Proc. 20th Conf. on Coastal Engng., Taipei 1986.

Mynett, A.E., J. Bosma and **P. van Vliet**, (1984). Effects of directional seas in coastal regions. Symposium on Description and Modelling of Directional Seas, Paper B7, Lyngby, Denmark.

Willmott, C.J., (1981). On the validation of models. Physical Geography 2(2), 1981 pp. 219-232.

Willmott, C.J., (1984). On the evaluation of model performance in physical geography. In: Spatial statistics and models (Eds. G.L. Gaile and C.J. Willmott), pp. 443-460, Reidel 1984.

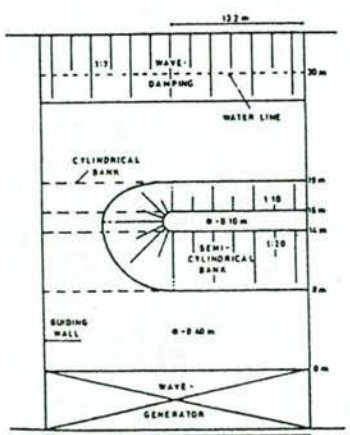

Fig. 1 Wave basin lay out

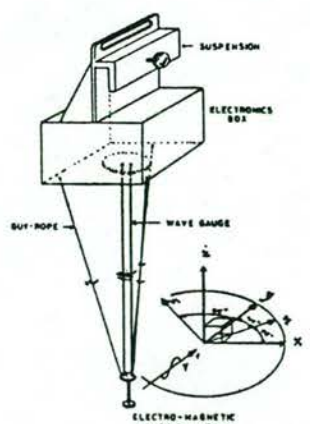

Fig. 2 Wave direction meter

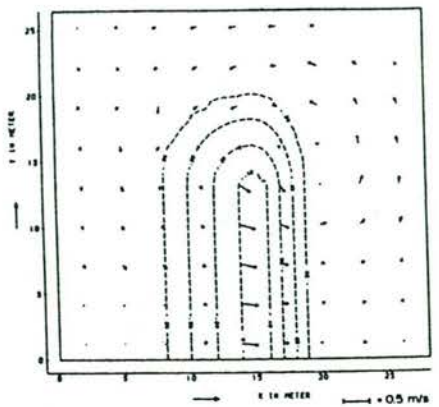

Fig. 10 Measured current vectors, me35

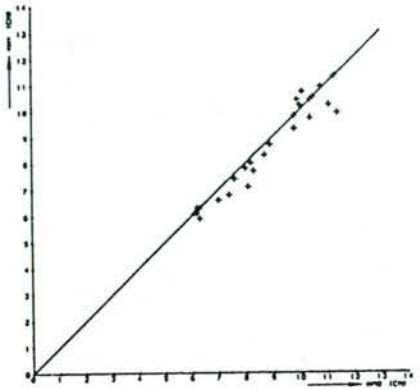

Fig. 11 Scatter plot wave heights, ve35s1

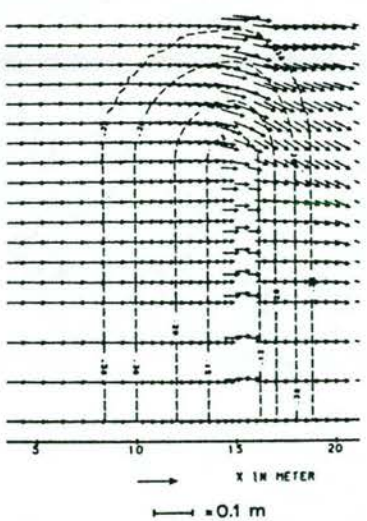

Fig. 12 Vector plot wave heights and directions, ve35a

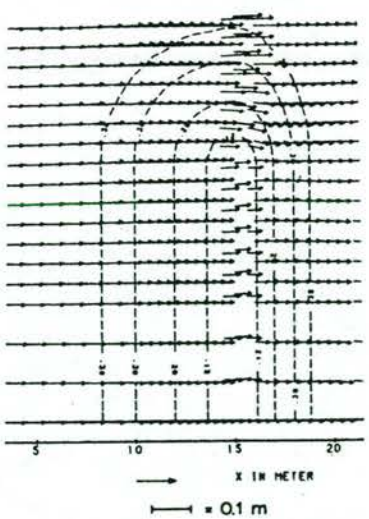

Fig. 13 Vector plot wave heights and directions, ve35s1

HET SPEKTRUM,

DE ENERGIEBALANS

EN ENKELE

FYSISCHE PROCESSEN DAARIN

Han Vogel
mei 09

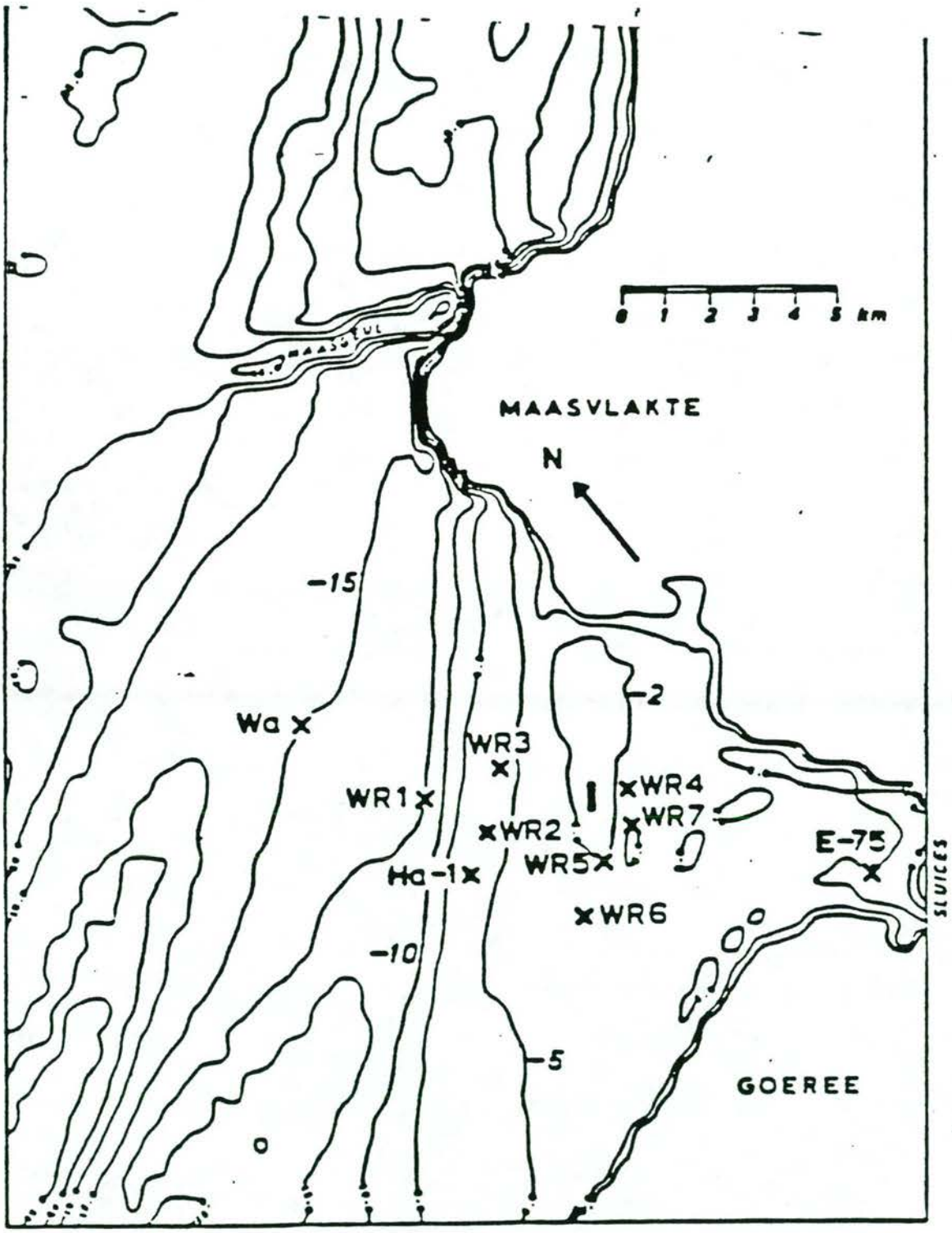

Bottom contours, estuary of Haringvliet.

Hoe veranderen de golven hier?

Hoe beschrijf je een **uiterst grillig oppervlak**?

⟹ geheel afhankelijk van het DOEL:

met welke nauwkeurigheid? welke tijds-/ruimteschaal?

10^{4} j

* ontwerp van constructie
* suppletie / zachte constructie
* deiningsprediktie, werkbaarheid
* erosie
* opwarreling van zand
* turbulentie
* atomaire bewegingen

10^{-4} s

10^{-4} m ⟵ ····· ⟶ 100 km

proces ↔ deelproces

meerdere mogelijkheden om „golven" te beschrijven :

1. Probeer de vorm van het oppervlak van de trilling te berekenen

Bijv. als simplificatie : monochromatisch

CREDIZ , PHAROS

nadeel : veel rekenpunten

andere mogelijkheid om „golven" te beschrijven :

2. probeer de „golven" te beschrijven als
   stochastisch proces waarvan de procesparameters
   deterministisch bepaald worden (voldoen aan d.v.)

   bijv. een vergelijking voor de variantie of
   voor het spektrum → fysische interpretatie : energie!

Bijv. als simplificatie : proces is Gaussisch ; dan
wordt het proces volledig beschreven door 't spektrum

dus.

golfkoestanden gelijk ⇔ spektra gelijk

variantie $\leftrightarrow$ energie :

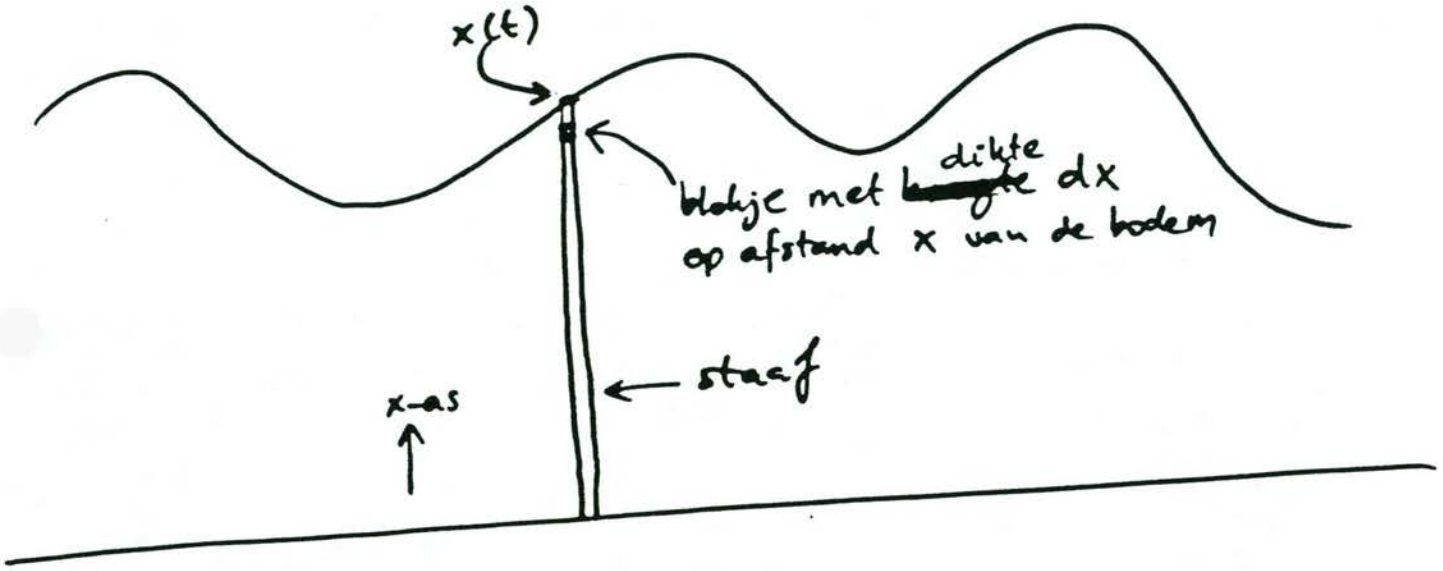

Totale potentiele energie van de staaf =

$\int$ potentiele energie van blokjes $=$ $\int$ massa $\cdot\, g \cdot$ hoogte:

$$= \int_0^{x(t)} \underbrace{\rho\, dx}_{\text{massa}} \cdot g \cdot \underbrace{x}_{\text{hoogte blokje boven bodem}} = \rho \cdot g \cdot \int_0^{x(t)} x\, dx =$$

$$= \rho g \cdot \left[\tfrac{1}{2}x^2\right]_0^{x(t)} = \tfrac{1}{2}\rho g \cdot x(t)^2$$

Gemiddelde potentiele energie van de staaf : $\frac{1}{T}\int_0^T \tfrac{1}{2}\rho g\, x(t)^2\, dt$

$\rightsquigarrow$ variantie

SPEKTRUM

Een trilling kan geschreven worden als een som van sinussen en cosinussen :

$$f(t) = \sum_{\omega} \left(a_\omega \cdot \cos \omega t + b_\omega \cdot \sin \omega t \right)$$

* als er maar eindig veel ω's zijn, geeft $E_\omega = \frac{1}{2}\left[a_\omega^2 + b_\omega^2 \right]$ aan hoeveel <u>energie</u> in de ω-trilling aanwezig is.

* als er continuum veel ω's zijn, geeft

$$\int_{\omega_1}^{\omega_2} \underbrace{\tfrac{1}{2}\left[a(\omega)^2 + b(\omega)^2 \right]}_{E(\omega)} d\omega$$

aan hoeveel energie in het <u>frequentiebandje</u> (ω_1, ω_2) aanwezig is.

vb. als $f(t) = \sin t + \frac{1}{2}\sin 2t + \frac{1}{4}\sin 3t$

dan spectrum:

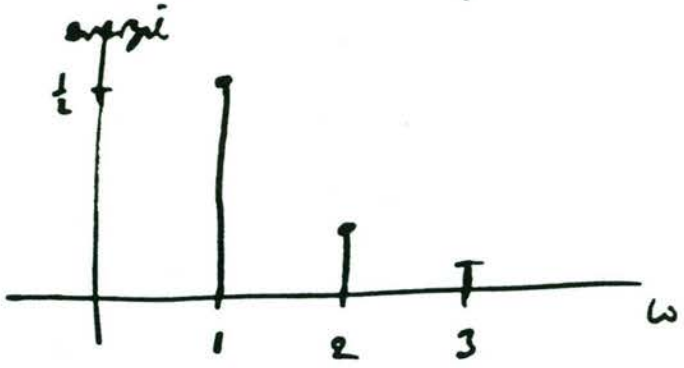

b. als $f(t) = \sin 2t$ + ruis

dan spectrum:

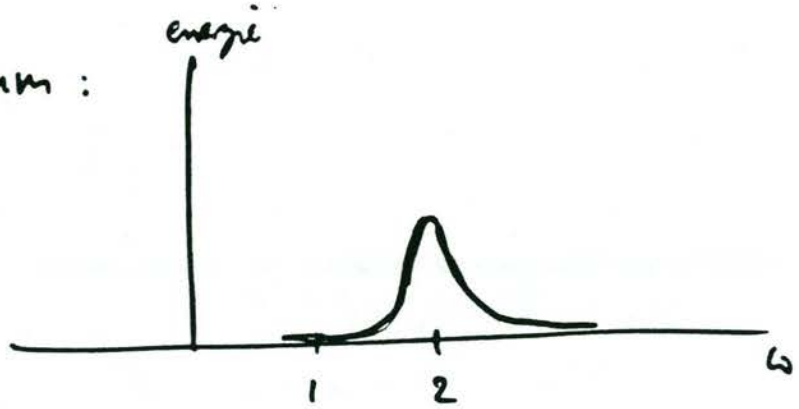

veel/weinig ruis

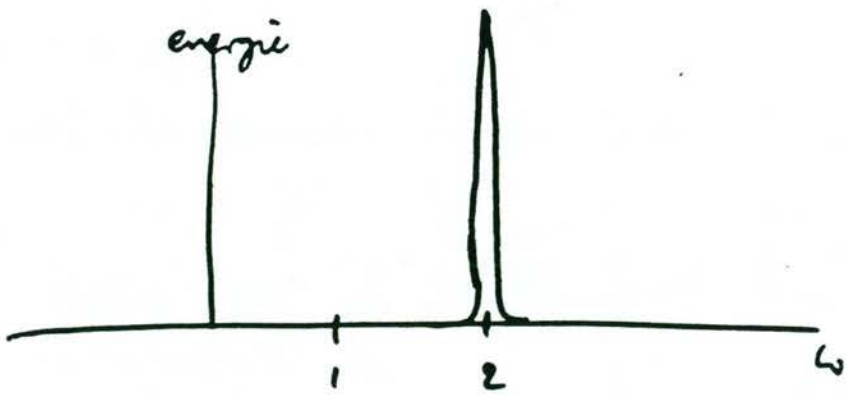

eerste voorbeeld: eigenlijk δ-pieken

* Dit waren tijdsfunkties $f(t)$.

Voor ruimtefunkties geldt het zelfde.

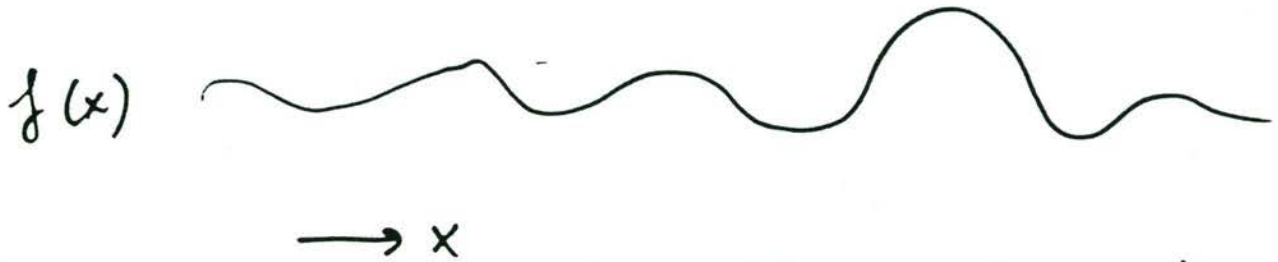

$$f(x) = \sum a_k \cos kx + b_k \sin kx$$

(dimensie k: 1/meter ; dimensie ω: 1/sec

* Voor <u>tweedimensionale ruimtefunkties</u> geldt ook iets analoogs.

$$f(x,y) = \sum \left(a_{k_1} \cos k_1 x + b_{k_1} \sin k_1 x\right) * \left(c_{k_2} \cos k_2 y + d_{k_2} \sin k_2 y\right)$$

$$= \sum a(k_1, k_2) \cdot e^{i(k_1 x + k_2 y)}$$

$t \longleftrightarrow \omega$

$x \longleftrightarrow k$

$(x,y) \longleftrightarrow (k_1, k_2)$

Het spektrum is dan een funktie van 2 variabelen:

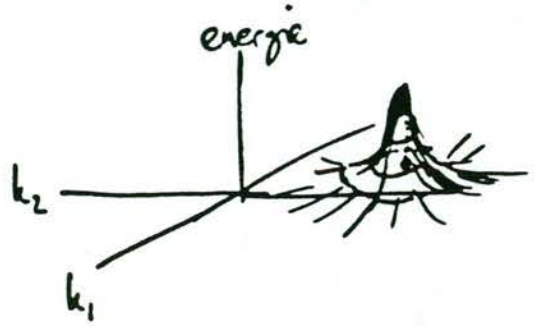

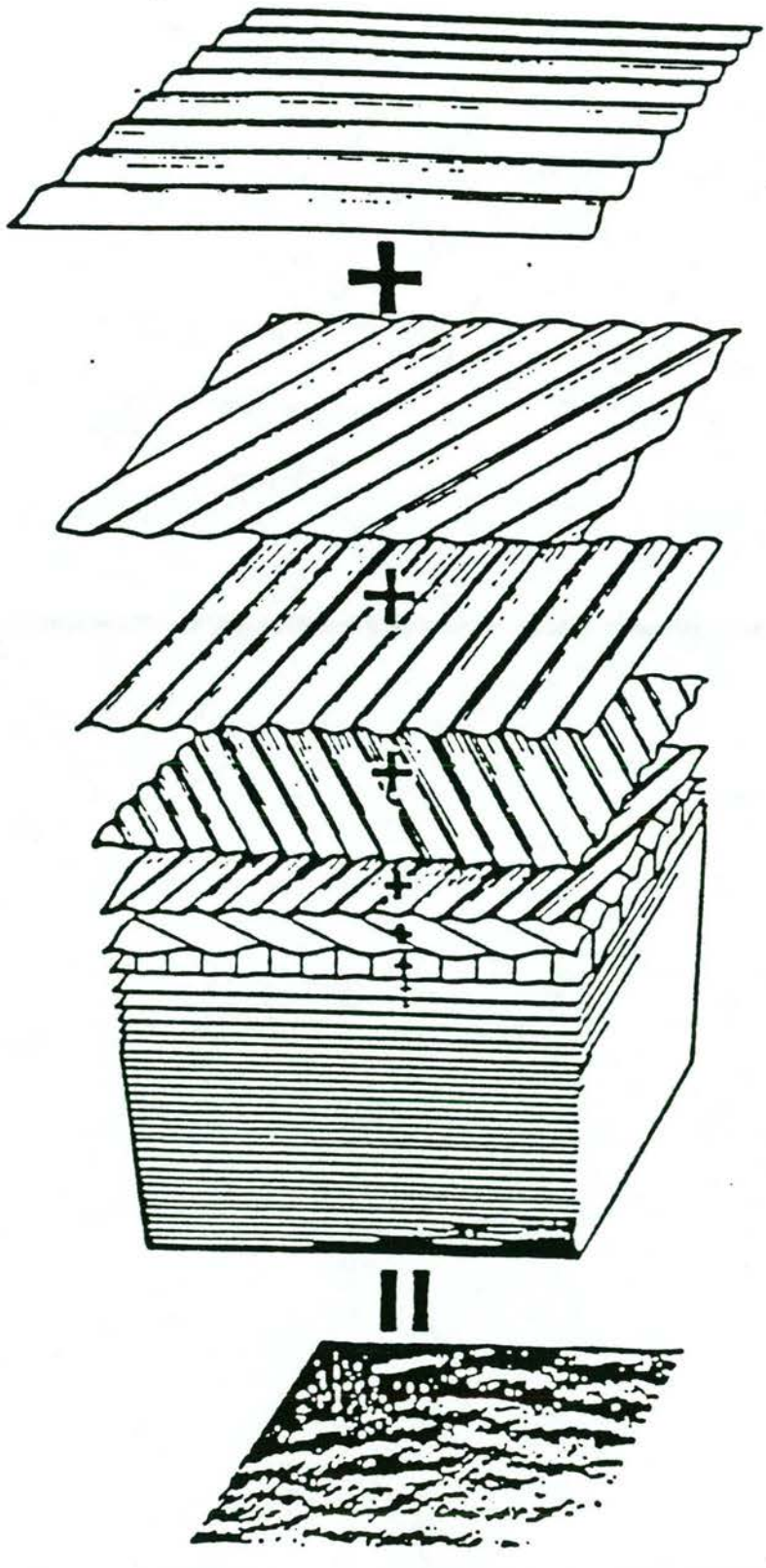

<u>vb</u> als $f(x,y) = \cos(2x + 3y)$

dan is f constant op lijnen $2x + 3y = \text{constant}$

dus $\perp$ vector $(2,3)$

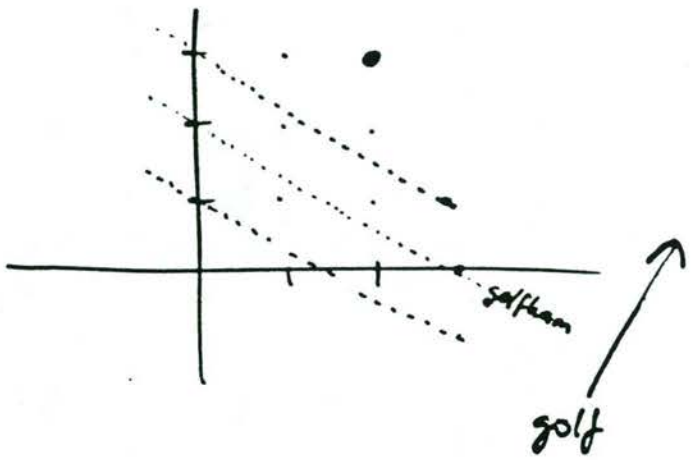

dan is het spectrum :

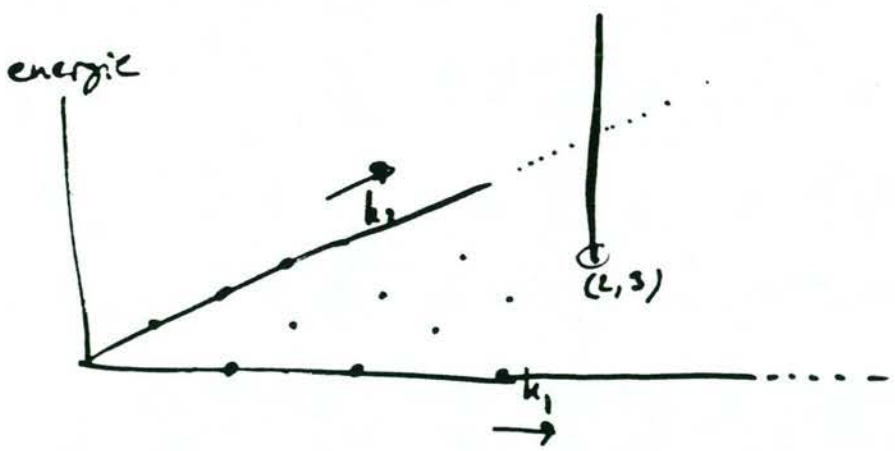

algemene functie $f(x,y)$ is te schrijven als :

$$f(x,y) = \sum a(k_1,k_2)\cos(k_1x + k_2y) + b(k_1,k_2)\sin(k_1x + k_2y)$$

I.p.v. met k_1 en k_2 kan ook gewerkt worden met k en θ (richting)

2.3.10 a

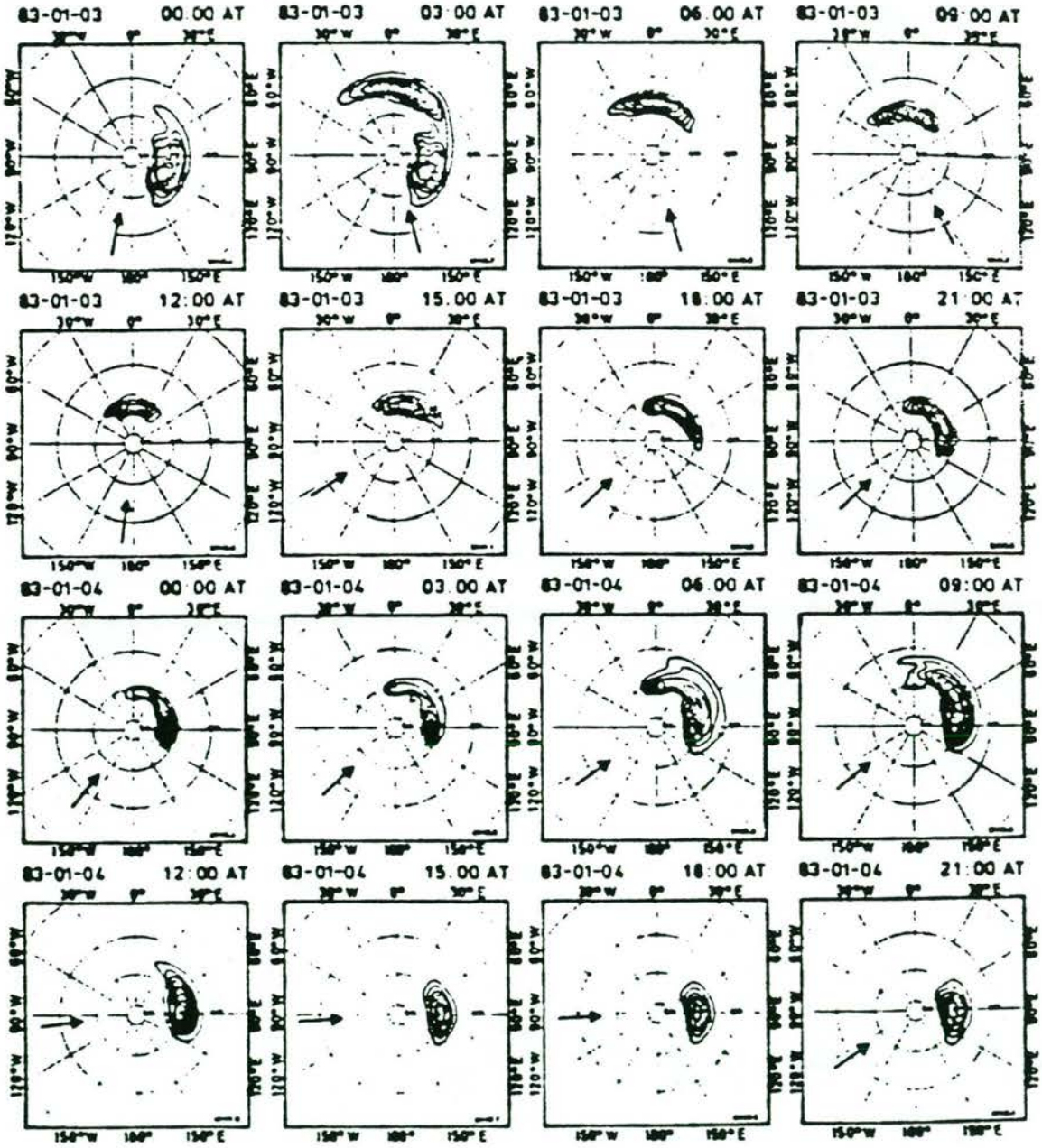
83-01-03 00:00 AT
83-01-03 03:00 AT
83-01-03 06:00 AT
83-01-03 09:00 AT
83-01-03 12:00 AT
83-01-03 15:00 AT
83-01-03 18:00 AT
83-01-03 21:00 AT
83-01-04 00:00 AT
83-01-04 03:00 AT
83-01-04 06:00 AT
83-01-04 09:00 AT
83-01-04 12:00 AT
83-01-04 15:00 AT
83-01-04 18:00 AT
83-01-04 21:00 AT

2 opmerkingen:

(1.) Bij veel trillingsproblemen is er een verband tussen het k-spektrum en het ω-spektrum, dat gelegd wordt door een afbeelding van de k-as naar de ω-as: de dispersierelatie. Voor korte golven:

$$\omega^2 = g k \cdot \tanh(kh)$$

(ω: hoekfreq., g: zw.kr.vers., k: golfgetal, h: waterdiepte)

(2.) Het tweedimensionale $\vec{k}$-spektrum (oftewel het (k,ϑ)-spektrum, ofkewel het (ω,ϑ)-spektrum) wordt vaak weer teruggebracht naar een eéndimensionaal k-spektrum of ω-spektrum door te middelen over de richtingen

Niet $E(\omega,\vartheta)$ maar $\tilde{E}(\omega) = \int_0^{2\pi} E(\omega,\vartheta)\, d\vartheta$

(bijv. bij een meetinstrument dat geen richtingen kan onderscheiden)

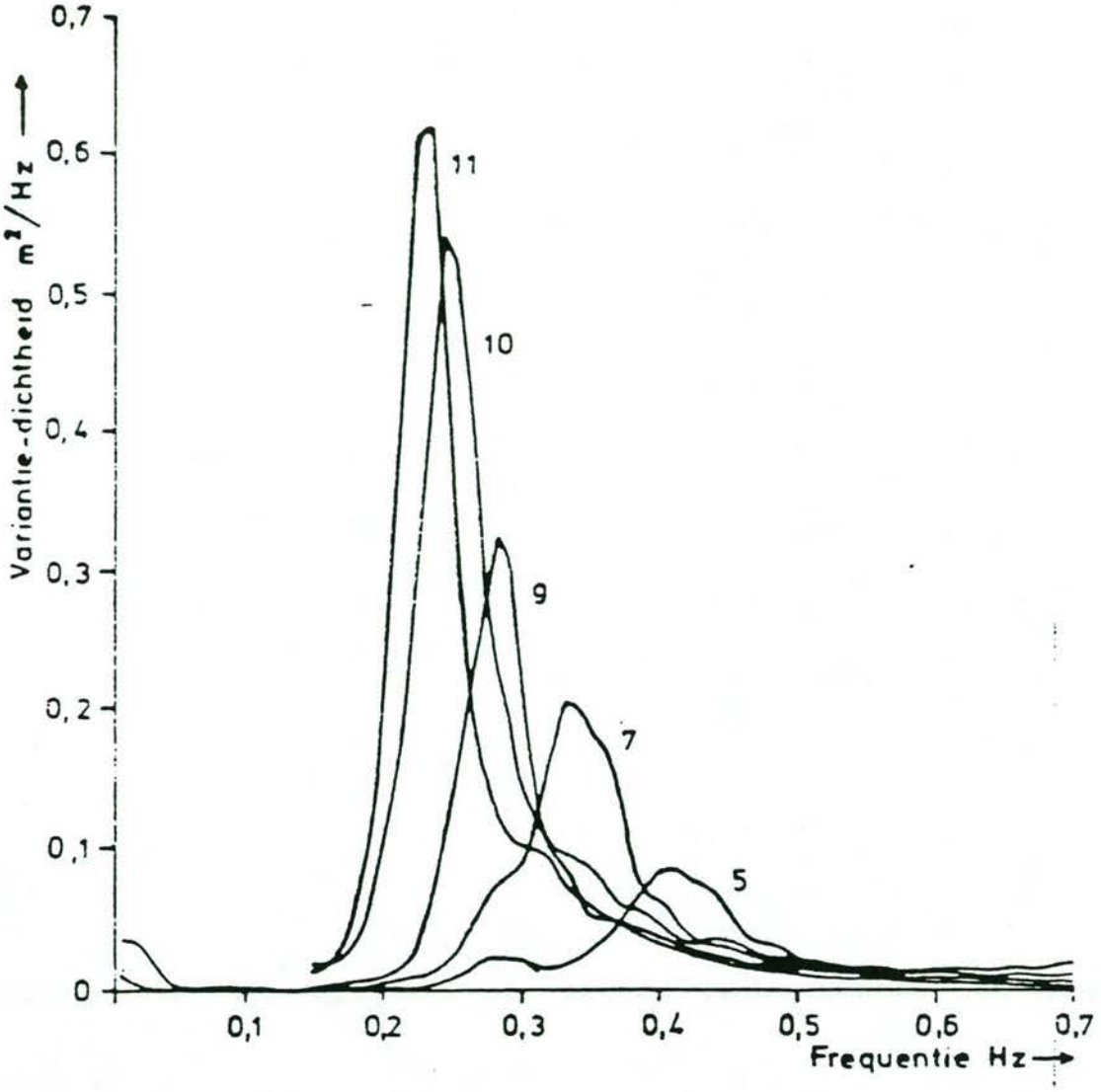

Fig. 22 Ontwikkeling van het frequentiespectrum voor zeegang bij toenemende windbaan tijdens de aflandige wind bewesten Sylt.
De nummers geven de stations aan:

station no.	5	7	9	10	11
windbaan (km)	9.5	20	37	52	80
windsnelheid	7.0 m s (15 sept. 1968, 11-12 h)				

2.3.11 b

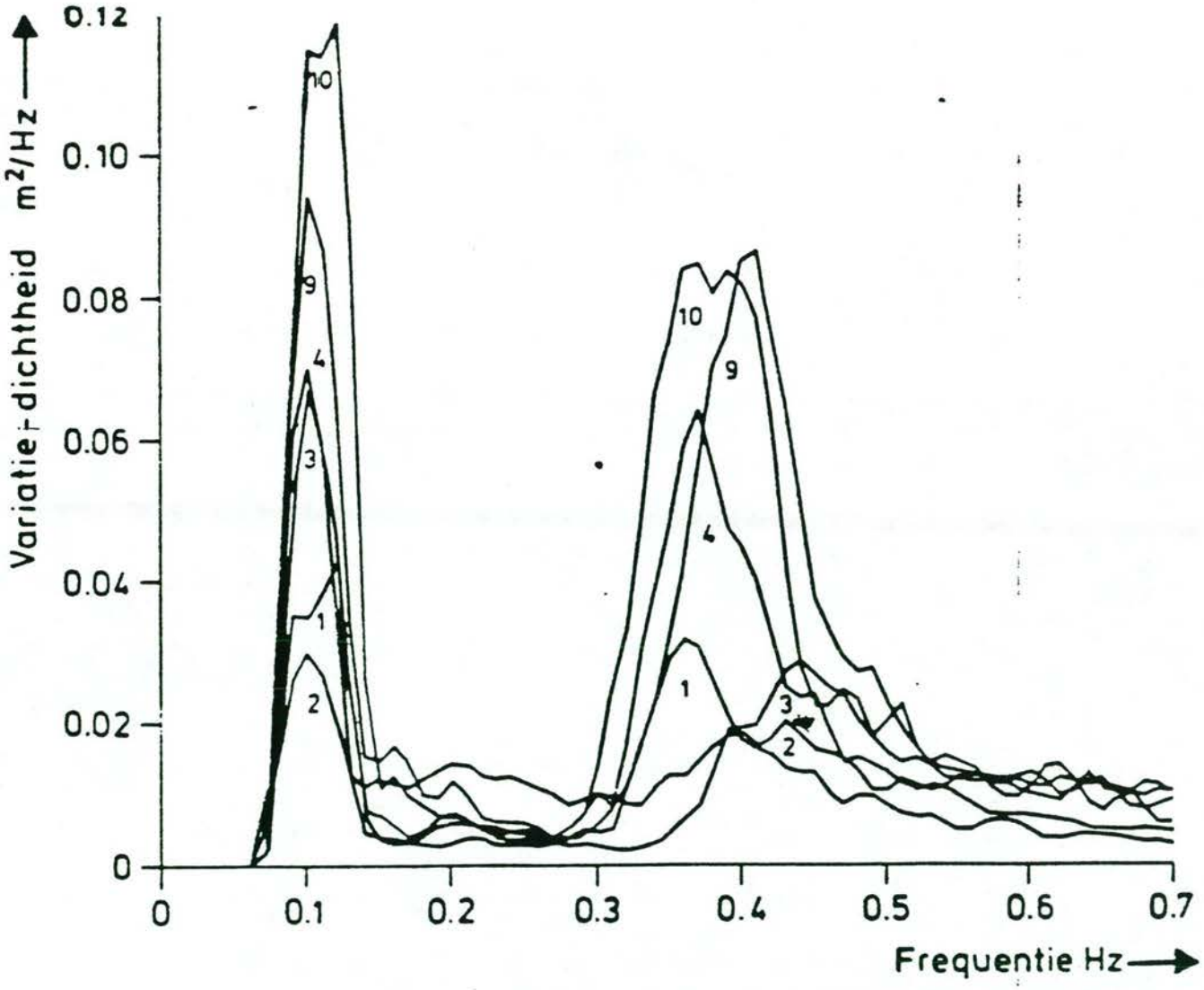

Fig. 18B Reeks van spectra, verkregen uit gelijktijdige registraties langs een raai lopende van Sylt in westnoordwesteiijke richting. De nummers geven de waarnemingsstations aan:

station no.	1	2	3	4	9	10
afstand tot kust van Sylt (km)	1	2	4	6,5	37	52
zeediepte (m)	6	8	10	12	18	21

Ongeveer 2 uren vóór de registraties stak een wind op uit zuidoost met een snelheid van ca 8 m/s (16 juli 1969, 6h 30).

Spektrale parameters:

2-dim. ding

Soms wordt hier met het totale (spektrum) gewerkt, maar met een functie daarvan; bijvoorbeeld:

* totale energie: $E_0 = \iint E(\omega,\vartheta)\, d\omega\, d\vartheta$

  sign. golfhoogte: $H_s = 4 \cdot \sqrt{E_0}$

* gem. frequentie: $\omega_0 = \iint \omega \cdot E(\omega,\vartheta)\, d\omega\, d\vartheta$

* „deining": $E_{[10]} = \int_0^{2\pi}\int_0^{\square} E(\omega,\vartheta)\, d\omega\, d\vartheta$

* spektrale momenten: $M_k = \iint \omega^k \cdot E(\omega,\vartheta)\, d\omega\, d\vartheta$

* allerlei „perioden": $TM01 = M_0 / M_1$; $TM02 = (M_0 / M_2)^{1/2}$

* piekfrequentie: ω_{piek}

* totale x-component van de energiestroom:

$$F_x = \iint c_g \cdot E(\omega,\vartheta) \cdot \cos\vartheta \; d\omega\, d\vartheta$$

$$F_y = \qquad\qquad \sin\vartheta$$

Mogelijkheden om „golven" te beschrijven :

① Het oppervlak berekenen ← Crediz

② Het spektrum berekenen ← Endec HISWA
(of spektrale parameters)

⋮

(niet-lineair :
stokes, KdV .....
Hamiltonformalisme
Na S)

Elke mogelijkheid heeft wél - en nadelen.

Keuze hangt af van de toepassing.

2.3.14

recapitulatie :

* fysische processen waardoor „golven" veranderen
* spektrum als beschrijvingswijze van golven

Nu : het verband hiertussen :

een vergelijking die de spektrumverandering beschrijft
ten gevolge van fysische processen

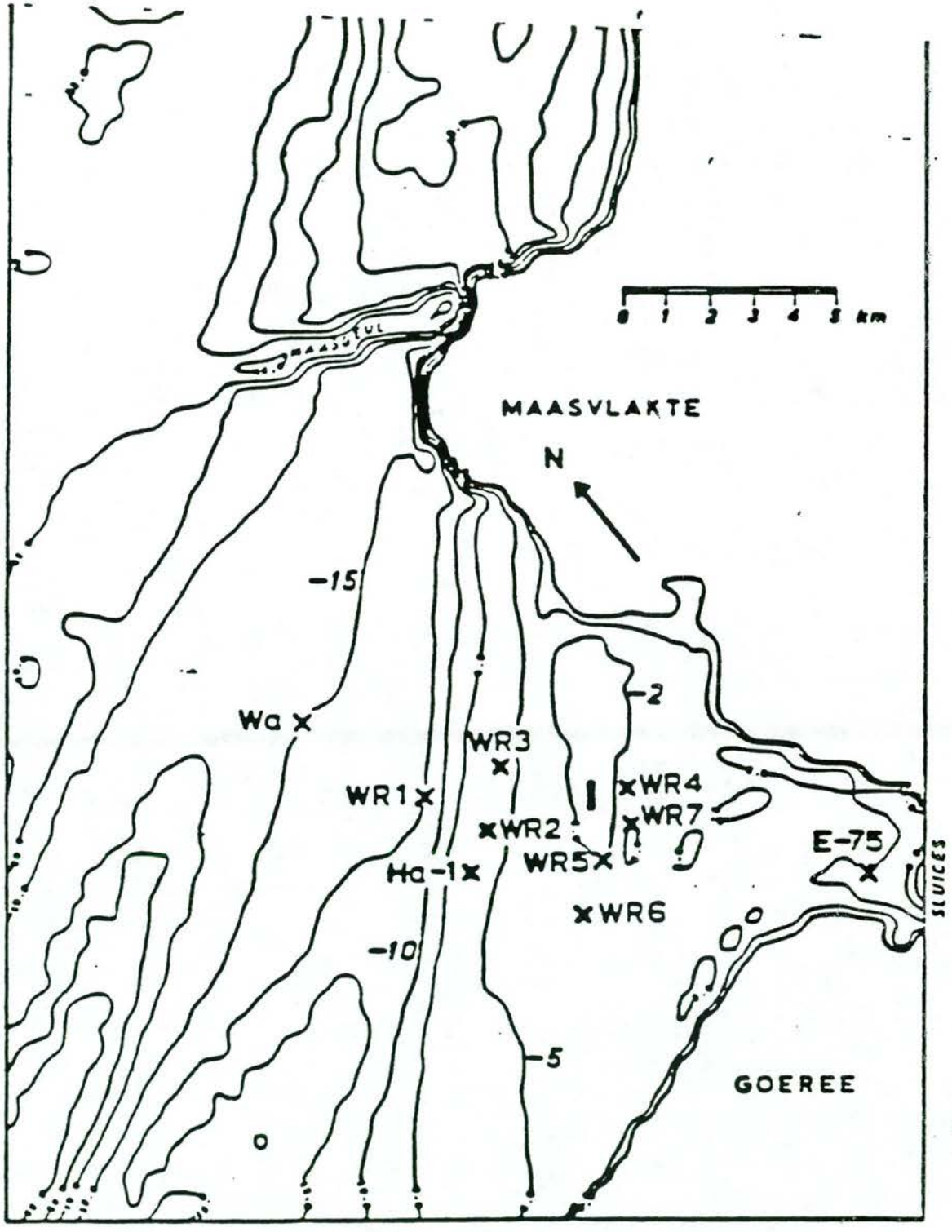

Bottom contours, estuary of Haringvliet.

- Hoe ziet (het) spektrum op de diverse locaties eruit?
  → op die-en-die dag
- Waardoor worden de verschillen bepaald?

Energiebalans :

$$\frac{\partial E}{\partial t} + (\vec{c}_g \cdot \nabla) E = S$$

in de (x, y, k_1, k_2)-ruimte

(of $(x, y, \omega, \vartheta)$)

$\vec{c}_g$ beschrijft de stralen

↳ volgt direkt uit de dispersierelatie

Veel modellen gebaseerd op :

$$\frac{\partial E}{\partial t} + (\vec{c}_g \cdot \nabla) E = S$$

① Benaderingen linkerlid :

a. stationair

b. homogeen

c. vaste frequentie

d. geen variatie in y-richting

e. diep water : geen refraktie

f. reflektie

g. stroming

(energie ⟶ aktie)

$$\frac{\partial E}{\partial t} + (\vec{c}_g \cdot \nabla) E = S$$

② Benaderingen [redacted] rechterlid :

a. bodem wrijving

b. percolatie

c. windtoevoer

d. breken op steilheid

e. breken op ondiepte

f. stromingsverliezen

g. niet-lineaire wisselwerkingen

③ Benaderingen van de hele vergelijking :

a. integreren over richtingen en frequenties, daarna oplossen

b. integreren over frequenties, daarna oplossen

⋮

Het resultaat is een vergelijking waarin spectrale parameters voorkomen (niet $E(x,y,\omega,\theta)$

samenvatting :

* in voorbeeld : enkele fysische processen

* hoe „golven" beschreven kunnen worden

* spektrum ; spektrale parameters

* energiebalans

* parametrisering van de energiebalans